T.C.

BURSA TECHNICAL UNIVERSITY

GRADUATE EDUCATION INSTITUTE

SEMI-ACTIVE AND ACTIVE SUSPENSION CONTROL WITH ROAD PREVIEW

PhD THESIS

Mert BÜYÜKKÖPRÜ

Department of Mechanical Engineering

Doctorate Programme

July 2023

T.C.
BURSA TECHNICAL UNIVERSITY
GRADUATE EDUCATION INSTITUTE

SEMI-ACTIVE AND ACTIVE SUSPENSION CONTROL WITH ROAD PREVIEW

PhD THESIS

Mert BÜYÜKKÖPRÜ
(171080204)
ORCID:

Department of Mechanical Engineering

Doctorate Programme

Thesis Advisor: Dr. Erdem UZUNSOY
ORCID:
Thesis Co-Advisor: Dr. Xavier MOUTON
ORCID:

July 2023

Mert BÜYÜKKÖPRÜ a PhD student of BTU Graduate Education Institute student ID 171080204, successfully defended the thesis/dissertation entitled "SEMI-ACTIVE AND ACTIVE SUSPENSION CONTROL WITH ROAD PREVIEW", which he prepared after fulfilling the requirements specified in the associated legislations, in front of the jury whose signatures are below.

Thesis Advisor :	**Dr. Erdem UZUNSOY** Bursa Technical University	.....
Co-advisor :	**Dr. Xavier MOUTON** Groupe Renault	.....
Jury Members :	**Prof. Dr. Haluk EROL** Istanbul Technical University	.....
	Dr. Hakan ÜLKER Bursa Technical University	.....
	Dr. Ekrem DÜVEN Bursa Technical University	.....
	Dr. Kutluk Bilge ARIKAN TED University	.....

Submission Date :

Defence Date : 04 July 2023

In accordance with Articles 9/2 and 22/2 of the Postgraduate Education and Training Regulation published in the Official Gazette dated 20.04.2016; for this postgraduate thesis, a report was received in accordance with the criteria determined by the Graduate Education Institute by using the plagiarism software program that Bursa Technical University is subscribed to.

STATEMENT OF PLAGIARISM

I declare that all the information and results presented in visual, auditory and written form in this thesis were obtained by me in accordance with academic and ethical rules, I have documented all the results and information in the thesis that are not specific to this study, by citing the source in the thesis, and I accept all kinds of legal consequences if the opposite arises.

Student's Name Surname: Mert BÜYÜKKÖPRÜ

Signature :

To my spouse and children,

FOREWORD

I would like to thank my family and my spouse for their endless support. I am really grateful to my advisor Dr. Erdem Uzunsoy, who guided me in every step of this way that we worked together in the academic field, for his guidance, reviews and recommendations. I am really grateful to my industrial advisor Dr. Xavier Mouton who has been believing and encouraging me to remove barriers in the way of science and innovations in the industrial field and also for his guidance in all matters. I would like to thank these people for always listening to me patiently and broadening my learning horizons. I would also like to thank my managers who made it possible to work on this full-time project at Oyak-Renault.

May 2023

Mert Büyükköprü
Mechanical Engineer, MSc.

TABLE OF CONTENTS

Page

ABBREVIATIONS

4WS : Four-wheel steering control
ABS : Anti-Lock Braking System
ADAS : Advance Driver Assistance Systems
ADD : Active Driven Damper
ASR : Anti Slip Regulation
CPU : Central Processing Unit
CRG : Curved Regular Grid
DBSCAN : Density Based Spatial Clustering of Applications with Noise
DoF : Degree of Freedom
EPAS : Electrical power assisted steering system
IDT : Input Decoupling Transformation
ISO : International Standard Organisation
LPV : Linear Parameter Varying
LQR : Linear Quadratic Regulator
MF : Magic Formula
MIMO : Multi-input-multi-output
MPC : Model Predictive Control
PDD : Power Driven Damper
PSD : Power Spectral Density
QP : Quadratic Programming
RMS : Root Mean Square
SAD : Sum of Absolute Differences
SAS : Semi-active suspension system
SH : Skyhook
TCS : Traction Control System
VSC : Vehicle Stability Control

SYMBOLS

$\boldsymbol{F_{net}}$	**:** Net force
$\boldsymbol{k_s}$	**:** Spring constant
$\boldsymbol{z}$	**:** Distance from initial position
$\boldsymbol{m_s}$	**:** Mass of 1DOF model
$\ddot{\boldsymbol{z}}$	**:** Body acceleration
$\boldsymbol{\omega_n}$	**:** Natural frequency (radians/second)
$\mathbf{z_0}$	**:** Amplitude
t	**:** Time
∅	**:** Phase angle
$\boldsymbol{f_N}$	**:** Natural frequency (Hertz)
$\boldsymbol{c_s}$	**:** Damping coefficient
$\boldsymbol{\zeta}$	**:** Damping ratio
$\boldsymbol{\omega_d}$	**:** Damped natural frequency
$\boldsymbol{\alpha}$	**:** Damping factor
F	**:** Force
Q	**:** Chamber pressure
V	**:** Stroke speed
F_d	**:** Damper force
c	**:** Damper control parameter
$\boldsymbol{c^{sym}}$	**:** Damper control parameter
$\boldsymbol{c^{nl}}$	**:** Damper control parameter
$\dot{\boldsymbol{x}}$	**:** Stroke speed

$\boldsymbol{I}$	**:** Control input current
$\boldsymbol{c_0, k_0, x^0, \gamma, \beta, \delta, A, n}$	**:** Nonlinear dynamic model coefficients
z	**:** Internal state parameter
$\boldsymbol{f_x, f_y, f_z}$	**:** Focal lengths
$\boldsymbol{u_l, u_r}$	**:** Disparity values
$\boldsymbol{x, y, z}$	**:** Coordinates of point
$\boldsymbol{E_l, E_r}$	**:** Pixels in the left and right images
$\boldsymbol{f_1, f_2, f_3, f_4}$	**:** Force components
$\boldsymbol{Z_s, \dot{Z}_s, \ddot{z}_s}$	**:** Body position, velocity, acceleration
$\boldsymbol{Z_u, \dot{Z}_u, \ddot{z}_u}$	**:** Wheel position, velocity, acceleration
X	**:** System states
$\boldsymbol{k_t}$	**:** Tyre stiffness
$\boldsymbol{Z_r}$	**:** Road input
$\boldsymbol{L_f}$	**:** Distance between front axle and center of gravity
$\boldsymbol{L_r}$	**:** Distance between rear axle and center of gravity
$\boldsymbol{M_s}$, M_{uf}	**:** Vehicle sprung and unsprung masses
$\boldsymbol{h_s}$	**:** Center of gravity height from ground
$\boldsymbol{a_x}$	**:** Longitudinal acceleration
$\boldsymbol{F_{s,f}, F_{s,r}}$	**:** Front and rear spring forces
$\boldsymbol{I_{xx}, I_{yy}}$	**:** Inertia moments
A, B, C, D	**:** State space system matrices
$\boldsymbol{\ddot{\theta}}$	**:** Pitch acceleration
$\ddot{\emptyset}$	**:** Roll acceleration
$\boldsymbol{a_{rms}}$	**:** Root mean square of a signal
$\boldsymbol{Z_{r_i}, \ddot{Z}_i}$	**:** Road inputs, body acceleration for each input and output

w_i	**:** Signal's frequency
Facc	**:** Variance gain
y(t)	**:** Discrete signal
$E\{.\}$	**:** Averaging operator
r(k)	**:** Autocovariance sequence
R_m	**:** Covariance matrix
M	**:** Hermitian matrix
s	**:** Laplace variable
C_{sky}	**:** Virtual skyhook damper damping coefficient
C_{min} , C_{max}	**:** Minimum and maximum damping coefficient
α	**:** Switching parameter
$E(t)$	**:** Total Energy
$P(t)$	**:** Power flow
$P_{sd}, P_{ss}, P_{ud}, P_{us}, P_{net}$	**:** Power components
A_d, B_d, C_d, D_d	**:** Discrete state space system matrices
A, B_u, B_w	**:** System, control inputs, disturbance matrices
u, w	**:** Control inputs, disturbance inputs
$\hat{y}$	**:** Estimated outputs
Q, R	**:** Output and control signal penalty matrix
H	**:** Hessian matrix
lb, ub	**:** Lower and upper bound
$Fd'_{i,j}$	**:** Actuators produced output force
$F_z, M_\theta, M_\emptyset$	**:** Force and moments around CoG
C_{skyB} , C_{skyP}, C_{skyR}	**:** Virtual skyhook dampers
$\dot{Z}_s, \dot{\theta}, \dot{\emptyset}$	**:** Bounce, pitch, roll rate
W	**:** A representative matrix

$\boldsymbol{X_i, V_j}$	**:** Distance of point i and the vehicle speed
$\boldsymbol{\Delta t}$	**:** Processing time
$\boldsymbol{\overline{Z}}$	**:** Weighted arithmetic mean road height point
$\boldsymbol{\omega_i}$	**:** Weighting factors
$\boldsymbol{f_{lpf}, f_{hpf}}$	**:** Low pass and high pass filter cut-off frequency
$\boldsymbol{I}$	**:** Electric current
T	**:** Time delay

LIST OF TABLES

Page

LIST OF FIGURES

Page

YARI VE TAM AKTİF SÜSPANSİYONUN YOL BİLGİSİ ÖNGÖRÜSÜ İLE KONTROLÜ

ÖZET

Çalışma Groupe Renault'nun Vehicle Motion Control projesi kapsamında düşey eksende, taşıtın kontrol edilerek seyir ve sürüş dinamiklerinin iyileştirilmesi amacı ile 2019 haziran ve 2023 yılları arasındaki dört yıllık çalışmanın sonucunda ortaya çıkmıştır.

Günümüz taşıtlarında konfor beklentisi giderek artmakta, artan sayıda araç üreticisinin de pazara girmesi ile rekabet de giderek artmaktadır. Pasif süspansiyon sistemlerinin performansı, araç gövdesi ve lastiğin titreşimlerinin sönümlenmesi için tek bir eyleyici kullanılması ve bu nedenle ikisi arasında bir denge sağlanarak, sabit bir sönüme kalibre edilmesi sebebi ile sınırlıdır. Damperin performansının artırılması amacı ile değişken sönüm oranlı elektronik kontrollü süspansiyon sistemleri geliştirilmiştir, iki kademeli ve ardından daha gelişmiş sürekli değişken yarı-aktif süspansiyon sistemleri taşıtları, hem spor hem konfor odaklı karakterize etmeye olanak sağlamıştır. Aktif süspansiyon sistemleri ise üreticiler tarafından genellikle üst sınıf araçlar için geliştirilmektedir. Yarı-aktif süspansiyon sistemlerin, marketin talebine bağlı olarak daha alt sınıf araçlara da entegre edilmesi beklenmekte ve bu sistemlerin rekabet açısından önemi daha da artmaktadır.

Yarı-aktif süspansiyon sistemleri üzerine yapılan çalışmalar, sadece otomotiv endüstrisinin değil aynı zamanda akademinin de uzun süredir ilgisini çekmekte, bu alanda pek çok çalışma ortaya konmaktadır. Günümüzde taşıtlarda giderek artan elektronik donanımların etkisi ile birlikte artan sensör miktarı, direksiyon, fren, dört çeker kontrol, içten yanmalı veya elektrikli tahrik sistemlerinin yarı-aktif ve aktif süspansiyon sistemlerinin etkileşimi ayrıca bu alanın önemini artırmaktadır.

İleri sürüş destek sistemleri, aracın çevresinin algılanması sağlaması ile birlikte aracın önündeki yol profilinin algılanmasına ve bu sayede süspansiyon sisteminin yol profiline bağlı olarak öngörülü kontrol edilmesine olanak sağlamıştır. Çalışmanın ilk bölümünde, geri beslemeli yarı-aktif süspansiyon kontrol yöntemleri incelenmiş ve araca uygulanması için yöntemler birbirleri ile kıyaslanmıştır. Ardından, sürüş destek sistemi elemanı olan ön kameradan, testler vasıtası veri toplanmıştır. Kamera tarafından üretilen ham yol profili ölçümlerinin, verimli şekilde işlenmesi için DBSCAN yöntemi ortaya konmuş ve diğer yöntemlerle kıyaslanmıştır. Ön görülü yarı-aktif süspansiyonu kontrol amacı ile MPC yöntemi ile tam taşıt modeline uygulanmıştır ve geri beslemeli SH kontrol yöntemleri ile kıyaslanmıştır. Sonrasında sanal taşıt modeli, yedi serbestlik dereceli dinamik taşıt kullanılarak, kamera tarafından taranmış veya bilinen bir yol profili üzerinde taşıtın önünde aynı hızla giden

bir dinamik modelin çıktılarını kullanarak zıplama, kafa vurma ve yalpa hareketleri birbirlerine göre önceliklendirilmesi araştırılmıştır.

Yarı-aktif süspansiyon sistemleri ile ilgili son kısımda ise MPC içerisine dahil edilen 7 serbestlik dereceli modelin, sanal sönüm oranları SH yöntemine benzetilerek optimize edilmiş, bu sayede sistemde manipüle edilen değişken sayısı 3'e indirilmiştir. Ağırlık merkezi civarında hesaplanan kontrol kuvvet ve momentleri IDT yöntemi ile yarı-aktif damperlere aktarılmıştır.

Yarı-aktif ve aktif kontrol yöntemleri, yüksek serbestlik dereceli taşıt modeli ve test pistinin nümerik hali kullanılarak IPG Carmaker ve Matlab ile ortak simüle edilmişledir. Yapılan simülasyonlar sonucunda, öngörülü kontrol yöntemleri ile geri beslemeli kontrol yöntemlerinin birbirilerine yakın performans gösterdiği tespit edilmiştir. MPC kontrol yönteminden elde edilen sonuçların umut verici olduğu, performansının artırılması için daha hassas taşıt, lastik modelleri ve yol profiline ihtiyaç olduğu çıkarımı yapılmıştır.

Anahtar kelimeler: Skyhook, MPC, Yarı-aktif damper, Aktif-süspansiyon, Sürüş, Seyir

SEMI-ACTIVE AND ACTIVE SUSPENSION CONTROL WITH ROAD PREVIEW

SUMMARY

This thesis presents the four-year work on improving vehicle ride and handling with vertical vehicle control between 2019 and 2023 as part of Groupe Renault's Vehicle Motion Control Project. The comfort expectation and competition in today's vehicles are increasing with the involvement of many automobile manufacturers in the market. Passive suspension systems have limited performance, since there is only one actuator that dampen the body and wheels, thus, the damper has to be calibrated with a constant damping coefficient considering the balance between the body and the wheels. Electronically controlled dampers with variable damping ratio have been developed to improve damper performance. First, two–stage, then an improved continuously variable dampers were developed, and this system made possible to change the vehicle characteristics between comfort and sport.

Active suspension systems are generally developed by manufacturers for high-end vehicles. On the other hand, semi-active suspension systems are expected to be integrated into lower class vehicles because of its lower cost compared to active systems and depending on market demand. Thus, the importance of these systems in terms of competition is increasing.

Studies on semi-active dampers have long been of interest not only to the automobile industry but also to researchers in academia, and plenty of studies have been presented in the field. Ever-increasing electronic components in vehicles nowadays increase the number of sensors in vehicles, and the interaction of steering, braking, four-wheel control, conventional or electric engines' traction systems with semi-active dampers increases the importance of this field.

Advanced driving assistance systems made it possible to detect the environment of the vehicle as well as the road profile in front of the vehicle and to control the suspension systems with this preview information. At the beginning of this study, feedback control methods were examined and compared with each other in terms of their performance and applicability to the vehicle. Later in the tests, road data was acquired with a front camera. For efficient evaluation of raw data that produced by the camera, the DBSCAN method were proposed and compared with the existing method. Model Predictive Control (MPC) method with semi-active dampers were applied to the full vehicle model and compared with Skyhook control methods. Then, a 7-DoF virtual vehicle model was moved at the same speed as the vehicle on the camera-detected road profile. Thus, the outputs of virtual vehicle were examined to be used in prioritizing the vehicle motions such as bounce, pitch and roll.

In the last section, SH-like derivative MPC controller was introduced to control the vehicle body by controlling global forces and moments instead of forces on the actuators. Calculated forces and moments around the CoG were distributed to the dampers by the IDT method.

Semi-active and active control methods were co-simulated using high fidelity IPG® Carmaker® models and Matlab®. The simulation results showed that the preview and feedback model performances were similar. The results of the MPC were promising, and it was deduced that a more accurate vehicle model, tyre model and road profile information may be needed to improve its performance.

Key words: Skyhook, MPC, Semi-active damper, Active-suspension, Ride, Handling.

1. INTRODUCTION

1.1 Scope

The development of vehicles, especially due to the increase in the use of electronic components in the last century, forces vehicle manufacturers continuously improve the technological level of their vehicles due to high customer expectations. Comfort and safety are the forefront facts of the customer expectations and quality perception. Therefore, in this direction, especially ABS and VSC systems have become an industry standard, and many studies have been carried out on suspension systems related to comfort and safety. Suspension systems play an important role in vehicle design in terms of ride and handling. The main goal of the suspension system is to isolate the vehicle from road disturbances and to ensure the contact between the tyre contact patch and the road surfaces. In this context, the suspension system concept is designed at an early stage, depending on parameters such as type, dimensions, weight, engine power of the vehicle. Predefined characteristics determine whether the vehicle is comfort or sport oriented and are fixed for the life of the vehicle. However, controllable suspension system has been used for the last four decades to dominate one of the conflicted characteristics such as comfort and sport. Configurable, that is, controllable suspensions can change the ride and handling characteristics according to the vehicle states and the selected mode. Therefore, it enhances safety and comfort.

One step further to improve comfort is to take into account the states of the vehicle by sensing the vehicle itself and its environment, and to adapt the vehicle to environmental disturbances with appropriate decisions using the preview information.

In this study, it was aimed to improve comfort and safety by controlling semi-active and active suspension systems with preview information. In this context, research was carried out mainly in these areas with the aim of focusing on Skyhook control. Later, it was decided to integrate the environmental sensing system into the research by comparing the current technological level of the competitors and the literature surveys. First, the conversion of the output from the advanced driver assistance system (ADAS) into a preview road information was studied. An environmental sensing system was

selected, and road tests were conducted to collect road information. Second, the recorded test data was used to develop the algorithm to generate a preview road profile. Then, the mathematical model of the vehicle was developed, and the actuators were identified. Some well-known control logics such as Two-state Skyhook, Continuous Skyhook, centralized and decentralized skyhook, Active Driven Damper (ADD), Power Driven Damper (PDD), mixed Skyhook-ADD, skyhook-PDD and Model Predictive Control (MPC) were developed. The developed control logics were simulated and compared with a high-fidelity vehicle model in a highly realistic simulation environment. As a result, the agreed control logics were tested in a real test track to complete the study.

1.2 Literature Survey

1.2.1 Brief vehicle dynamics – approach to comfort measure

Vehicle dynamics examines the vehicle performance, ride and handling dynamics. Performance refers to longitudinal dynamics and measures acceleration, braking, fuel consumption, climbing under different conditions due to driver input. Handling, on the other hand, defines the vehicle's response and stability under the steering, road and environmental inputs. Ride (Comfort) refers to the isolation performance of the vehicle due to the disturbance from the road in addition to the vehicle manoeuvring responses.

Since the vehicles move under different road conditions and different driving conditions, they are affected by a wide spectrum of vibrations. These vibrations are transmitted tactilely, visually and audibly to the passengers and the driver. Ride terms are mainly tactile and visually related. Vibrations in the range of audibility are classified as noise. In other words, Vibrations can be divided into two parts according to their frequency range. The 0-25Hz range is classified as ride and 25-20000Hz range is classified as noise and harshness. 25Hz is almost the lower frequency threshold of hearing, as well as the upper frequency limit of simpler vehicle vibrations (Gillespie, 1992). The perceived vibration sources are road roughness, tyre and wheel, gearboxes, transmission and engines (Wong, 2008).

Main responsibilities of a typical suspension system can be expressed below (Rajamani, 2012).

- Isolating the vibration coming from the road to provide good comfort,
- Providing good road holding for turning, braking, acceleration and reducing vertical normal force variation on the tyre
- Provides good handling dynamics and minimizes roll and pitch motions during cornering
- Supporting the static weight of the vehicle

Determining human ride comfort and discomfort zone under vibration inputs is difficult due to human tolerance difference and lack of common criteria (Wong, 2008). Human physiology and dimensional differences are at the forefront of individual differences. The natural frequencies of human organs are particularly in the range of 3-6Hz. Therefore, vibrations in this frequency range may cause discomfort and sickness (Table 1.1). Dimensional differences from person to person also requires consideration of a wide frequency range.

Table 1.1: Human body resonances, reproduced from (Mastinu & Manfred, 2014).

Excitation Frequency (Hz)	Human Body Response
3–4	Strong resonance in the cervical vertebrae
3-6	Resonance of the stomach
4	Peak resonance of the lumbar vertebrae
4-5	Resonance in the hands (difficult to make aiming motions)
4-6	Resonance in the heart
5	Very strong resonance in the shoulder girdle
5-20	Resonance in the larynx (voice changes)
5-30	Resonance in the head
10-18	Resonance in the bladder (urge to urinate)
20-70	Resonance in the eyeballs (difficult to see)
100-200	Resonance in the lower jaw

Although it is a difficult problem to evaluate the response of the human body to vibration within a generally accepted standard due to the abundance of subjective parameters, there are various comfort evaluation criteria developed by different researchers in the literature, which take into account a small number of objective parameters. In the evaluation of vibration, in addition to the acceleration in the vertical axis, jerk, which is the derivative of the acceleration with respect to time, has also been developed as an evaluation criterion (Eager et al., 2016). The Janeway comfort

criterion depends on three basic relationships, each of which is related to specific frequency ranges. According to this, in the 1-6Hz range, the peak value of the jerk should not exceed 12.6m/s^3. The peak value of acceleration in the 20-60Hz range should not exceed 0.33m/s^2. In the 20-60Hz range, the peak velocity value should not exceed 2.7mm/s as shown also in Figure 1.1 (Janeway, 1975).

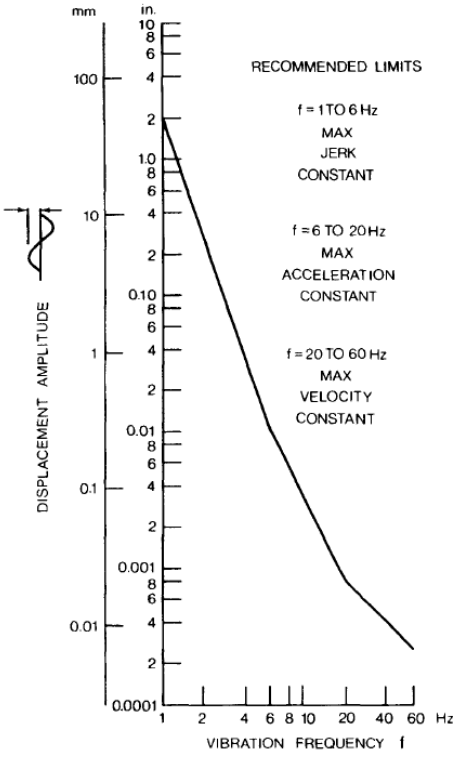

Figure 1.1: Vertical axis vibration limits for passenger comfort by Janeway (Wong, 2008).

The ISO 2631 standard is also used to determine the frequency-dependent quantities of vibrations that affect human health and comfort and are associated with motion sickness (ISO 2631, 1997).

1.2.2 Basic vibration theory

A complete suspension system in a vehicle is a complex structure that provides comfort and handling under vibratory environments and includes masses, spring, damper, visco-elastic bushings, bump-stops. A complete analysis of the system may require a multi-body dynamics approach. However, many times, even single-degree-of-freedom models can be quite useful, for example, for determining the role of a damper in a vibration system.

- *Free vibration of undamped system (1DoF)*

It is a simple vibration system with mass and spring, without dampers. The mass has only vertical translation and the linear spring is positioned between the mass and the ground. If the mass is vertically translated by a distance z from its initial position, the spring force will react in the opposite direction.

$$F_{net}=-k_s z \tag{1.1}$$

The motion of the body can be calculated by Newton's second law,

$$m_s \ddot{z}=F_{net} \tag{1.2}$$

Then, the Equation 1.1 turns into the well-known differential expression as in Equation 1.3,

$$\ddot{z}-\frac{k_s z}{m_s}=0 \tag{1.3}$$

By defining the circular frequency ω_n by the equation $\omega_n^2=\frac{k_s}{m_s}$, in (radians/second) as a positive quantity, since the spring constant and mass are positive, the differential equation can be solved to obtain the Equation 1.4.

$$z=z_0 \sin(\omega_n t+\emptyset) \tag{1.4}$$

Physically, it means that the mass is freely excited sinusoidally under constant frequency and phase angle, $\emptyset$, depending on its initial position.

From the natural period of the idealised system's oscillation, the natural frequency can be expressed in Hertz depending on the mass and spring stiffness.

$$f_N=\frac{1}{2\pi}\sqrt{\frac{k_s}{m_s}} \tag{1.5}$$

- *Free vibration of damped system (1DoF)*

The vehicle body tends to vibrate around its natural frequencies, some damping must be added to control this (Dixon, 2007). Damping dissipates the energy in the system. In other words, vibrations in the system can be removed with dampers. A linear damper is integrated into the suspension system and the damping force is expressed as in Equation 1.6.

$$F_d=-c_s \dot{z} \tag{1.6}$$

The negative damping sign indicates a force against the direction of motion. The parameter c_s is the damping coefficient, and its unit is Ns/m.

If the mass is displaced, the net force acting on the mass is given as in Equation 1.7,

$$F_{net}=-k_s z-c_s \dot{z} \tag{1.7}$$

Call Newton's second law and

$$m_s \ddot{z}=-k_s z-c_s \dot{z} \tag{1.8}$$

Then, the equation of motion equation can be arranged and solved

$$\ddot{z}+\frac{k_s}{m_s} z+\frac{c_s}{m_s} \dot{z}=0 \tag{1.9}$$

$$\frac{d^2}{dt^2} z+\frac{k_s}{m_s} z+\frac{d}{dt}\frac{c_s}{m_s} z=0 \tag{1.10}$$

$$\frac{d}{dt}=\frac{b^2-\sqrt{4ac}}{2a} \tag{1.11}$$

$$\frac{d}{dt}=-\frac{c_s}{2m_s}\pm\sqrt{\left(\frac{c_s}{2m_s}\right)^2-\frac{k_s}{m_s}}=\alpha\pm\sqrt{\alpha^2+\omega_n{}^2} \tag{1.12}$$

α is the real part of the root and called the damping factor. It is a negative value, and its unit is 1/s. ω_n is undamped natural frequency (rad/s). The solution will be complex, i.e. the oscillation will be damped. When $\omega_n > -\alpha$, in which case there is an undamped natural frequency ω_n, a damping ratio ζ and a damped natural frequency ω_d. The basic form of the equation including these terms is

$$\ddot{z}+2\zeta\omega_n \dot{z}+z\omega_n{}^2=0 \tag{1.13}$$

$$\omega_n=\sqrt{\frac{k_s}{m_s}} \tag{1.14}$$

$$\zeta=\frac{c_s}{\sqrt{2m_s k_s}} \tag{1.15}$$

$$\omega_d=\omega_n\sqrt{1-\zeta^2} \tag{1.16}$$

The actual displacement at time t may be expressed as

$$z=z_0\, e^{\alpha t}\sin(\omega_d t+\emptyset) \tag{1.17}$$

Parameters α and ω_d depend on the system properties. The amplitude z_0 and phase angle $\emptyset$ depend on initial conditions. As for vehicle dynamics terminology, basic ride motion is less than critically damped since subcritical damping provides a good balance between ride and handling (Dixon, 2007). It should be noted that the damped natural frequency is derived from the undamped natural frequency If damping is critical (ζ=1), the undamped natural frequency goes to zero. The additional exponential term $e^{\alpha t}$ removes the free oscillation, and it was the purpose of the damping.

1.2.3 Passive suspension systems

The suspension system, which has the task of absorbing and damping the vibrational inputs included in the vehicle system from the road and the environment, consists of a classical spring and damper, and is called passive suspension with no external intervention in the system.

Vehicle suspension plays an essential role in providing compromise between better comfort and a good handling especially during manoeuvres with road irregularities that cause the body to pitch and roll. In the next decade, the suspension will become increasingly important in ride comfort since the human role in vehicle control will become less than today (Iskander et al., 2019). This will take more attention to human comfort and requires different perspectives for performance evaluation.

The use of springs to ensure vertical movement of the wheels relative to the chassis on rough roads extends to horse-drawn carriages. Therefore, this well-known old method improved ride in the early history of the automobile. A damper was introduced between the unsprung mass and sprung mass to dampen the oscillation and control the movement (Milliken, William F. Milliken, 1995).

Telescopic type dampers have been used in modern passenger cars since the 1950s (Dixon, 2007). The telescopic type of damper can be categorised as

- Through-rod (Double-ended)
- Mono-tube
- Dual-tube

Through-rod damper has the advantage of volume as the rod passes through the chamber, while its seal is disadvantageously under high pressure. The dual tube

telescopic damper consists of two concentric tubes, with some gas at the end of the tube to adjust the displacement. Mono tube damper can contain some gas along with oil, the chamber is divided into two sections by floating piston as shown in Figure 1.2.

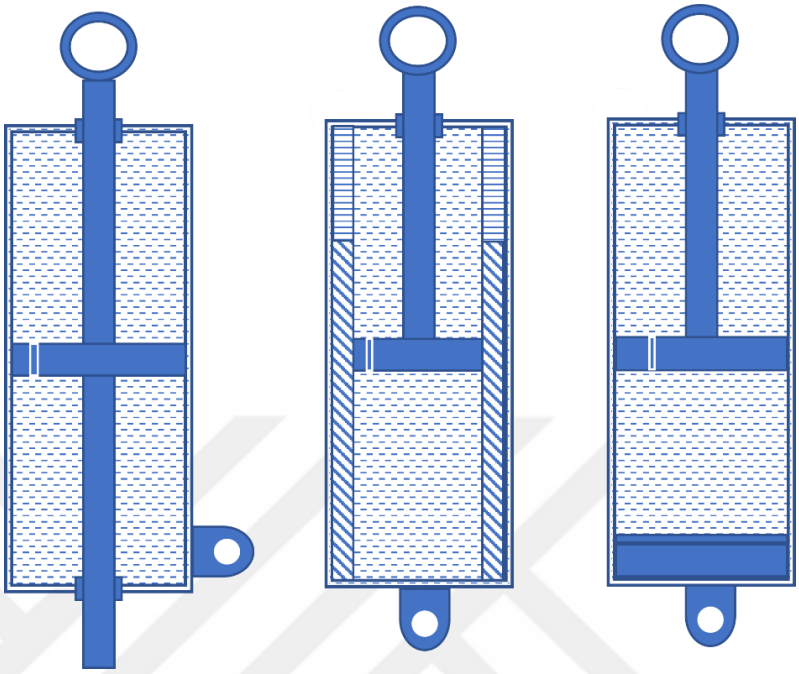

Figure 1.2: Basic types of telescopic dampers from the left; through-rod, dual tube, monotube.

A viscous fluid oil is used inside the damper, and the fluid passes from one chamber to the other through channels. Depending on the design of the flow channels, a damper has soft or hard characteristics (Łuczko and Ferdek, 2020). The damper is characterized by dimensions, force characteristic and other factors. The passive damping characteristic is usually explained by the relationship between force and stroke speed, F(V). The relationship between the damper F(V) characteristic and the P(Q) characteristics of various valves is quite straightforward, in principle. For incompressible flow, a given damper speed results in a volumetric flow rate through the relevant valves. The damper forces can be deduced from the valve P(Q) curves as they allow the various chamber pressures (Dixon, 2007). P(Q) curve can also be seen in the Figure 1.3. A typical damper force-velocity characteristic can be seen in Figure 1.4.

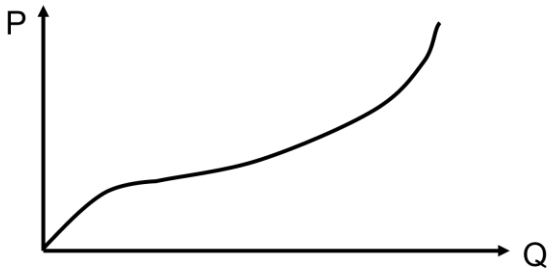

Figure 1.3: Typical valve test result reproduced from (Dixon, 2007).

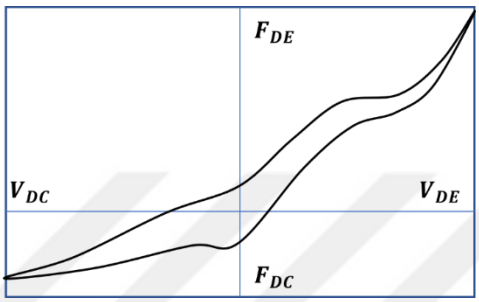

Figure 1.4: Example damper force velocity loop, F(V), resulting from stiffness reproduced from (Dixon, 2007).

The damping characteristic must be designed considering the ride and handling requirements in order to apply damping where it is needed. A study revealed that damping characteristics must be aligned with stroke rather than just stroke speed. Hence, optimum damping characteristics could be defined(Fukushima et al., 1983). The brief findings and handling and ride methodologies used in Fukushima's study were as follows:

- Handling

8-turn and lane change manoeuvres are defined as a simulation input for handling. When slow steering speed is applied, spring force rate is greater than the damper force. On the other hand, if the steering speed increases, in the case of a lane change manoeuvre, the rate of damper tends to increase.

- Ride

According to the study, damper force rate is 90% on a smooth road while damper force rate is still 75% on a rough road. This result indicated that the damper force excites the body and therefore reduces comfort.

Fukushima studied the necessity of damping in various driving conditions. The function of the damper is to damp the sprung and unsprung mass motions when the vehicle rapidly steered, to damp body roll and pitch motion, and to damp unsprung mass to keep the tyre-road contact. On the other hand, low damping improves the comfort on the smooth road.

According to Figure 1.5, the piston stroke is large when steering, but small when driving on a smooth road. For the same piston velocity, if the damping force is increased when the piston stroke is large and decreased when the piston stroke is small, an improvement in ride can be achieved without reducing performance. This result leads to optimum damping characteristics depending on the piston stroke in Figure 1.6.

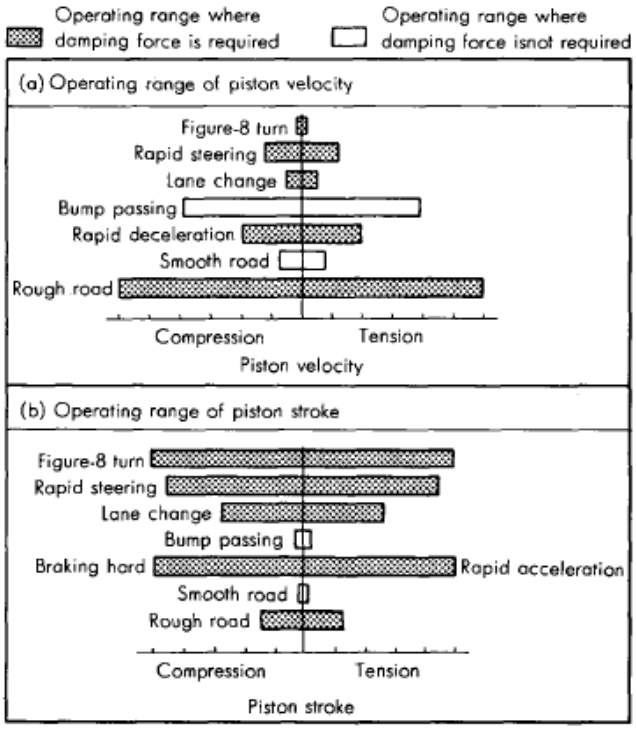

Figure 1.5: Damper operating range (Fukushima et al., 1983).

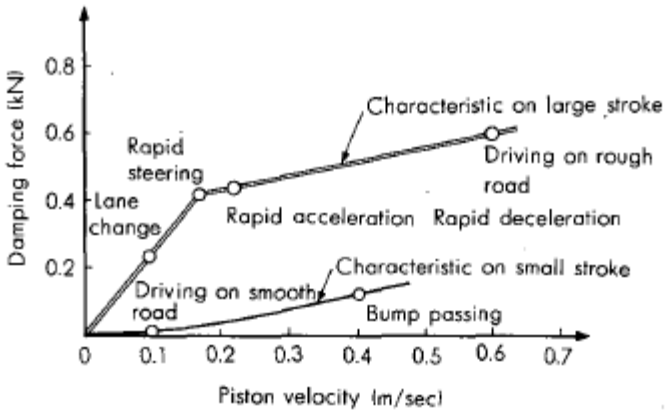

Figure 1.6: Optimum damping characteristic depending on piston stroke (Fukushima et al., 1983).

In view of the optimum damping characteristics, it seems that obtaining these different damping values under various conditions with a conventional damper is not an easy task. However, different types of semi-active dampers can change the damping ratio, and easily overcome the above-mentioned challenge.

1.2.4 Electronically controlled suspension system types and classification

Although there are many mechanical and elastic elements in the suspension system of a modern vehicle, the two important elements that will be examined within the scope of the study are springs and dampers. While the vehicle body is suspended by the spring, road-induced disturbance inputs are damped by the dampers. The suspension system is subjected to a wide range of vibration inducing inputs. For this reason, it is expected that these vibrations in a wide range are isolated by the suspension system, so that the driver and passengers can travel as comfortably as possible, while providing good road holding and reducing the vehicle body movements such as roll and pitch (Els et al., 2007). Car manufacturers have offered the controllable suspension system in high-end vehicles dealing with conflicting parameters of road holding and comfort (Soliman and Kaldas, 2021). Controlled suspension systems can be divided into two groups as active and semi-active suspension systems according to their functions. Active suspension systems are divided into two groups as slow active and fully active. The most important differences between fully active and slow active systems are energy consumption levels and control bandwidths.

Energy consumption levels of fully active systems are in the range of 5-10kW, while slow-active systems are in the range of 1-5kW, and systems in this group can operate with linear electric motor, fluid or air. (Fischer and Isermann, 2004; Koch et al., 2010).

Another component of controllable suspension systems is semi-active dampers. In classical systems, fully active systems correspond to spring, semi-active systems correspond to dampers. Vehicle height and spring coefficient can be changed in fully active systems. However, only the damping coefficient can be changed in semi-active systems. Semi-active dampers control the system by converting road-source inputs into force without external energy. This control is provided by valves that can change the damping ratio. The damping ratio change is provided in the order of 10-20W with much less energy compared to active systems (Fischer and Isermann, 2004; S. Savaresi et al., 2010).

Approximate energy consumption values depending on the control bandwidth are presented in Table 1.2. Low energy consumption has led researchers in the field of vehicle dynamics and control to be particularly interested in semi-active systems (Tseng and Hrovat, 2015). Semi-active dampers can be used with passive springs or with fully active suspension systems. If the vehicle is equipped with a fully active suspension system, semi-active dampers can be designed as integrated or independent with fully active systems, depending on the design and control bandwidth of the fully active actuator. (Göhrle et al., 2015).

Table 1.2: Energy consumption and control bandwidth of active and semi-active suspensions.

Class	Control Bandwidth	Energy Consumption
Semi-Active	30-40Hz	10-20W
Slow Active	1-5Hz	1-5kW
Fully Active	20-30Hz	5-10kW

Another classification fact is the force-generation limits of semi-active suspension systems in certain regions, which are seen in Figure 1.7, and this is expressed as the passivity constraint in the literature (S. Savaresi et al., 2010).

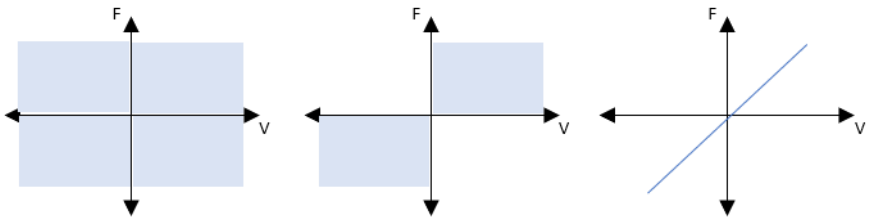

Figure 1.7: Left: active suspension, middle: semi-active suspension, right: passive suspension system.

The passivity constraint given by Equation 1.18 shows that the force of semi-active dampers can develop force in the grey areas of the graph given in the middle of the Figure 1.7.

$$F_d.V \geq 0 \tag{1.18}$$

Semi-active suspension systems, simply dampers, change the damping ratio with various technologies. The orifice between the chambers of the classical passive-type damper determines the characteristic of the damper. Electro-hydraulic dampers are hydraulic actuators like conventional dampers, but unlike conventional dampers, they change the damping ratio by using a solenoid valve located between the chambers.

A schematic representation of an electro-hydraulic type of damper can be seen in Figure 1.8. Variable damping occurs when the viscous fluid in the damper, which is connected to the vehicle body and the wheel joint, passes over the valve(s) from one chamber to another during the movement of the piston.

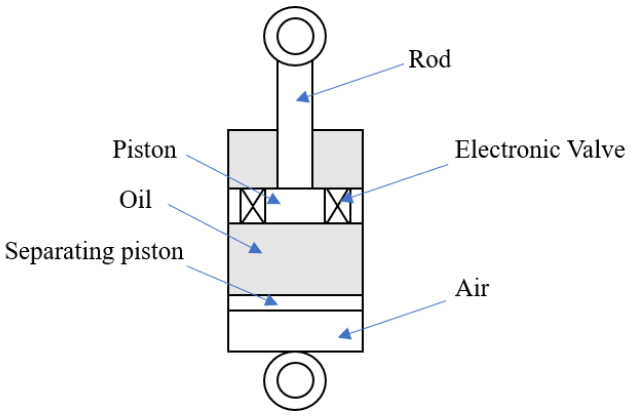

Figure 1.8 :Schematic representation of an electro-hydraulic type damper.

Figure 1.9 : Electronically controlled semi-active dampers. Right to left, Electrohydraulic damper with Solenoid valve (Sachs), Magnetorheological damper (Delphi), Electrorheological damper (Fludicon) (S. Savaresi et al., 2010).

Magnetorheological fluids are obtained by suspending ferromagnetic particles in a carrier fluid. These fluids exhibit rheological properties that can be controlled by the magnetic field effect. This feature is used to provide different damping forces according to the magnetic field formed inside the damper. (Song et al., 2005). Electrorheological fluids belong to a class of colloidal suspensions [1] that exhibit large reversible variations in their behaviour when exposed to external electric fields (Choi et al., 1998). Three dampers which have different damping technology can be seen in Figure 1.9.

1.2.5 Modelling methods of semi-active dampers

In semi-active suspension systems, the bi-viscous behaviour of the fluid, temperature-dependent viscosity variability and hysteresis cause nonlinear behaviour of the damper and make modelling difficult. Although many approaches are used in modelling, basically three types of models are used: static, dynamic, nonlinear and nonlinear black box. (S. M. Savaresi, Bittanti, et al., 2005). The static with coulomb friction and with hysteresis and and first order nonlinear dynamic models are defined as follows:

- Static Model (with Coulomb friction)

$$F_d = c(I)\dot{x} - c^{sym}(I)|\dot{x}| + c^{nl}(I)\sqrt{|\dot{x}|}\,\mathrm{sign}(\dot{x}) \tag{1.19}$$

[1] Colloidal suspension: a very finely dispersed mixture so that the particles do not tend to settle in any way.

In the static model, the parameters c, c^{sym}, c^{nl} depend on the damper control parameter I. This model presents the static friction coefficient as a function of stroke speed (S. Savaresi et al., 2010)

- Static Model (with Hysteresis)

$$F_d=A_1(I)\tanh\left[A_3(I)\left(\dot{x}+\frac{V_0(I)}{X_0(I)}x\right)\right]+A_2(I)\left(\dot{x}+\frac{V_0(I)}{X_0(I)}x\right) \quad (1.20)$$

- First order nonlinear dynamic model

$$\begin{cases} F_d=c_0(I)\dot{x}-k_0(I)(x-x^0)+\gamma(I)z \\ \dot{z}=\beta(I)|\dot{x}||z|\left|z^{n-1}\right|-\delta(I)(\dot{x})+A(I)\dot{x} \end{cases} \quad (1.21)$$

In the dynamic model, the parameters that depend on the damper control input I are $\{c_0, k_0, x^0, \gamma, \beta, \delta, A, n\}$. Z is the internal state parameter that expresses the hysteresis (S. Savaresi et al., 2010).

1.2.6 Suspension mechanisms

Suspension mechanisms are the elements that provide the connection between the tyres and the chassis. Different types and geometries of suspension mechanisms are used in vehicles. Vehicle suspension systems can be divided into three classes: solid axle (dependent suspension), independent suspension and semi-independent suspensions. As an example of the semi-independent type shown in Figure 1.10, twist or torsion beam suspension allows the tyres on the axle to move in the opposite direction with the flexibility provided (Dogru, 2017). Rear axle arrangements of this type of suspension systems are widely used in middle segment front wheel drive vehicles due to their advantages such as packaging and easy assembly (Albak et al., 2021).

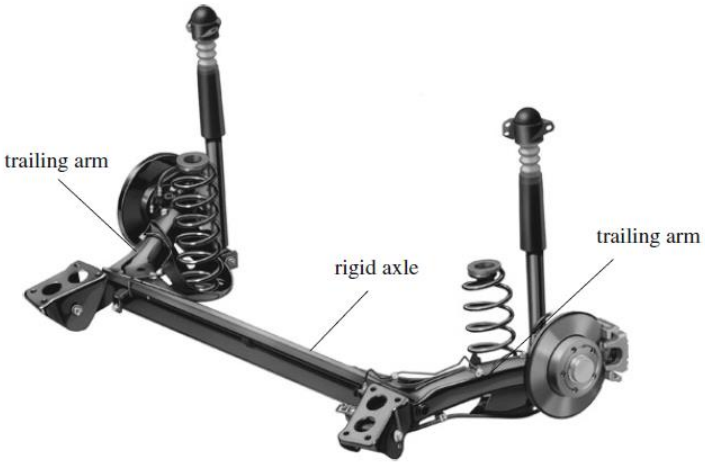

Figure 1.10: Torsion beam rear axle Wolkswagen Golf IV (Schramm et al., 2014).

Independent suspension mechanisms allow the tyres to move independently of each other, depending on different road inputs. Although there are different types of independent suspension systems, the most common and simple mechanisms are the double A-arm/wishbone and McPherson strut as shown in Figure 1.11 (Jazar, 2017).

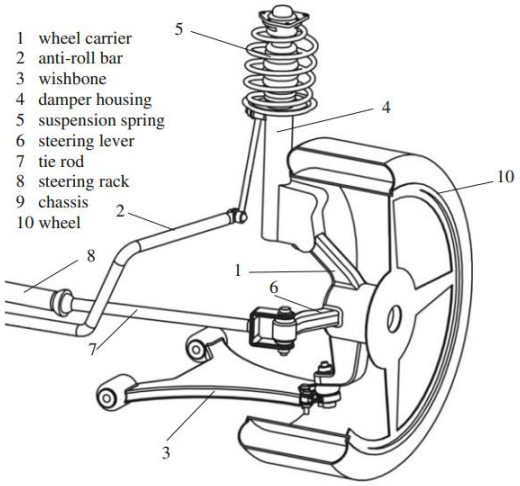

Figure 1.11: McPherson type Suspension Mechanism (Schramm et al., 2014).

1.2.7 Environmental sensing systems

Although the idea of predictive control emerged about half a century ago (Bender, 1968), non-contact measurement systems could not be used in practice due to the lack of desired technological level at that time (Hac, 2007). Sensors developed in the last quarter century; thanks to lidar, stereo and mono cameras, it has been possible to detect the vehicle's surroundings. The first use of environmental sensing systems in the suspension system started in 1988 when Nissan integrated sonar technology into the

vehicle and used the active suspension system for control. (Kishi and Yamamoto, 1985). Then, one of the first studies on suspension control was proposed by Mercedes Benz to measure the road profile by lidar (Streiter, 2008). The stereo camera, on the other hand, was first used by Mercedes Benz to measure the road profile and to provide predictive control of the suspension system (Weist et al., 2013).

As a result of the examination and comparison of environmental sensing systems in terms of suspension system requirements, it has been stated that lidar and camera systems are advantageous compared to radar and ultrasonic systems in terms of measurement distance, angular resolution and sampling time. When lidar and camera are compared, the measurement tolerance of lidar is less than 2mm, which is stated as its biggest advantage over the camera. (Schindler, 2009a). On the other hand, lidar is quite costly compared to cameras. However, while lidar causes us to perceive objects in high resolution, we cannot perceive the images of objects, or rather their colours, so we perceive, for example, a cardboard box on the road as a complete obstacle.

Thanks to image processing, objects can be distinguished by their colour and are similar to the perception of the human eye. The disadvantage of the camera compared to lidar is the inability of distinguishing the light refraction, shadow, etc., so that the image formed as a result of shadows is perceived as real (Staniek, 2017). In addition, the camera only works in daylight. Nevertheless, the existing use of the ADAS infrastructure in the vehicle has reduced the cost of suspension-specific environmental sensing, making the multi-purpose camera preferable for environmental sensing (Missel, J. Mehren, D. Reichmann M., Lallinger, 2013). Along with the cameras, which are a part of driving support systems, whose integration into vehicles has increased rapidly in the last decade; pedestrian detection, lane keeping assist, traffic sign detection, collision avoidance systems, etc. usage is increasing (Ziebinski et al., 2016)

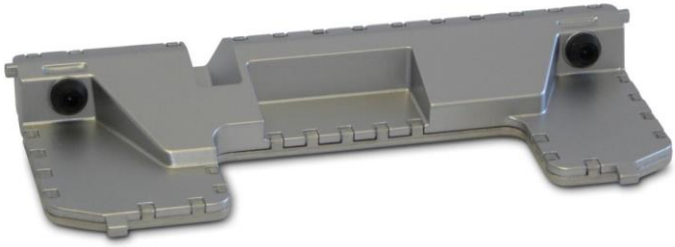

Figure 1.12 :Continental "ContiGuard" stereo camera (Coxworth, 2022).

Road profile detection with the camera is done in two ways, depending on the number of cameras. The first of these is based on the creation of a depth map by obtaining an image of disparity between the two images by establishing a mathematical relationship between pixels on images obtained from different perspectives (stereo camera-depending on focal length) (Labayrade et al., 1998; Saxena et al., 2007). The second method accomplishes to create a depth map by obtaining disparity from consecutive images captured with a monocular camera. (Kaneko and Yamamoto, 2017). Disparity, by definition, is the difference in the image position of the same three-dimensional point from two different camera angles. The typical stereo and monocular camera can be seen in Figures 1.12 and 1.13, while Figure 14 shows the stereo camera principle in detail, respectively.

Figure 1.13: ZF monocular camera (ZF, 2022).

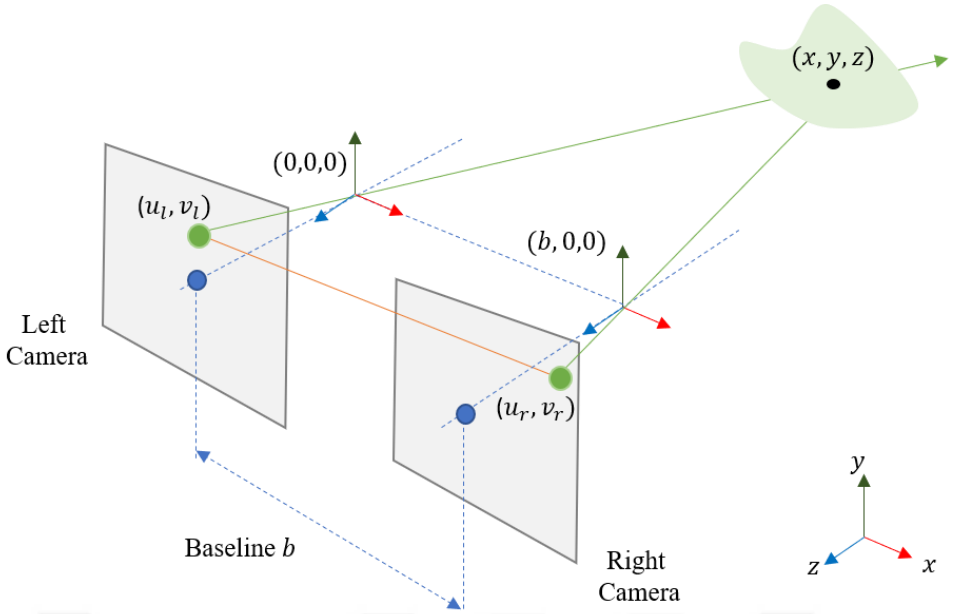

Figure 1.14 : Stereo camera schematic physical point and camera axes schematic.

Equations 1.22 and 1.23 are obtained for the right and left camera, respectively, due to the perspective projection. f_x,f_y,f_z focal lengths are the distance between the image plane and the projection centre. $u_l - u_r$ is the disparity value.

$$(u_l,v_l)=(f_x\frac{x}{z},f_y\frac{y}{z}) \tag{1.22}$$

$$(u_r,v_r)=(f_x\frac{x\text{-}b}{z},f_y\frac{y}{z}) \tag{1.23}$$

The coordinates of the point (x,y,z) are calculated by the equations 1.24 to 1.26.

$$x=\frac{b(u_l)}{u_l\text{-}u_r} \tag{1.24}$$

$$y=\frac{bf_x(v_l)}{f_y(u_l\text{-}u_r)} \tag{1.25}$$

$$z=\frac{bf_x}{f_y(u_l\text{-}u_r)} \tag{1.26}$$

In the next step, the images obtained with the right and left cameras are matched with each other. For example, part of the image from the left camera will be matched with the image from the right camera. For this purpose, different matching methods are used; one of them is the sum of absolute differences given by the Equation 1.27 (SAD: Sum of Absolute Differences) (Hamzah et al., 2010). $E_l(i,j)$and $E_r(i+k,j+l)$ are the left image pixel and its conjugate in the right image, respectively.

$$SAD = \sum_{(i,j) \in R} |E_l(i,j) - E_r(i+k,j+l)| \quad (1.27)$$

Pitch, roll or bounce movements of the vehicle will change the perspective of the acquired images and cause distortions in the creation of the disparity map. For this reason, these vehicle movements must be taken into account during the matching. (Shen et al., 2014). In a study with lidar, angular position changes due to body movements were calculated with a gyroscope placed near the lidar and correction was made when mapping point clouds (Gong et al., 2019). By comparing the consecutive images obtained with the camera for a similar purpose, the angular and positional differences between them were calculated and ego-motion estimation was made (Stein et al., 2000). Depending on the disparity, a road elevation profile is generated as a result of matching the images. In order to optimize the calculation time, the profile is generated on the projection of the road surface in front of the vehicle and the wheels shown in Figure 1.15 (Shen et al., 2014).

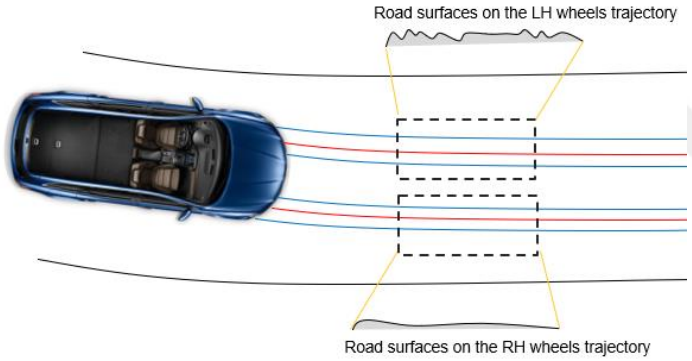

Figure 1.15: Areas measured on the wheel projection in front of the vehicle.

The accuracy of the camera's road profile elevation calculation depends on the texture of the road surface, light reflection, weather condition, and ego-motion. Therefore, a reliability value calculated by many different methods is also assigned to each measurement value (Pfeiffer et al., 2013). Left-right difference and naive peak ratio are the methods which are used to calculate the reliability value (Hu and Mordohai, 2012). When the confidence values decrease, the effect of low confidence values can be reduced by using statistical methods to calculate a more reliable road elevation profile. The first step of a road profile detection procedure is the image processing processes and the creation of the elevation profile, while the second step is the conversion of the obtained measurement points to the road elevation profile.

In this context, it is seen that the studies in the literature are mostly focused on image processing (Deigmoeller et al., 2018; Lee and Yoon, 2018; Suhr and Jung, 2015). There are very limited resources in the literature on the problem of how to combine available measurement points in the most efficient way. The general method mentioned in the literature is to divide the cloud of measurement points evenly along the x-axis and transform the points in each window into a road profile by statistical operations (Göhrle et al., 2015; Schindler, 2009b).

1.2.8 Vehicle model

One of the purposes of vehicle models is to have sufficient DoF to examine a specific vehicle motion and enable efficient analysis of the system's response. For example, suspension parameters which are damping coefficient and spring stiffness can be tuned to obtain the required damping characteristics for a vehicle. At the same time, one of the purposes of the vehicle model is to use it as a plant to design a controller. In order to design a controller for vertical motion control, it is essential to understand the vehicle dynamics and obtain the plant model that best reflects the control requirements of the system. For this reason, a vehicle dynamics model must be developed to calculate the vehicle's responses to external and internal inputs. The non-linear behaviour of vehicle elements such as spring, damper and bushing in the suspension system and the non-linearity of the suspension kinematics increase the complexity of the modelling (Blundell M. & Harty D., 2017). Because linear plant models are developed for linear systems, they can be easily designed with most controller design tools. Half, full and quarter vehicle models are commonly used in the literature. The rigid vehicle body has three rotational and three translational degrees of freedom (DoF) as shown in Figure 1.16.

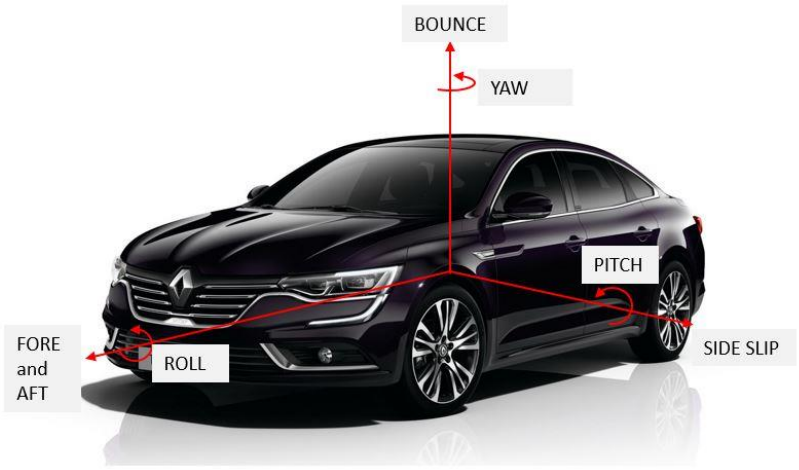

Figure 1.16: Degrees of freedom of a vehicle in space.

The vehicle dynamics terminologies that define the subject of motions in relation to the DoF are given in Table 1.3.

Table 1.3: Degrees of freedom of a vehicle (Bayar, 2006).

FREEDOM	SUBJECT
BOUNCE	RIDE
SIDE SLIP	HANDLING
FORE AND AFT	PERFORMANCE
YAW	HANDLING
PITCH	RIDE
ROLL	HANDLING, RIDE

1.2.8.1 Quarter car model

The quarter car model is one of the most used models to examine the basic suspension characteristics because it does not include the complex kinematics of the suspension system, roll and pitch movements (Maher and Young, 2011). Thus, the linear quarter car model can be considered to provide important information about the problem, although it is quite simple to make a comprehensive analysis of the vehicle's motion (Türkay and Akçay, 2005). The main advantages are as follows (Maher and Young, 2011):

- The relationship between comfort and performance is easily understood
- Includes several design parameters

- Single input system
- Control theories can be easily applied and their characteristics evaluated.

The quarter-car model includes two-degree-of-freedom model road inputs and force inputs of an actuator such as active and semi-active damper, and the quarter car equipped with semi-active damper is shown in Figure 1.17. It allows to examine the vertical axis movements of the sprung mass (Body) and the unsprung mass (Wheel) (Maher and Young, 2011).

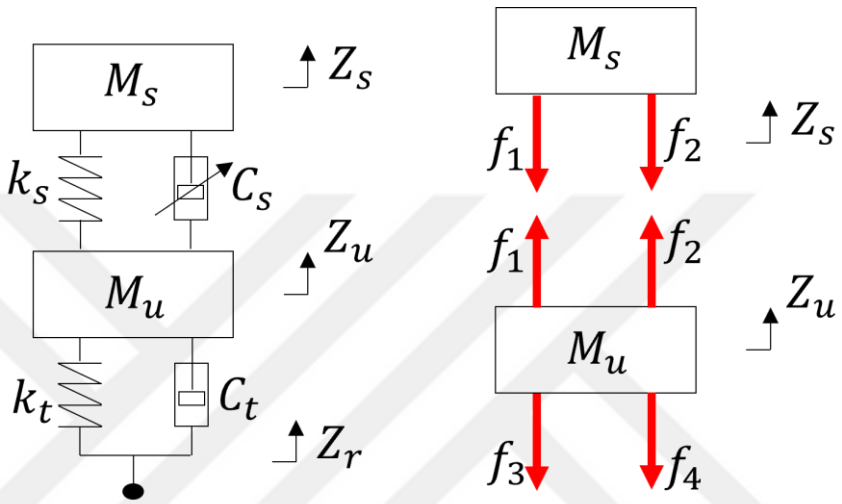

Figure 1.17: Quarter car model and its decomposition.

It is possible to obtain the equations for the quarter car model by applying Newton's second law. f_1 and f_2 are suspension spring and damping forces, depending on stroke and stroke speed, respectively, as given in equations 1.28 and 1.29 f_3 and f_4 are the spring and damping force of the tyre as the tyre is modelled linear spring and damper with a point contact, as given in equations 1.29 and 1.30. Since the tyre-road relationship is represented by point contact in this type of model, the enveloping effect of the tyre cannot be obtained.

$$f_1=k_s(Z_s-Z_u) \quad (1.28)$$

$$f_2=C_s(\dot{Z}_s-\dot{Z}_u) \quad (1.29)$$

$$f_3=k_t(Z_u-Z_r) \quad (1.30)$$

$$f_4=C_s(\dot{Z}_u-\dot{Z}_r) \quad (1.31)$$

Equation 1.32, which describes the motion of the sprung mass, is obtained by summing the forces acting on the sprung mass. Equation 1.33 is provided in the same way for the unsprung mass. The input F_d, is integrated into equations 1.32 and 1.33. It can

then be defined as semi-active damper force or active suspension force for different purposes.

$$M_s\ddot{z}_s=-k_s(Z_s-Z_u)-C_s(\dot{Z}_s-\dot{Z}_u)-F_d \tag{1.32}$$

$$M_u\ddot{z}_u=-k_t(Z_u-Z_r)-C_t(\dot{Z}_u-\dot{Z}_r)+k_s(Z_s-Z_u)+C_s(\dot{Z}_s-\dot{Z}_u)+F_d \tag{1.33}$$

The system can be expressed in state space representation by defining the states as follows,

$$\begin{bmatrix} X_1 \\ X_2 \\ X_3 \\ X_4 \end{bmatrix} = \begin{bmatrix} Z_s \\ \dot{Z}_s \\ Z_u \\ \dot{Z}_u \end{bmatrix} \tag{1.34}$$

The damping characteristic of the tyre can sometimes be neglected for convenience, but this parameter will be taken into account as an option in this study. Therefore, the state space representation of the system with tyre damping is given in equation 1.35 while the option without tyre damping force is given in equation 1.36. In case the tyre-damping force is neglected, the input matrix size is reduced from 3x1 to 2x1, and the element of matrix A(4,4) is also changed. The output Y matrix gave the body acceleration, stroke and wheel deflection speed.

$$\begin{bmatrix} \dot{X}_1 \\ \dot{X}_2 \\ \dot{X}_3 \\ \dot{X}_4 \end{bmatrix} = \begin{bmatrix} 0 & 1 & 0 & 0 \\ \frac{-k_s}{M_s} & \frac{-C_s}{M_s} & \frac{k_s}{M_s} & \frac{C_s}{M_s} \\ 0 & 0 & 0 & 1 \\ \frac{k_s}{M_u} & \frac{C_s}{M_u} & \frac{-k_s-k_t}{M_u} & \frac{-C_s-C_t}{M_u} \end{bmatrix} \begin{bmatrix} X_1 \\ X_2 \\ X_3 \\ X_4 \end{bmatrix} + \begin{bmatrix} 0 & 0 & 0 \\ 0 & 0 & \frac{-1}{M_s} \\ 0 & 0 & 0 \\ \frac{k_t}{M_u} & \frac{C_t}{M_u} & \frac{1}{M_u} \end{bmatrix} \begin{bmatrix} Z_r \\ \dot{Z}_r \\ F_d \end{bmatrix} \tag{1.35}$$

$$\begin{bmatrix} \dot{X}_2 \\ X_1-X_3 \\ \dot{X}_3 \end{bmatrix} = \begin{bmatrix} \frac{-k_s}{M_s} & \frac{-C_s}{M_s} & \frac{k_s}{M_s} & \frac{C_s}{M_s} \\ 1 & 0 & -1 & 0 \\ 0 & 0 & 0 & 1 \end{bmatrix} \begin{bmatrix} X_1 \\ X_2 \\ X_3 \\ X_4 \end{bmatrix} + \begin{bmatrix} 0 & 0 & 0 \\ 0 & 0 & \frac{-1}{M_s} \\ 0 & 0 & 0 \\ 0 & 0 & 0 \end{bmatrix} \begin{bmatrix} Z_r \\ F_d \end{bmatrix} \tag{1.36}$$

$$\begin{bmatrix} \dot{X}_1 \\ \dot{X}_2 \\ \dot{X}_3 \\ \dot{X}_4 \end{bmatrix} = \begin{bmatrix} 0 & 1 & 0 & 0 \\ \frac{-k_s}{M_s} & \frac{-C_s}{M_s} & \frac{k_s}{M_s} & \frac{C_s}{M_s} \\ 0 & 0 & 0 & 1 \\ \frac{k_s}{M_u} & \frac{C_s}{M_u} & \frac{-k_s-k_t}{M_u} & \frac{-C_s}{M_u} \end{bmatrix} \begin{bmatrix} X_1 \\ X_2 \\ X_3 \\ X_4 \end{bmatrix} + \begin{bmatrix} 0 & 0 \\ 0 & \frac{-1}{M_s} \\ 0 & 0 \\ \frac{k_t}{M_u} & \frac{1}{M_u} \end{bmatrix} \begin{bmatrix} Z_r \\ F_d \end{bmatrix} \tag{1.37}$$

(1.38)

$$\begin{bmatrix} \dot{X}_2 \\ X_1\text{-}X_3 \\ \dot{X}_3 \end{bmatrix} = \begin{bmatrix} \frac{-k_s}{M_s} & \frac{-C_s}{M_s} & \frac{k_s}{M_s} & \frac{C_s}{M_s} \\ 1 & 0 & -1 & 0 \\ 0 & 0 & 0 & 1 \end{bmatrix} \begin{bmatrix} X_1 \\ X_2 \\ X_3 \\ X_4 \end{bmatrix} + \begin{bmatrix} 0 & 0 \\ 0 & \frac{-1}{M_s} \\ 0 & 0 \\ 0 & 0 \end{bmatrix} \begin{bmatrix} Z_r \\ F_d \end{bmatrix}$$

1.2.8.2 Half car models

In the literature, half-car models are generally used for pitch or roll motion evaluation in addition to bounce (Krtolica and Hrovat, 1990; Prabakar et al., 2009; Wakeham and Rideout, 2018). A typical half-car model for bounce and pitch motion evaluation can be seen in Figure 1.18. It is less complex than the full-car model and does not consider complex kinematics of suspension systems as in quarter car models. L_f and L_r are the distance between front and rear axles and the CoG while I_{yy} refers to the pitch moment of inertia. Equation 1.39 and 1.40 define the total front and rear suspension forces. Equations 1.41, 1.42 and 1.43 define the front and rear unsprung masses, pitch and bounce acceleration, respectively. The term$(M_s h_s)a_x$ was considered in the vehicle model and it defines the moments around the y-axis resulting from longitudinal acceleration or deceleration.

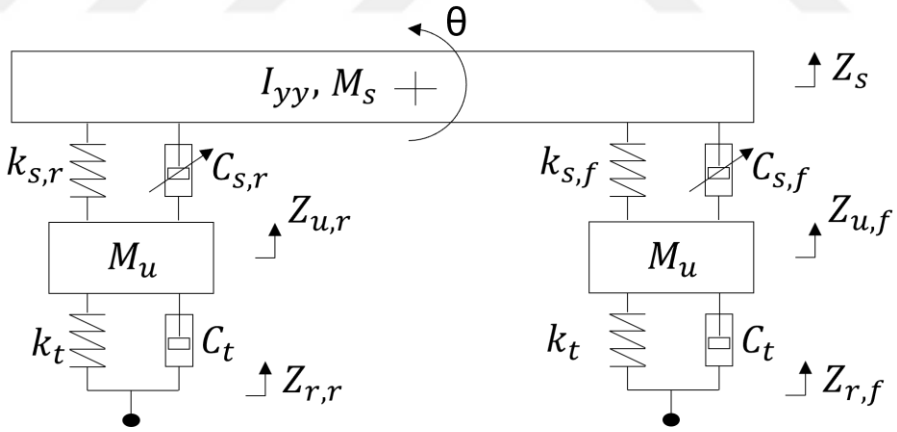

Figure 1.18: Four degree of freedom half car model

$$F_{s,f}=-k_{s,f}(Z_s-Z_{u,f}-L_f\theta)-c_{s,f}(\dot{Z}_s-\dot{Z}_{u,f}-L_f\dot{\theta})-u_f \quad (1.39)$$

$$F_{s,r}=-k_{s,r}(Z_s-Z_{u,r}-L_r\theta)-c_{s,r}(\dot{Z}_s-\dot{Z}_{u,r}-L_r\dot{\theta})-u_r \quad (1.40)$$

$$\ddot{Z}_{u\{i\}}=\frac{1}{M_{u\{i\}}}\left[k_{t\{i\}}(Z_{r\{i\}}-Z_{u\{i\}})+c_{t\{i,j\}}(\dot{Z}_{r\{i\}}-\dot{Z}_{u\{i\}})-F_{s,\{i\}}\right] \quad (1.41)$$

$$\ddot{\theta}=\frac{1}{I_{yy}}\left[-L_f(F_{sFL}+F_{sFR})+L_r(F_{sRL}+F_{sRR})-(M_s h_s)a_x\right] \quad (1.42)$$

$$\ddot{Z}_s=\frac{1}{M_s}\left[F_{s,f}+F_{s,r}\right] \quad (1.43)$$

1.2.8.3 Full car model

A rigid vehicle body in space, has three translational and three rotational degrees of freedom (Bayar, 2006). This means that a rigid vehicle body itself has 6 DoF. However, generally, a vehicle model developed for vertical motion control includes bounce in the z-axis, roll movement around the x-axis, pitch movements around the y-axis of the body. Additionally, in the vertical motions control-oriented models, the movement of the unsprung mass, which includes the sum of tyres, axles, rims, hubs, brake calliper and discs, adds 4 more degrees of freedom to a 2-axle, 4-wheel vehicle model (Zhao et al., 2014). In the literature, many vehicle models have been developed for ride and handling dynamics studies separately (Kissai et al., 2019; Poussot-Vassal et al., 2008). But for some cases, lateral and/or longitudinal (2 DoF of rigid body's 6 DoF) motions are also needed to be controlled within vertical motions control-oriented model, simultaneously as in this study (D. Chen et al., 2021). The vehicle model in this study, as shown in Figure 1.19, was developed based on the ISO axis system and it contains 7 equations of motion as the vehicle body has 3 motions and unsprung mass has 4 degrees of freedom.

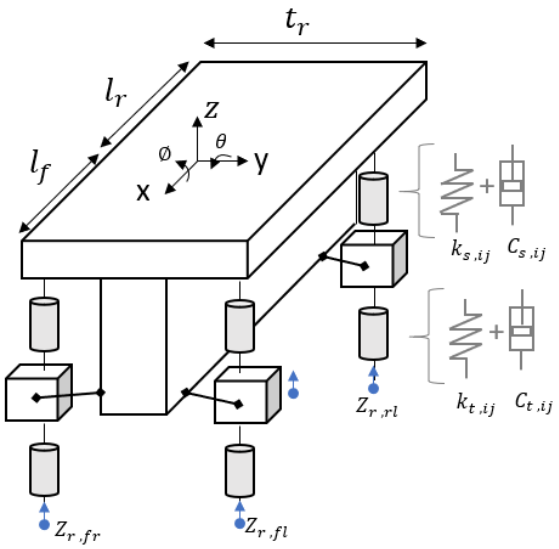

Figure 1.19: Full vehicle model for suspension control.

$$\ddot{z}=\frac{1}{M_s}\left[F_{sFL}+F_{sFR}+F_{sRL}+F_{sRR}\right] \tag{1.44}$$

$$\ddot{\theta}=\frac{1}{I_{yy}}\left[-L_f(F_{sFL}+F_{sFR})+L_r(F_{sRL}+F_{sRR})-(M_s h_s)a_x\right] \tag{1.45}$$

$$\ddot{\emptyset}=\frac{1}{I_{xx}}\left[\frac{-t_f}{2}(F_{sFL}-F_{sFR})+\frac{t_r}{2}(F_{sRL}-F_{sRR})-(M_s(h_{cog}-h_{rol})a_y\right] \tag{1.46}$$

$$\ddot{Z}_{u\{i,j\}}=\frac{1}{M_{u\{i,j\}}}\left[k_{t\{i,j\}}(Z_{r\{i,j\}}-Z_{u\{i,j\}})+c_{t\{i,j\}}(\dot{Z}_{r\{i,j\}}-\dot{Z}_{u\{i,j\}})-F_{sFL}\right] \tag{1.47}$$

$$\{i,j\}=FL,FR,RL,RR$$

Equations 1.44 to 1.46 refer to the vehicle body and 1.47 is used for the four unsprung masses. Equation 1.48 to 1.50 represents the suspension forces at each corner considering body movements such as roll, pitch, roll rate and pitch rate. When Equations 1.48 to 1.50 are integrated into equations 1.44 to 1.47, a 7-DoF vehicle model can be generated. These equations are combined in state space matrix form as in Equations 1.52 to 1.55. This state space system has 14 states and 10 outputs.

$$F_{sFL}=-k_{sFL}(Z-Z_{uFL}-L_f\theta+\frac{t_f}{2}\emptyset)-c_{sFL}(\dot{Z}-\dot{Z}_{uFL}-L_f\dot{\theta}+\frac{t_f}{2}\dot{\emptyset}-u_{FL}) \tag{1.48}$$

$$F_{sFR}=-k_{sFR}(Z-Z_{uFR}-L_f\theta-\frac{t_f}{2}\emptyset)-c_{sFR}(\dot{Z}-\dot{Z}_{uFR}-L_f\dot{\theta}-\frac{t_f}{2}\dot{\emptyset}-u_{FR}) \tag{1.49}$$

$$F_{sRL}=-k_{sRL}(Z-Z_{uRL}+L_f\theta+\frac{t_f}{2}\emptyset)-c_{sRL}(\dot{Z}-\dot{Z}_{uRL}+L_f\dot{\theta}+\frac{t_f}{2}\dot{\emptyset}-u_{RL}) \tag{1.50}$$

$$F_{sRR}=-k_{sRR}(Z-Z_{uRR}-L_f\theta-\frac{t_f}{2}\emptyset)-c_{sRR}(\dot{Z}-\dot{Z}_{uRR}-L_f\dot{\theta}-\frac{t_f}{2}\dot{\emptyset}-u_{RR}) \tag{1.51}$$

$$A=\begin{bmatrix}
0 & 1 & 0 & 0 & 0 & 0 & 0 & 0 & 0 & 0 & 0 & 0 & 0 & 0 \\
\frac{-2(k_{sf}+k_{sr})}{M_s} & \frac{-2(c_{sf}+c_{sr})}{M_s} & 0 & 0 & \frac{2(L_f k_{sf}-L_r k_{sr})}{M_s} & \frac{2(L_f c_{sf}-L_r c_{sr})}{M_s} & \frac{k_{sf}}{M_s} & \frac{c_{sf}}{M_s} & \frac{k_{sf}}{M_s} & \frac{c_{sf}}{M_s} & \frac{k_{sr}}{M_s} & \frac{c_{sr}}{M_s} & \frac{k_{sr}}{M_s} & \frac{c_{sr}}{M_s} \\
0 & 0 & 0 & 1 & 0 & 0 & 0 & 0 & 0 & 0 & 0 & 0 & 0 & 0 \\
0 & 0 & \frac{-k_{sf}(t_f)^2+k_{sr}(t_r)^2}{2I_{xx}} & \frac{-c_{sf}(t_f)^2+c_{sr}(t_r)^2}{2I_{xx}} & 0 & 0 & \frac{k_{sf}t_f}{2I_{xx}} & \frac{c_{sf}t_f}{2I_{xx}} & \frac{-k_{sf}t_f}{2I_{xx}} & \frac{-c_{sf}t_f}{2I_{xx}} & \frac{k_{sf}t_f}{2I_{xx}} & \frac{c_{sf}t_f}{2I_{xx}} & \frac{-k_{sf}t_f}{2I_{xx}} & \frac{-c_{sf}t_f}{2I_{xx}} \\
0 & 0 & 0 & 0 & 0 & 1 & 0 & 0 & 0 & 0 & 0 & 0 & 0 & 0 \\
\frac{2(L_f k_{sf}-L_r k_{sr})}{2I_{yy}} & \frac{2(L_f c_{sf}-L_r c_{sr})}{2I_{yy}} & 0 & 0 & \frac{-2k_{sf}(L_f)^2+2k_{sr}(L_r)^2}{2I_{yy}} & \frac{-2c_{sf}(L_f)^2+2c_{sr}(L_r)^2}{2I_{yy}} & \frac{-L_f k_{sf}}{2I_{yy}} & \frac{-L_f c_{sf}}{2I_{yy}} & \frac{-L_f k_{sf}}{2I_{yy}} & \frac{-L_f c_{sf}}{2I_{yy}} & \frac{L_r k_{sr}}{2I_{yy}} & \frac{L_r c_{sr}}{2I_{yy}} & \frac{L_r k_{sr}}{2I_{yy}} & \frac{L_r c_{sr}}{2I_{yy}} \\
0 & 0 & 0 & 0 & 0 & 0 & 0 & 1 & 0 & 0 & 0 & 0 & 0 & 0 \\
\frac{k_{sf}}{M_{uf}} & \frac{c_{sf}}{M_{uf}} & \frac{k_{sf}t_f}{2M_{uf}} & \frac{c_{sf}t_f}{2M_{uf}} & \frac{-L_f k_{sf}}{M_{uf}} & \frac{-L_f c_{sf}}{M_{uf}} & \frac{-k_{sf}-k_{tf}}{M_{uf}} & \frac{-c_{sf}}{M_{uf}} & 0 & 0 & 0 & 0 & 0 & 0 \\
0 & 0 & 0 & 0 & 0 & 0 & 0 & 0 & 0 & 1 & 0 & 0 & 0 & 0 \\
\frac{k_{sf}}{M_{uf}} & \frac{c_{sf}}{M_{uf}} & \frac{-k_{sf}t_f}{2M_{uf}} & \frac{-c_{sf}t_f}{2M_{uf}} & \frac{-L_f k_{sf}}{M_{uf}} & \frac{-L_f c_{sf}}{M_{uf}} & 0 & 0 & \frac{-k_{sf}-k_{tf}}{M_{uf}} & \frac{-c_{sf}}{M_{uf}} & 0 & 0 & 0 & 0 \\
0 & 0 & 0 & 0 & 0 & 0 & 0 & 0 & 0 & 0 & 0 & 1 & 0 & 0 \\
\frac{k_{sr}}{M_{ur}} & \frac{c_{sr}}{M_{ur}} & \frac{k_{sr}t_r}{2M_{ur}} & \frac{c_{sr}t_r}{2M_{ur}} & \frac{L_r k_{sr}}{M_{ur}} & \frac{L_r c_{sr}}{M_{ur}} & 0 & 0 & 0 & 0 & \frac{-k_{sr}-k_{tr}}{M_{ur}} & \frac{-c_{sr}}{M_{uf}} & 0 & 0 \\
0 & 0 & 0 & 0 & 0 & 0 & 0 & 0 & 0 & 0 & 0 & 0 & 0 & 1 \\
\frac{k_{sr}}{M_{ur}} & \frac{c_{sr}}{M_{ur}} & \frac{-k_{sr}t_r}{2M_{ur}} & \frac{-c_{sr}t_r}{2M_{ur}} & \frac{L_r k_{sr}}{M_{ur}} & \frac{L_r c_{sr}}{M_{ur}} & 0 & 0 & 0 & 0 & 0 & 0 & \frac{-k_{sr}-k_{tr}}{M_{ur}} & \frac{-c_{sr}}{M_{uf}}
\end{bmatrix}$$

(1.52)

$$B=\begin{bmatrix} 0 & 0 & 0 & 0 & 0 & 0 & 0 & 0 & 0 & 0 \\ 0 & 0 & 0 & 0 & 0 & 0 & -\frac{1}{M_s} & -\frac{1}{M_s} & -\frac{1}{M_s} & -\frac{1}{M_s} \\ 0 & 0 & 0 & 0 & 0 & 0 & 0 & 0 & 0 & 0 \\ 0 & 0 & 0 & 0 & \frac{1}{I_{xx}} & 0 & -\frac{t_f}{2I_{xx}} & \frac{t_f}{2I_{xx}} & -\frac{t_r}{2I_{xx}} & \frac{t_r}{2I_{xx}} \\ 0 & 0 & 0 & 0 & 0 & 0 & 0 & 0 & 0 & 0 \\ 0 & 0 & 0 & 0 & 0 & -\frac{1}{I_{yy}} & \frac{l_f}{I_{yy}} & \frac{l_f}{I_{yy}} & -\frac{l_r}{I_{yy}} & -\frac{l_r}{I_{yy}} \\ 0 & 0 & 0 & 0 & 0 & 0 & 0 & 0 & 0 & 0 \\ \frac{kt_f}{M_{uf}} & 0 & 0 & 0 & 0 & 0 & \frac{1}{M_{uf}} & 0 & 0 & 0 \\ 0 & 0 & 0 & 0 & 0 & 0 & 0 & 0 & 0 & 0 \\ 0 & \frac{kt_f}{M_{uf}} & 0 & 0 & 0 & 0 & 0 & \frac{1}{M_{uf}} & 0 & 0 \\ 0 & 0 & 0 & 0 & 0 & 0 & 0 & 0 & 0 & 0 \\ 0 & 0 & \frac{kt_r}{M_{ur}} & 0 & 0 & 0 & 0 & 0 & \frac{1}{M_{ur}} & 0 \\ 0 & 0 & 0 & 0 & 0 & 0 & 0 & 0 & 0 & 0 \\ 0 & 0 & 0 & \frac{kt_r}{M_{ur}} & 0 & 0 & 0 & 0 & 0 & \frac{1}{M_{ur}} \end{bmatrix} \quad 1.53$$

C is identity matrix 14 by 14, and D is zero matrix 14 by 10.

$$C=\begin{bmatrix} 1 & \cdots & 0 \\ \vdots & \ddots & \vdots \\ 0 & \cdots & 1 \end{bmatrix} \quad (1.54)$$

$$D=\begin{bmatrix} 0 & \cdots & 0 \\ \vdots & \ddots & \vdots \\ 0 & \cdots & 0 \end{bmatrix} \quad (1.55)$$

1.2.8.4 Simplified and externally excited full car model

Some states may not be considered as output since they are not used in control. For instance, the body's vertical position, wheel positions, roll and pitch angles can be eliminated. The body's vertical velocity, roll and pitch rates and unsprung mass vertical speeds can be considered as output. Thus, the number of controlled parameters was reduced from 14 to 7. It is also possible to add external forces and moments acting on the system around the CoG. F_z is the force in vertical direction, and the moments are M_x and M_y around x and y axis. In this way, the system can be considered as 7 inputs and 7 outputs. While these inputs can be used simultaneously, some cannot.

$$\ddot{z}=\frac{1}{M_s}[F_{sFL}+F_{sFR}+F_{sRL}+F_{sRR}+F_z] \quad (1.56)$$

$$\ddot{\theta}=\frac{1}{I_{yy}}[-L_f(F_{sFL}+F_{sFR})+L_r(F_{sRL}+F_{sRR})+M_x] \quad (1.57)$$

$$\ddot{\emptyset}=\frac{1}{I_{xx}}\left[\frac{-t_f}{2}(F_{sFL}-F_{sFR})+\frac{t_r}{2}(F_{sRL}-F_{sRR})+M_y\right] \tag{1.58}$$

The new body equations 1.56, 1.57 and 1.58 were combined with equation 1.47 for the four unsprung masses. Then, the matrix B and C were obtained. Matrix A was same as previous and matrix D is 7 by 11 zeros. The reason for adding external inputs is explained in section 3.3.

$$B=\begin{bmatrix}
0 & 0 & 0 & 0 & 0 & 0 & 0 & 0 & 0 & 0 \\
0 & 0 & 0 & 0 & 0 & \frac{1}{M_s} & -\frac{1}{M_s} & -\frac{1}{M_s} & -\frac{1}{M_s} & -\frac{1}{M_s} \\
0 & 0 & 0 & 0 & 0 & 0 & 0 & 0 & 0 & 0 \\
0 & 0 & 0 & 0 & \frac{1}{I_{xx}} & 0 & -\frac{t_f}{2I_{xx}} & \frac{t_f}{2I_{xx}} & -\frac{t_r}{2I_{xx}} & \frac{t_r}{2I_{xx}} \\
0 & 0 & 0 & 0 & 0 & 0 & 0 & 0 & 0 & 0 \\
0 & 0 & 0 & 0 & 0 & -\frac{1}{I_{yy}} & \frac{l_f}{I_{yy}} & \frac{l_f}{I_{yy}} & -\frac{l_r}{I_{yy}} & -\frac{l_r}{I_{yy}} \\
0 & 0 & 0 & 0 & 0 & 0 & 0 & 0 & 0 & 0 \\
\frac{kt_f}{M_{uf}} & 0 & 0 & 0 & 0 & 0 & \frac{1}{M_{uf}} & 0 & 0 & 0 \\
0 & 0 & 0 & 0 & 0 & 0 & 0 & 0 & 0 & 0 \\
0 & \frac{kt_f}{M_{uf}} & 0 & 0 & 0 & 0 & 0 & \frac{1}{M_{uf}} & 0 & 0 \\
0 & 0 & 0 & 0 & 0 & 0 & 0 & 0 & 0 & 0 \\
0 & 0 & \frac{kt_r}{M_{ur}} & 0 & 0 & 0 & 0 & 0 & \frac{1}{M_{ur}} & 0 \\
0 & 0 & 0 & 0 & 0 & 0 & 0 & 0 & 0 & 0 \\
0 & 0 & 0 & \frac{kt_r}{M_{ur}} & 0 & 0 & 0 & 0 & 0 & \frac{1}{M_{ur}}
\end{bmatrix} \tag{1.59}$$

$$C=\begin{bmatrix}
0 & 1 & 0 & 0 & 0 & 0 & 0 & 0 & 0 & 0 & 0 & 0 & 0 & 0 \\
0 & 0 & 0 & 1 & 0 & 0 & 0 & 0 & 0 & 0 & 0 & 0 & 0 & 0 \\
0 & 0 & 0 & 0 & 0 & 1 & 0 & 0 & 0 & 0 & 0 & 0 & 0 & 0 \\
0 & 0 & 0 & 0 & 0 & 0 & 0 & 1 & 0 & 0 & 0 & 0 & 0 & 0 \\
0 & 0 & 0 & 0 & 0 & 0 & 0 & 0 & 0 & 1 & 0 & 0 & 0 & 0 \\
0 & 0 & 0 & 0 & 0 & 0 & 0 & 0 & 0 & 0 & 0 & 1 & 0 & 0 \\
0 & 0 & 0 & 0 & 0 & 0 & 0 & 0 & 0 & 0 & 0 & 0 & 0 & 1
\end{bmatrix} \tag{1.60}$$

1.2.9 Tyre models

While Pneumatic Tyres create the forces and moments necessary for movement on the tyre contact patch, they also have the important function of isolating some of the road-induced vibrations. There are different tyre models in the literature and the model complexity is determined by the frequency range of interest (Schmeitz, 2004). Some of the tyre models can be shown in Figure 1.20.

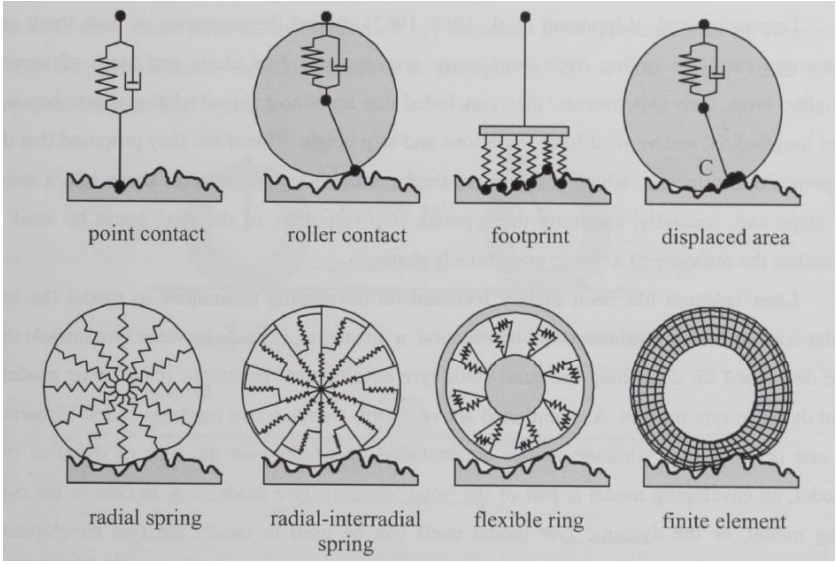

Figure 1.20: Some of the well-known tyre model figures (Schmeitz, 2004).

Simple point contact tyre models are generally used in the low and mid frequency range. Point-contact tyre models include a linear spring and a linear viscous damper. These models are considered relatively good approximations for representing low amplitude long wavelength path profiles. Since the models do not include the tyre geometry and elasticity, the enveloping effect of the tyres is not taken into account in these models (Schmeitz, 2004). Although deformation is not included in the model, point contact is not limited to the vertical axis. Thus, the contact point can be moved longitudinally and filter out short wavelength bumps. (Badalamenti and Doyle, 1988).

Radial spring models contain a certain number of springs and dampers in the radial direction. The vertical and longitudinal forces on the axis are obtained by summing the horizontal and vertical forces resulting from the deformations on the local radial springs. However, the independent movement of the springs in the model from the neighbouring springs reduces the accuracy of the model. This problem occurs when the ground or bump does not fully support the tyre. Later, with the addition of intermediate springs, the model was able to show the tyre enveloping behaviour for aircraft tyres by working in conjunction with adjacent springs (Badalamenti and Doyle, 1988).

There are different models in the literature for non-smooth surfaces such as solid ring models, Multibody models, Finite Element Models. The requirements that the models must meet can be expressed as reliability of the calculated loads originating from the

road –tyre interface, low computational load, and easy parameter acquisition (Schmeitz, 2004).

The rigid ring model neglects the deformation of tyre belt by considering the primary tyre modes. The ring is attached to the rim, elastically by spring and damper elements to represent the stiffness and damping characteristics of the pneumatic tyre. In general, there are two models used to represent the contact for the interface between the tyre and road surface; an enveloping model to consider micro and some macrotexture of road surface and a slip model (Schmeitz, 2004).

Multibody models include point masses, springs, dampers and tread elements as shown in Figure 1.21.

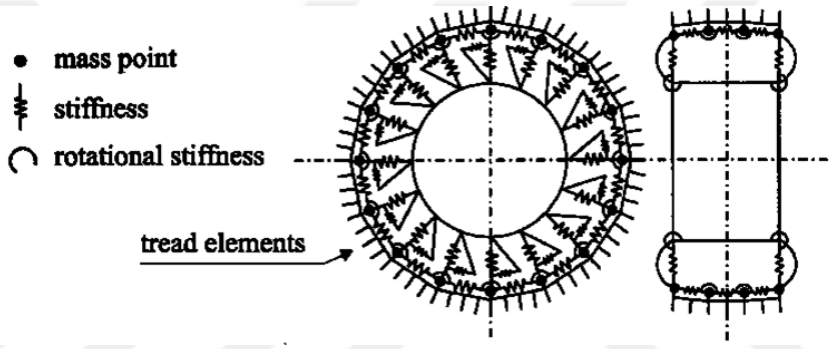

Figure 1.21 Three-dimensional multibody tyre model (Schmeitz, 2004).

The tyre belt is expressed as a three-dimensional mass point system. The model reduces the elasticity of the belt to a ring of mass points connected by tension and torsion springs. The sidewall is considered massless and is connected to the point masses by tension and torsion springs. In the lateral direction, the belt consists of elastic rings connected to each other by tension and torsion springs. Tyre treads, on the other hand, are modelled as elastically deformable brushes by sticking or slipping on the road surface. (Eichler, 1997).

One of the known commercial tyre models is FTyre® and it offers the simulation analysis up to 250Hz inputs. (Cosine scientific software AG, n.d.). Another commercial model frequently used in the literature is MF SWIFT. Since Magic Formula (MF) tyre model was first introduced by Pacejka in 1987 (Bakker et al., 1987), it has become almost the most popular tool in vehicle handling simulations.

The MF tyre model is now able to handle combinations of brake slip, lateral slip, camber, tyre pressure effects and transient responses up to 8 Hz. In the 90s, Delft and

TNO started to work on developing a driving tyre model for rough road surfaces. Especially in vehicle dynamics models where active control systems such as ABS, ESP, ASR, TCS will be considered, the frequency values that tyre models can address are expected to be greater than 8Hz and at least 30Hz for wavelengths shorter than 0.2m. For this purpose, MF-SWIFT was developed as a short-wavelength, medium-frequency tyre model (Schmeitz et al., 2007). Finite element models are unsuitable for vehicle dynamics simulations due to their computational load. On the other hand, due to their highly non-linear structure, they are particularly suitable for examining the tyre's response to small roughness. (Schmeitz, 2004).

1.2.10 Road

Studies in the literature generally use simple sinusoidal (Figure 1.22) or Chirp-increasing sinusoidal (Figure 1.23) path inputs to examine the relationship between the input and output of control systems.

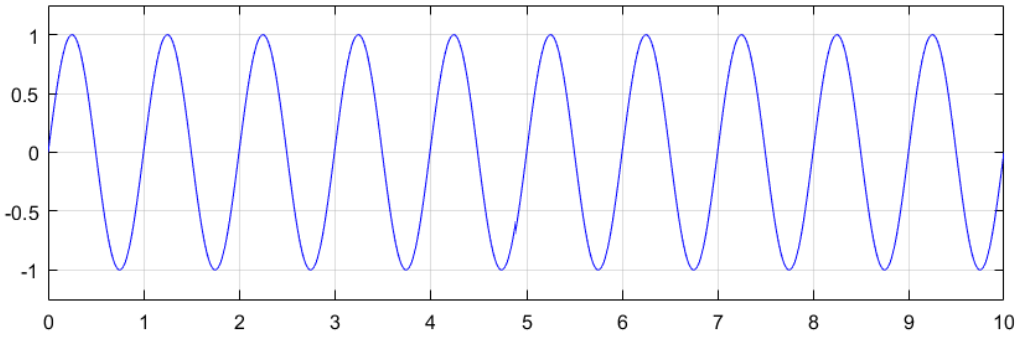

Figure 1.22: Sinusoidal input.

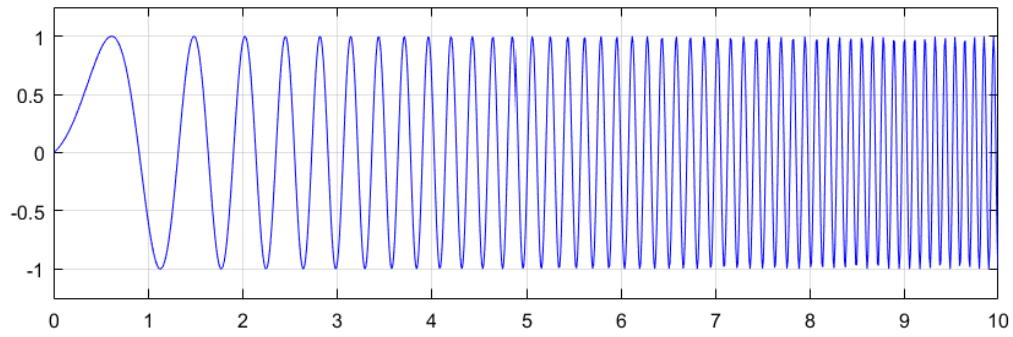

Figure 1.23: Chirp input with increasing frequency.

However, road surfaces have a very broad frequency spectrum. Road roughness is defined as the elevation profile on the surface with which the tyres of the vehicle are in contact. Road profiles generally fit into the category of broadband random signals. Therefore, profiles are defined by their statistical properties. One of the most useful presentation methods is the Power Spectral Density (PSD) function. Like any random signal, the elevation profile measured along the path is converted into sine curves by the Fourier transform. It is expressed as amplitude versus spatial frequency with a PSD plot. Spatial frequency is expressed as the wavenumber and in units of cycles/meter. (Gillespie, 1992).

Simple sinusoidal profiles are practical for evaluating input-output relationship, especially for studies in the frequency domain. On the other hand, ISO profiles have a more complex frequency content than sinusoidal inputs. ISO road profiles have classes from A to H, very good to bad, as shown in Figure 1.24. These classes give the flexibility to test a system in a wide range and against a standard. However, they have stationary characteristics (Loprencipe and Zoccali, 2017). Stationary characteristics may be misleading in interpreting results since both sinusoidal and ISO profiles are artificial. Artificial means they do not include road slopes or non-symmetrical variations on the horizontal and lateral plane as in a real road profile.

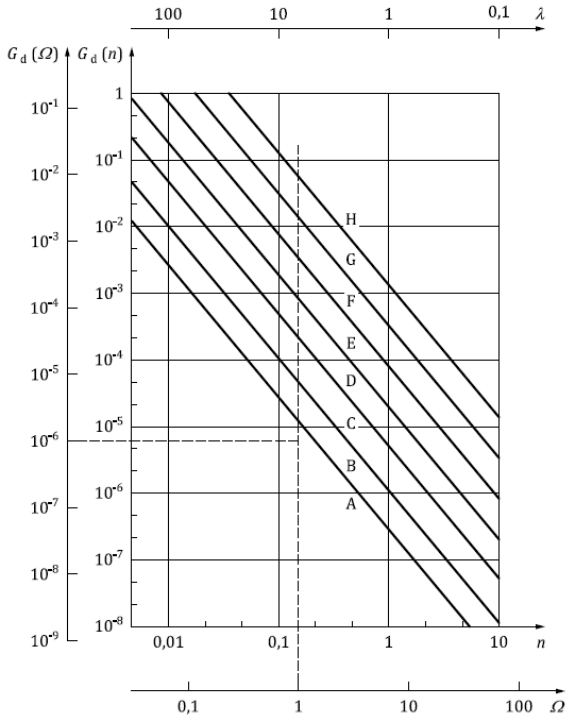

Figure 1.24: ISO Road Class (ISO 8608:2016(E), 2016).

In addition to standard road profiles, Daimler AG developed Curved Regular Grid (CRG) to use high precision measured road surfaces for tyre, vibration and driving simulation purposes and later made it available to the public as open source (*ASAM OpenCRG®*, n.d.). The open source CRG file format, which can also contain the digital road surfaces of the tracks belonging to the vehicle manufacturers' own test tracks, can be edited or used in an environment such as MATLAB® (Figure 1.25), or commercial vehicle dynamics software.

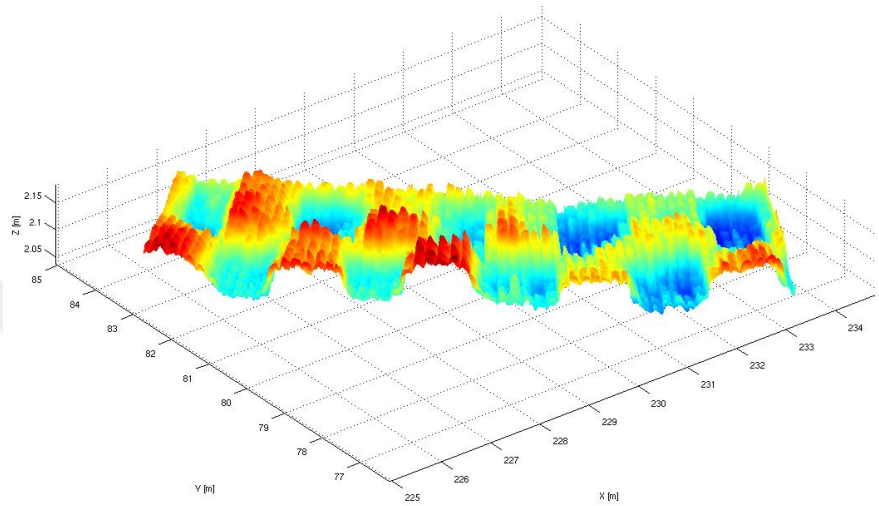

Figure 1.25: Belgian Block X, Y and Z coordinates in Open CRG Matlab®.

1.2.11 Sensors

Depending on the methodology, semi-active damper control methods require knowing the stroke, stroke speed, sprung mass and unsprung mass velocity, and acceleration. Therefore, these parameters need to be measured. Accelerometers, as in Figure 26, are widely used for these purposes (Carratù et al., 2017; Thenozhi et al., 2012). It can be used to measure sprung and unsprung mass acceleration, then the accelerations can be converted into velocities. Thus, stroke speed can also be obtained. Alternatively, a stroke sensor can be used to measure stroke and the stroke can be converted into velocity. It should be noted that the stroke sensor option still requires knowing at least the sprung mass speed.

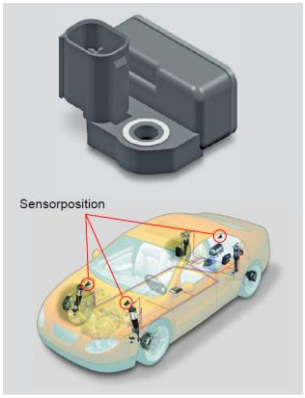

Figure 1.26: Continental Chassis Acceleration Sensor.

Figure 1.27 shows a stroke sensor between the chassis and suspension lower arm where it can be placed. Since the assembly position of the sensor is not aligned with the suspension, a geometrical transformation is needed to calculate the suspension stroke. One of the purposes of stroke sensors is to estimate the levelling of vehicles in order to adjust the headlight to prevent glazing.

Figure 1.27: Stroke sensor Hella®.

As shown in Figure 1.28, eight accelerometers need to be placed on the sprung masses and unsprung masses at the four corners of the vehicle.

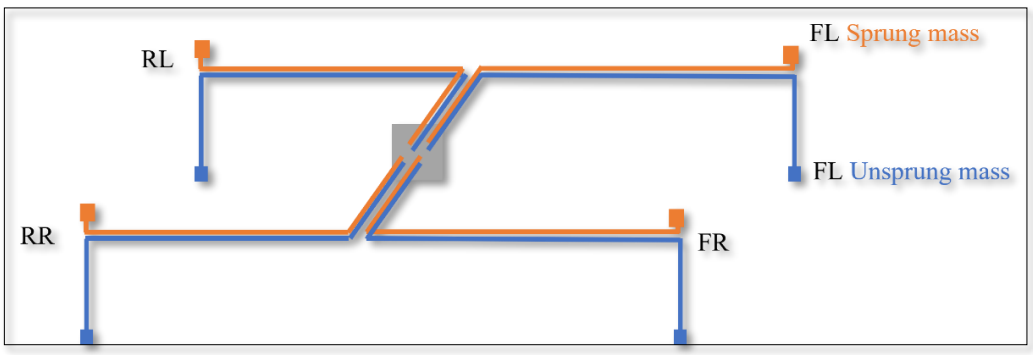

Figure 1.28:Sensor architecture in a chassis

Velocity can be obtained through the integration of acceleration since it cannot be measured directly. However, the accelerometer is fixed not only to the vehicle reference system but also to the road reference system. Therefore, accelerometers are affected by road slope. The road slope offsets the measurements. Moreover, the velocity signal may drift and includes offset as a result of the integration.

It has been reported that the calibrations of each automotive sensors produced must be interchangeable within ±1 % difference of each sensor, and the automotive environmental operating requirements are very severe, with vibrations up to ±10g (Fleming, 2001). The measurement should ideally have zero offsets and bias, i.e., aligned to zero. If there is some offset, a wrong direction can be obtained. A high pass filter can be used to remove the offset in the acceleration signal. Above the correctly chosen cut-off frequency, a low pass filter can be used as an anti-drift integration.

- *Reducing the number of sensors*

Even though sensor costs tend to decrease with advancing technology and high-volume production, it is still a substantial cost factor for automakers. Therefore, some OEMs and researchers have studied to reduce the number of sensors for suspension control or remove them altogether.

A group of researchers used a single sensor per quarter car model to estimate stroke speed with the Kalman Filter (G and Serpa, 2010). Another study estimates vehicle body attitude states based on wheel speed variation by wheel speed sensors (Liu et al., 2015). Another study controlled the dampers based on wheel rotation speed, considering the potential performance degradation of slow communication cycle of wheel speed sensors in-vehicle network (Hironobu and Kazuaki, 2022).

- *Virtual sensors*

Recent developments on deep learning and neural network allows to build a connection between measured and estimated information by fusing already available sensors to have virtual sensors for external outputs. In this way, significant advantages emerges to estimate some of information which is highly infeasible to measure in a serial vehicle and eliminate current sensors in the system (Šabanovi˘c, E.; Kojis et al., 2021).

1.2.12 Performance evaluation methods

Comfort expectation may differ significantly for passengers and drivers. While the driver wants to take all the necessary steps to control the vehicle depending on the road and vehicle conditions, the majority of passengers tend to demand smoother cruising and driving.

In this context, a comfortable vehicle for passengers can actually be described as a comfortable living space, namely a house on wheels (Mastinu and Manfred, 2014). Certainly, the performance of a suspension system is the most important criterion in evaluating the level of comfort that can be provided. Subjective and objective evaluation methods are used in the literature to evaluate suspension performance. (Demić et al., 2002; Els, 2005).

1.2.12.1 Subjective evaluation

Subjective rating is the oldest method used to evaluate comfort. The human body is equipped with a large number of different biological sensors to detect quantities within its physiological limits, and experienced evaluators use these biological sensors effectively. The following basic rules were adapted from (Mastinu and Manfred, 2014).

1. Clear definition of evaluation criteria and precise definition of evaluation conditions.

Comfort is multidimensional. This means that several independent criteria need to be defined and separated from each other. For each criterion, there must be a task critical or boundary condition where the differences between good and bad design are evident. Many benchmarks require real driving exercises on the test track.

2. Reference vehicle.

Comparing two vehicle is much easier than evaluating a single vehicle and makes the assessment more meaningful.

3. Descriptive rating scale.

The rating scale should be clearly defined. It is important that all raters have the same understanding of a given rating level.

4. Customer-oriented weighting.

The multidimensional comfort rating must be combined with an overall score for each vehicle. A representative picture can only be obtained if all the important comfort elements are captured and weighted according to customer preference for the particular vehicle type.

5. Trained evaluators

The evaluator needs a lot of experience, the ability to focus on specific aspects, and the ability to distinguish differences caused by boundary conditions from differences in performance.

6. Sufficient evaluation.

Even trained evaluators do not always come to the same conclusion. However, fewer observations are required compared to regular customers. For an appropriate comfort assessment, it is necessary to cover a certain range of the population with a certain number of selected assessors, as comfort performance in some comfort respects, such as vibration damping, postural or lateral support, also depends on the size of the occupant.

1.2.12.2 Objective evaluation methods

- *Root Mean Square (RMS) value*

Calculating the root mean square value of a variable is a method used, for example, to measure the amplitude of a wave that oscillates in the positive and negative direction. It is widely used especially in the evaluation of the performance of the suspension system. (Akçay and Türkay, 2008; Tudon-Martinez et al., 2013).

RMS values of n number of values, $\{a_1^2 + a_2^2 + \ldots . a_n^2\}$, are calculated by equation 1.61.

$$a_{rms} = \sqrt{\frac{1}{n}\sum_{i=1}^{n} a_i^2} = \sqrt{\frac{a_1^2 + a_2^2 + \ldots . a_n^2}{n}} \tag{1.61}$$

- *Nonlinear Frequency Response*

The performance of a semi-active suspension system can be evaluated in the frequency domain by the relationship between output (control system response) and input. The suspension model or control method may not be linear, in which case the closed loop control system will also not be linear. Bode diagrams cannot be used in non-linear situations. In order to examine the frequency response of nonlinear systems, an algorithm called variance gain, whose output is pseudo bode, has been developed. (S. M. Savaresi, Silani, et al., 2005). The variance gain procedure is expressed in the following order (S. Savaresi et al., 2010).

1. According to this algorithm, the closed loop system is fed with N number of sinusoidal inputs at increasing frequency.

$$Z_{r_i}(t)=A\sin(w_i t)\ ;\ i=1,2,....,N\ t\in[0,T] \tag{1.62}$$

2. The output signal is recorded. For each input, the output signal such as body acceleration is measured.

$$\ddot{Z}_i(t)=A\sin(w_i t)\ ;\ i=1,2,....,N\ t\in[0,T] \tag{1.63}$$

3. The approximate variance gain can be expressed with the equation 1.64. The discrete Fourier transforms, and PSDs of the input and output signals are calculated.

$$Facc(w_i)=\sqrt{\frac{\frac{1}{T}\int_0^T(\ddot{Z}_{si})^2}{\frac{1}{T}\int_0^T(Z_{ri})^2}}\qquad i=1,2,3..N \tag{1.64}$$

Although the RMS value is an effective method for calculating the amplitudes of signals that change direction, it hides the details of the signal, which includes a wide frequency range. For this reason, although the RMS value gives an idea in general, it is necessary to make detailed analysis over the entire frequency range with variance gain and similar approaches in order to make a detailed analysis depending on the frequency.

- *Power Spectral Density*

A power spectral density (PSD) is a measure of the power content of the signal versus frequency. PSD is typically used for characterising random wide bandwidth signals. The amplitude of the PSD is normalized with spectral resolution to digitize the signal.

The unit is g^2/Hz for the vibrations. A random signal usually has a finite average power and can be characterized by its average power spectral density (PSD) (Stocia P., 2005).

The discrete-time signal {y(t); t=0,±1,±2,...} is assumed to be a sequence of random variable with zero mean:

$$E\{y(t)\}=0 \text{ for all } t \tag{1.65}$$

E{.} denotes the averaging operator. The autocovariance sequence of y(t) is defined as

$$r(k)=E\{y(t)y^*(t-k)\} \tag{1.66}$$

The autocovariance sequence r(k) has useful properties given in equation 1.67 and 1.68.

$$r(k)=r^*(-k) \tag{1.67}$$

$$r(0)\geq|r(k)| \text{ for all } k \tag{1.68}$$

The covariance matrix of $\{y(t)\}$ was defined as follows

$$R_m=\begin{bmatrix} r(0) & r^*(1) & \cdots & r^*(m-1) \\ r(1) & r(0) & \ddots & \vdots \\ \vdots & \ddots & \ddots & r^*(1) \\ r(m-1) & \cdots & r(1) & r^*(0) \end{bmatrix}=E\left\{\begin{bmatrix} y^*(t-1) \\ \vdots \\ \vdots \\ y^*(t-m) \end{bmatrix}[y(t-1)...y(t-m)]\right\} \tag{1.69}$$

Equation 1.69 is positive semi-definite for all values of m. A Hermitian matrix M is positive semi-definite if $a*Ma\geq 0$ for every vector of a. Since equation 1.70 satisfies rule where z(t) as in equation 1.61 thus; R_m is positive semi-definite for every m.

$$a*R_m a=a*E\left\{\begin{bmatrix} y^*(t-1) \\ \vdots \\ \vdots \\ y^*(t-m) \end{bmatrix}[y(t-1)\ldots y(t-m)]\right\}a=E\{z^*(t)z(t)\}=E\{|z(t)|^2\}\geq 0 \tag{1.70}$$

$$z(t)=[y(t-1)...y(t-m)]a \tag{1.71}$$

The PSD is defined as discrete time Fourier transform of the covariance sequence:

$$\emptyset(\omega)=\sum_{k=-\infty}^{\infty} r(k)e^{-i\omega k} \text{ (Power Spectral Density)} \tag{1.72}$$

$$r(k)=\frac{1}{2\pi}\int_{-\pi}^{\pi}\emptyset(\omega)e^{i\omega k}d\omega \tag{1.73}$$

The equation 1.64 is obtained after inverse transform for equation 1.73.

$$r(0)=\frac{1}{2\pi}\int_{-\pi}^{\pi}\emptyset(\omega)d\omega \tag{1.74}$$

Since $r(0)=E\{|y(t)|^2\}$ measures the average power of $E\{y(t)\}$, the $\emptyset(\omega)$ is called PSD and it shows the average signal power over frequencies.

1.2.12.3 Control methods

A significant milestone for the control of a semi-active damper was the development of skyhook (SH) control, in particular the idea of using the semi-active suspensions as force generators (Karnopp et al., 1973). Skyhook was a simple feedback control logic with unique advantages for noise attenuation around the vehicle body resonant frequency (Emura et al., 1994). After the first conceptual idea, various SH control methods have been developed to solve different problems. For instance, to balance the trade-off between sprung and unsprung mass, the SH damping force equation was modified, thus the damping force was shared between sprung and unsprung mass (Besinger et al., 1995). The skyhook control strategy was completely modified and adapted for road holding, then called ground-hook control (Valášek et al., 1997). When SH control was introduced, the semi-active damper technology was not mature enough, and the damping coefficient could only be changed between minimum and maximum. With the improvement of damping technology, an infinite number of damping has been allowed to be applied. After that, SH-continuous was introduced (S. Savaresi et al., 2010). Later, gain adaptive SH control was introduced, the gain was modified according to the estimated road condition using a sensor (Hong et al., 2002).

Then, the researchers focused on extending the control zone of the SH control and bringing it closer to the optimal bound. A new approach called acceleration driven damper (ADD) was proposed using the Pontrygain's maximum principle. ADD improved the comfort by minimizing vertical acceleration and could reach the optimum bound beyond the resonant frequency (S. M. Savaresi, Silani, et al., 2005). Next, the researchers mixed the SH and ADD and introduced SH-ADD to reach the optimum bound for comfort for the entire frequency range (S. M. Savaresi and Spelta, 2007). Although the semi-active damper has many advantages such as energy

consumption and cost, an important disadvantage is its dissipative constraint. A semi-active suspension system has a limited force generation capability, due to the dissipative constraint, in other words, depending on the extension and compression of the damper and the requested force direction. Because semi-active dampers generate discontinuous forces, the control logic requires switching with respect to both body and wheel speed directions. Discontinuous force and system dynamics (instantaneous relations of damper and spring forces) may cause chattering (Margolis and Goshtasbpour, 1984). The SH control causes jerk and unwanted audible noise due to the sudden release of energy stored in the suspension elements. Therefore, the conventional SH control policy was modified. The modified control policy allowed the damper to release force in a controlled manner between high and low damping to reduce sudden force changes and jerk (Miller and Nobles, 1990). Since ADD uses acceleration directly as a switching parameter, it is quite sensitive to generate jerk in the case of sensor noise. The researchers proposed power driven damper (PDD) approach based on the control of the Port Hamiltonian system to solve the existing jerk problem in ADD (Morselli and Zanasi, 2008). The PDD approach improved the comfort beyond the body resonant frequency range as in ADD. Then, a mixed SH-PDD approach was introduced to extend the control range. Some filtering methods were also proposed to smooth the control forces by modulating the control force (Ahmadian et al., 2004; Liu and Zuo, 2016; Stamatov et al., 2008). Then, the energy driven damper (EDD) approach based on optimal control theory, which considers the kinetic energy of the suspension system, was introduced (Li et al., 2020).

While the SH and its variants remain popular and attractive to many researchers, many different control methods have been used for semi-active and active suspension control. Optimal control methods were used to optimize ride and handling behaviour, simultaneously (Brezas et al., 2015; Hirao et al., 2018). It has also been reported that the clipping method cannot ensure the performance and robustness of the controller, since dissipative constrains are not taken into account in the design (S. Savaresi et al., 2010). Further, H-infinity-LPV (Linear Parameter-Varying) approach has been used in many studies to build the robust controller considering the dissipative constraints in the design (Do et al., 2010; Tudon-Martinez et al., 2013).

The estimation of the road surface characteristic helps to improve the comfort by means of controller's gain adaptation. Some of these studies were rely on vibration-

based approaches such as evaluation of RMS on the vehicle body and wheels (Qin et al., 2015; Ward and Iagnemma, 2009). Although vibration-based approach is very helpful, they naturally yield the results as soon as the tyre passed over a vibratory input such as speed bump or pothole on their trajectory. In these methods starting from the moment that notable input can be detectable visually, there is an important time gap without any automatic control action. In fact, this gap can be transformed into a highly valuable period with some accumulated data depending on the preview information of the road profile characteristics, therefore, further improvements can be done on the level of comfort. At this point, preview control logic has been introduced as an acceptable improvement to the system. However, the idea of preview control logic was first developed by Bender (Bender, 1968) almost five decades ago. At the time, the contactless measuring technology was not at the desired level (Hac, 2007).

Recently developed sensing devices, such as Lidar, Stereo and Monocular cameras, have made the estimation of road profiles before passing the vehicle over its trajectory, possible (Oniga et al., 2007). However, early research studies in preview control have mostly been focused on the basic principles and improvement of the control logic and preview control as in these examples (Mehra et al., 1997; Tseng and Hrovat, 2015). A research study conducted on road profile implementation for the preview control was studied by (Streiter, 2008). Then, another research focused on the road profile generation with lidar measurement (Schindler, 2009b). Next, another study focused on the active suspension control using Model predictive control (MPC), with preview information by the sensor at the windshield (Göhrle et al., 2013). The main advantages of the MPC controller are that it can consider the constraints as hard or soft in the cost function (Hrovat et al., 2012). Therefore, for example, in the case of active suspension, the suspension stroke can be restricted to prevent reaching the bump stopper. Similarly, dissipative constraints can also be considered, this time for semi-active suspension case. The same researcher studied model predictive control of semi-active and active suspension together with road preview (Göhrle, 2014; Göhrle et al., 2013). In another study, the researcher compared MPC versus skyhook and feed forward controller performances by providing a methodology for how preview information is transformed into a road profile for low bandwidth active suspension (Göhrle et al., 2015). In the PhD thesis of the same researcher, it was concluded that MPC and Skyhook showed the same performances for active suspension. It was reported that the

Skyhook controller was selected because of the modular nature of the Skyhook and the computational cost of the MPC (Göhrle, 2014). Semi-active dampers are nonlinear and their characteristics change depending on stroke speed, sign, and the compression or extension (Pellegrini, 2013). Therefore, the damping force can be linearized to use in linear MPC. It is also possible to formulate the nonlinear damping characteristic into a cost function. Another study used nonlinear MPC with imperfect preview information and nonlinear damping characteristics. It was reported that the test results were worse than the simulation results but better than the passive damper (Kjellberg and Sundell, 2018). Online optimization complicates the real-time implementation of MPC as the computational cost is high. One study implemented region-free (also called regionless) explicit MPC for an active suspension with preview. The problem was solved offline, and the solutions were mapped, the optimal control inputs were stored. Moreover, this study decentralized the controller, i.e., each corner of the vehicle was controlled independently, thus reducing the computational cost. It should be noted that a precise solid state lidar was used for road profile measurement in this study (Theunissen et al., 2020).

The front camera accuracy is imperfect. A stereo camera accuracy was reported ± 2 cm in a study from (Göhrle et al., 2015). Moreover, another study shows that elevation profile measurement accuracy decreases with the length of the measured distance (Shen et al., 2014) as in table 1.4.

Table 1.4: Measurement accuracy variation with respect to measured surface length (Shen et al., 2014).

Downrange Distance	Height Measurement Variance
5m to 8m	+/- 1.2cm
8m to 12m	+/- 2.1cm
12m to 16m	+/- 3.7cm
16 to 21m	+/- 5.8cm
21 to 28m	+/- 8.8cm

MPC is the best candidate to implement preview control in a semi-active damper because only MPC can consider passivity constraint in control methods. The MPC has two-way preview capability to consider potential outputs of the model on the future horizon as well as considering the vehicle states and disturbances, i.e. the upcoming road profile. Thus, it makes the MPC sensitive to the measurement variance at the

centimetre level as preview control relies on an estimation of vehicle system behaviour based on disturbance in receding horizon and that may cause significant errors in control. In this section, different semi-active damper control methods were examined regarding advantages and disadvantages based on the literature survey. The aforementioned control methods' significant attributes were summarized briefly in terms of performance, calibration complexity, and application easiness in Table 1.5.

Table 1.5: Common control methods known for semi-active suspension.

Control Method	Advantages	Disadvantages
Skyhook (Two-state)	• High damping around the body resonance frequency • Easy to calibrate and apply • Does not need a system model	• High transmissibility in the mid and high frequency regions causes Jerk • Global control is not possible
Skyhook (Continuous)	• Infinite number of damping compared to two state Skyhook thanks to continuously variable damping • No abrupt transitions between High-Low Damping • Easy to calibrate and apply • Does not need a system model	
Skyhook (Global)	• Since it has global control, roll and head movements can be controlled with separate gain coefficients. • Easy to calibrate and apply • Prevents integral wind-up by considering the passivity constraint. • Does not need a system model	• Requires some of system parameters (vehicle dimensions) to ensure force distribution
Skyhook ADD	• Performance closes to optimal bound in the mid-frequency region • Possibility of control with a single accelerometer • Easy to calibrate and apply • Prevents integral wind-up by considering the passivity constraint.	• Not robust against to sensor noise and causes jerk • Due to the low damping at mid frequency range, bump stops prevent coupling.
Skyhook PDD	• Performance closes to optimal bound in the mid-frequency region • Robustness to the sensor noise • Less Jerk • Easy to calibrate and apply • Prevents integral wind-up by considering the passivity constraint.	• Too much control parameter compared to SH continuous
LQR	• No excessive calculation cost • Preview capability	• Less robust as passivity does not considered
H-infinity LPV	• Prevents integral wind-up by considering the passivity constraint. • Robustness	• Calibration and application is difficult •
MPC (with Preview)	• Preview capability • Prevents integral wind-up by considering the passivity constraint.	• Calculation cost or memory requirement • Application is difficult compared to SH
MPC (Without Preview)	• Prevents integral wind-up by considering the passivity constraint.	• Calculation cost or memory requirement • Application is difficult compared to SH • No preview capability
MPC (Linearized stroke)	• Linearized constraint • Relatively simple optimisation problem	• Calculation cost or memory requirement • Application is difficult compared to SH • Less accurate results and sometimes no feasible solution can be found
Explicit MPC	• Computationally less expensive compared to MPC	• Standard explicit MPC requires much memory

2. METHOD

In the method section, the study focused on the perspective of how the control methods would be applied to the vehicle. Therefore, preview and non-preview control methods were examined in detail. The non-preview semi-active suspension control methods were also examined in terms of energy perspective. Then, the study was conducted to obtain the preview information and data acquisition from the vehicle body for feedback control.

2.1 SH Control Principle

The well-known SH control principle can be defined as a fictitious damper mounted between the sprung mass and the virtual reference plane in the sky. The advantage of this method can be explained in the 1 DoF vehicle model with conventional and SH controlled suspensions as in Figure 2.1.

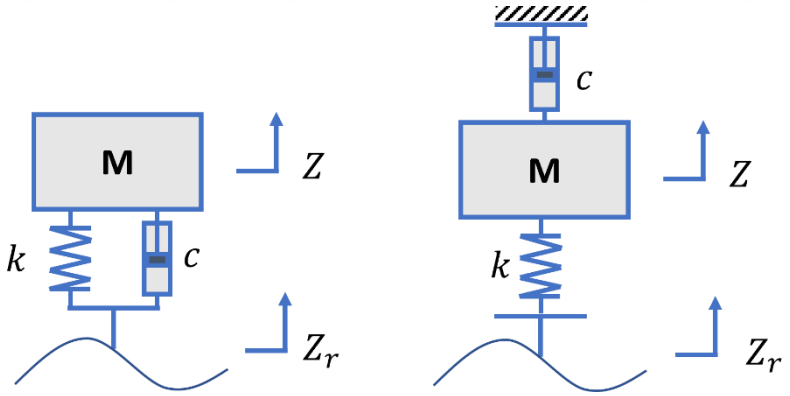

Figure 2.1: 1 DoF quarter car model; left: conventional, right: SH control.

The conventional quarter car model transfer function is as follows.

$$\frac{Z}{Z_r} = \frac{cs+k}{Ms^2+cs+k} \tag{2.1}$$

The transfer function of the SH-controlled quarter car model is as follows

$$\frac{Z}{Z_r} = \frac{k}{Ms^2+cs+k} \tag{2.2}$$

As can be seen, the transfer function of the SH-controlled suspension does not include damping coefficient in numerator since there is no damping between the road surface and the mass. On the other hand, in conventional quarter car, it is seen that the numerator has s, and the denominator has s^2. Therefore, it shows that conventional transfer function has 20dB/decade attenuation rate. Since SH does not include s in numerator, it has 40dB/decade attenuation ratio. This is the key factor of SH control (Duven, 2007).

As mentioned earlier, the SH damper is a fictitious damper and is assumed to be suspended in the sky. Since it is not possible to do this, a damper, which is mounted parallel to the suspension spring mimics the behaviour of a fictitious damper as shown in figure 2.2.

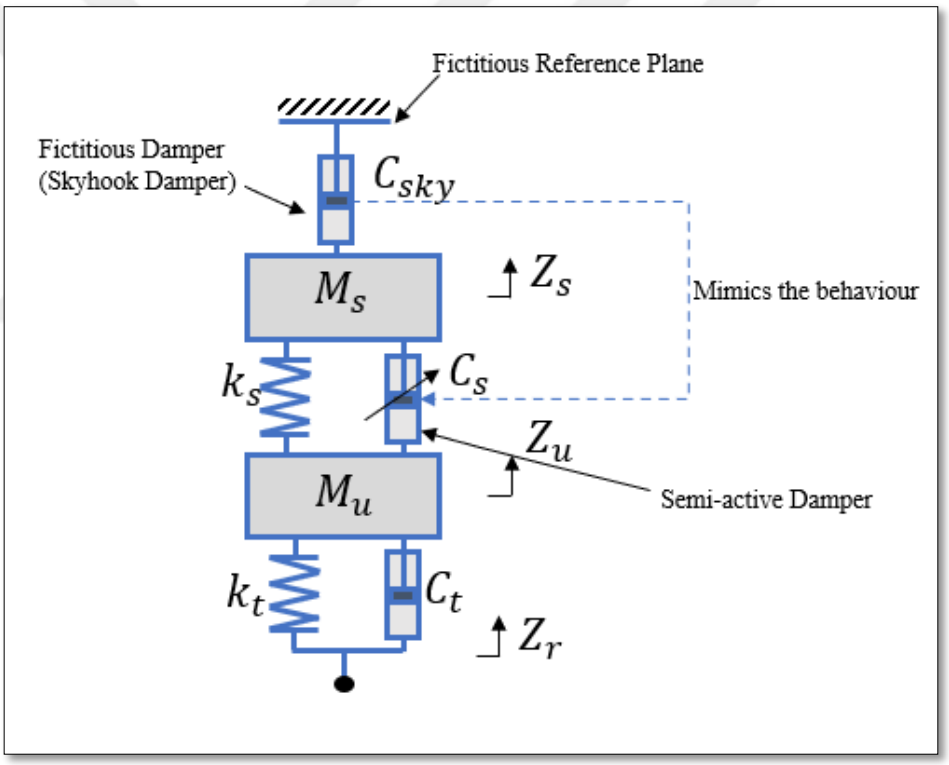

Figure 2.2: Quarter car model Skyhook control.

$$F_{csky}=C_{sky}\dot{Z}_s \tag{2.3a}$$

$$F_d=C_s(\dot{Z}_s-\dot{Z}_u) \tag{2.3b}$$

$$M_s\ddot{z}_s=-k_s(Z_s-Z_u)-F_d \tag{2.4}$$

$$M_u\ddot{z}_u=+k_t(Z_u-Z_r)+C_t(\dot{Z}_u-\dot{Z}_r)+k_s(Z_s-Z_u)+F_d \tag{2.5}$$

The skyhook damper force request, F_{csky}, is calculated in proportion to the sprung mass velocity, $\dot{Z}_s$ as given in Equation 2.3a. Then, the expected force F_{csky} is reproduced by the semi-active damper as the F_d force in equation 2.3b. Reproduction depends on the body and stroke speed signs criteria. If the criteria are satisfied, this means that the semi-active damper can reproduce the skyhook damper force in the same direction, as shown in conditions 1 and 3 in Figure 2.3. Otherwise, the semi-active damper applies the minimum force (conditions 2 and 4).

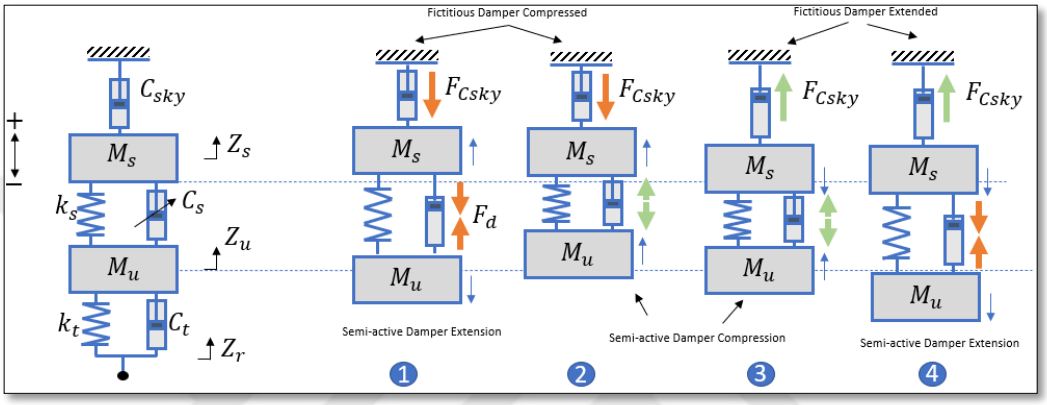

Figure 2.3: SH control criterions.

The skyhook-continuous method is defined in equation 2.6. If the term $\frac{C_{sky}\dot{Z}_s}{(\dot{Z}_s-\dot{Z}_u)}$ is replaced by the maximum damping coefficient, C_{max}, then, a two-state skyhook is obtained.

$$C_s=\begin{cases}\frac{C_{sky}\dot{Z}_s}{(\dot{Z}_s-\dot{Z}_u)}, & \&\dot{Z}_s(\dot{Z}_s-\dot{Z}_u)\geq 0\\ C_{min}, & \&\dot{Z}_s(\dot{Z}_s-\dot{Z}_u)<0\end{cases} \tag{2.6}$$

While the two-state target is to reduce the body speed to zero as much as possible, the SH-continuous damps the body motion in proportion to the vehicle body speed. The SH criteria were converted to a truth table for clarity, as seen in Table 2.1.

Table 2.1: SH conditions truth table.

Condition	$\dot{Z}_s$	$\dot{Z}_s - \dot{Z}_u$	Suspension Speed	Stroke	Body Movement (Ms)	Virtual Damper
1	+	+	extension		Body direction +	Skyhook Damper Compression
2	+	-	compression		Body direction+	Skyhook Damper Compression
3	-	-	compression		Body direction-	Skyhook Damper Extension
4	-	+	extension		Body direction-	Skyhook Damper Extension

Semi-active dampers have limited force generation capability, and this requires switching with respect to body and stroke speed direction. Hence, sudden changes in the damping coefficient between maximum and minimum cause force discontinuities depending on the relationship between spring and damping force. Therefore, this phenomenon has been reported as chattering or jerk in the literature (Margolis and Goshtasbpour, 1984). It was also reported that phenomenon causes unwanted audible noise due to the sudden release of the energy stored in the suspension elements. To reduce jerk and sudden force changes, Miller (Miller and Nobles, 1990) modified the SH procedure and designed the logic to have controllable force release. Some other jerk reducing, and signal filtering methods were also proposed to smooth the control force by manipulating the control policy and modulating the force request (Ahmadian et al., 2004; Collette and Preumont, 2010; Stamatov et al., 2008). However, it was reported that semi-active dampers have a time delay, and the damping properties cannot be changed instantaneously as in theoretical studies, and this may reduce chatter and jerk to some extent (Liu et al., 2005).

2.2 Active Driven Damper (ADD)

After the development of the SH concept, ADD was introduced like many other approaches. However, ADD had a significant difference with a new approach proposed to reach an optimal bound using Pontryagin's maximum principle. ADD improved comfort by minimising vertical acceleration and was able to reach the optimum bound beyond the resonant frequency (S. M. Savaresi, Silani, et al., 2005).

The ADD approaches, given in Equation 2.7, use body acceleration, $\ddot{Z}_s$, instead of the velocity variable of SH. While it may seem like an advantage to use acceleration directly without converting it to velocity, acceleration data requires some noise filtering due to measurement noise, drift and offset.

$$C_s=\begin{cases} C_{min} \ , \ \&\ddot{Z}_s(\dot{Z}_s-\dot{Z}_u) \leq 0 \\ C_{max} \ , \ \&\ddot{Z}_s(\dot{Z}_s-\dot{Z}_u) \ >0 \end{cases} \tag{2.7}$$

2.3 Skyhook-Active Driven Damper (SH-ADD)

ADD improves the comfort beyond the body resonant frequency, while SH provides the best filtering around the body resonant frequency. A simple switching parameter, α, is designed to combine SH and ADD to provide benefits across the entire frequency range.

$$C_s=\begin{cases} C_{max}, \ \left[\ddot{Z}_s^{\ 2}-\alpha^2\dot{Z}_s^{\ 2} \leq 0 \wedge \dot{Z}_s(\dot{Z}_s-\dot{Z}_u)>0\right] \vee \left[\ddot{Z}_s^{\ 2}-\alpha^2\dot{Z}_s^{\ 2} >0 \wedge \ddot{Z}_s(\dot{Z}_s-\dot{Z}_u)>0\right] \\ C_{min} \ , \ \left[\ddot{Z}_s^{\ 2}-\alpha^2\dot{Z}_s^{\ 2} \leq 0 \wedge \dot{Z}_s(\dot{Z}_s-\dot{Z}_u)\leq 0\right] \vee \left[\ddot{Z}_s^{\ 2}-\alpha^2\dot{Z}_s^{\ 2} >0 \wedge \ddot{Z}_s(\dot{Z}_s-\dot{Z}_u)\leq 0\right] \end{cases} \tag{2.8}$$

2.4 Power Driven Damper (PDD)

Since the conditions of the ADD are directly dependent on acceleration (if the actuator bandwidth is wide enough), it may cause chatter and a large amount of jerk. Therefore, the PDD approach given in Equation 2.9 is set to the average damping value during transients $(\dot{Z}_s-\dot{Z}_u)=0 \wedge (Z_s-Z_u)\neq 0$ (Morselli and Zanasi, 2008). PDD requires additional information on the parameters such as spring stiffness k_s Z_s-Z_u.

$$C_s=\begin{cases} C_{max} \ , & k_s\&(Z_s-Z_u)(\dot{Z}_s-\dot{Z}_u) + C_{max}\ (\dot{Z}_s-\dot{Z}_u)^2<0 \\ C_{min} \ , & k_s(Z_s-Z_u)(\dot{Z}_s-\dot{Z}_u) + C_{min}\ (\dot{Z}_s-\dot{Z}_u)^2\geq 0 \\ (C_{max}+C_{min})/2, & (\dot{Z}_s-\dot{Z}_u)=0 \wedge (Z_s-Z_u)\neq 0 \\ -k_s(Z_s-Z_u)/(\dot{Z}_s-\dot{Z}_u), \& & \text{otherwise} \end{cases} \tag{2.9}$$

2.5 Skyhook-Power Driven Damper (SH-PDD)

The PDD control policy improved comfort beyond the resonant frequency like ADD. A similar approach to that for SH-ADD, the SH-PDD approach has also been proposed to improve comfort over the whole frequency range. A switching function is

implemented between SH and PDD to define the operating range. The primary objective of SH control policy is to dissipate energy from sprung mass as quickly as possible. On the contrary, ADD and PDD aim to decouple the energy between sprung and unsprung mass. In some periods, the conflict between SH and ADD/PDD can be used to switch between SH and ADD/PDD. If the sum of the power of the sprung mass absorbed by the semi-active damper and the power released by the semi-active damper to the unsprung mass is greater than zero, the suspension can transfer all the energy absorbed from sprung mass to the unsprung mass. Thus, SH can be applied in this period. Otherwise, PDD can be applied as more energy is absorbed by the suspension (Liu and Zuo, 2016). Consequently, $(\dot{Z}_s-\dot{Z}_u)^2$, is the switching function and the SH-PDD approach is given by Equation 2.10.

2.6 Explanations Of Logic From An Energy Perspective

$$C_s=\begin{cases} C_{max}\ ,\ \dot{Z}_s^{\,2}-\dot{Z}_u^{\,2}\geq 0 \vee\ \&k_s(Z_s-Z_u)(\dot{Z}_s-\dot{Z}_u)+C_{max}\ (\dot{Z}_s-\dot{Z}_u)^2<0 \\ C_{min}\ ,\ \dot{Z}_s^{\,2}-\dot{Z}_u^{\,2}<0\ \vee\ \&k_s(Z_s-Z_u)(\dot{Z}_s-\dot{Z}_u)+C_{min}\ (\dot{Z}_s-\dot{Z}_u)^2\geq 0 \\ -k_s(Z_s-Z_u)/(\dot{Z}_s-\dot{Z}_u),\ \text{otherwise} \end{cases} \tag{2.10}$$

Giving switching policies based on written explanations with formulas makes it difficult to understand intuitively. Therefore, it has been found that systematically making explanations from the energy perspective helps to internalize the physical insight of logic more easily. The energy perspective approach was introduced by (Liu and Zuo, 2016).

The equation 2.11 gives the stored mechanical energy of the 2 DoF quarter car model over a period of time. The kinetic energy of unsprung and sprung mass and the stored energy in the spring k_s, and equivalent stiffness of the tyre, k_t were summed. Since the damper has an energy dissipative functionality, it is not included in the energy equation.

$$E(t)=\frac{1}{2}m_s\dot{z}_s^{\,2}+\frac{1}{2}m_u\dot{z}_u^{\,2}+\frac{1}{2}k_s(z_s-z_u)^2+\frac{1}{2}k_t(z_u-z_r)^2 \tag{2.11}$$

The power flow, in equation 2.12, can be obtained by gathering energy input from road undulations and the energy output by the damper.

$$P(t)=k_u\dot{z}_r(z_u-z_r)-C_s\ (\dot{Z}_s-\dot{Z}_u)^2 \tag{2.12}$$

The first term of Equation 2.12, $k_u\dot{Z}_r(z_u-z_r)$ is power flow transferred from the road. The second term, $-C_s\,(\dot{Z}_s-\dot{Z}_u)^2$ is power dissipated by the damper. According to Newtonian mechanics, power is equal to force times velocity. The semi-active damper absorbs the power of the sprung mass as given in Equation 2.13.

$$P_{sd}=C_s\,(\dot{Z}_s-\dot{Z}_u)\dot{Z}_s \tag{2.13}$$

The power of sprung mass absorbed by the suspension spring is given in equation 2.14

$$P_{ss}=k_s\,(\dot{Z}_s-\dot{Z}_u)\dot{Z}_s \tag{2.14}$$

The power released by the semi-active damper to the unsprung mass is shown in equation 2.15.

$$P_{ud}=C_s\,(\dot{Z}_s-\dot{Z}_u)\dot{Z}_u \tag{2.15}$$

The power released by the suspension spring to the unsprung mass is given in equation 2.16

$$P_{us}=k_s\,(\dot{Z}_s-\dot{Z}_u)\dot{Z}_u \tag{2.16}$$

So, the net power on the suspension, P_{net} , can be calculated by Equation 2.17.

$$P_{net}=P_{sd}+P_{ss}+P_{ud}+P_{us}=C_s\,(\dot{Z}_s-\dot{Z}_u)\dot{Z}_s+k_s\,(\dot{Z}_s-\dot{Z}_u)\dot{Z}_s+C_s\,(\dot{Z}_s-\dot{Z}_u)\dot{Z}_u+k_s\,(\dot{Z}_s-\dot{Z}_u)\dot{Z}_u \tag{2.17}$$

- *The physical background of SH*

As explained in section 2.3, the SH control enforces the semi-active damper to mimic the behaviour of the fictitious damper hooked to the sky. Hence, equation 2.18 is given to recover the energy absorbed in the sprung mass by the suspension elements.

$$P_{sd}+P_{ss}=[C_s\,(\dot{Z}_s-\dot{Z}_u)+k_s\,(\dot{Z}_s-\dot{Z}_u)]\dot{Z}_s \tag{2.18}$$

The only controllable feature in equation 2.19 is the semi active damper. It can be deduced that the damper can dissipate the energy of the sprung mass in the shortest time by setting the damping coefficient as maximum, $C_s = C_{max}$. A positive P_{sd} satisfies the SH policy, which can be expressed by $(\dot{Z}_s-\dot{Z}_u)\dot{Z}_s>0$. Otherwise, when the damper is in the direction of transferring power to the sprung mass, the transmissibility is reduced to a minimum by setting the damping coefficient to a minimum, $C_s = C_{min}$ as given in Figure 2.4.

$$\text{Skyhook} \Leftrightarrow \min_{C_s} J(C_s \triangleq -P_{sd} + P_{ss}) \tag{2.19}$$

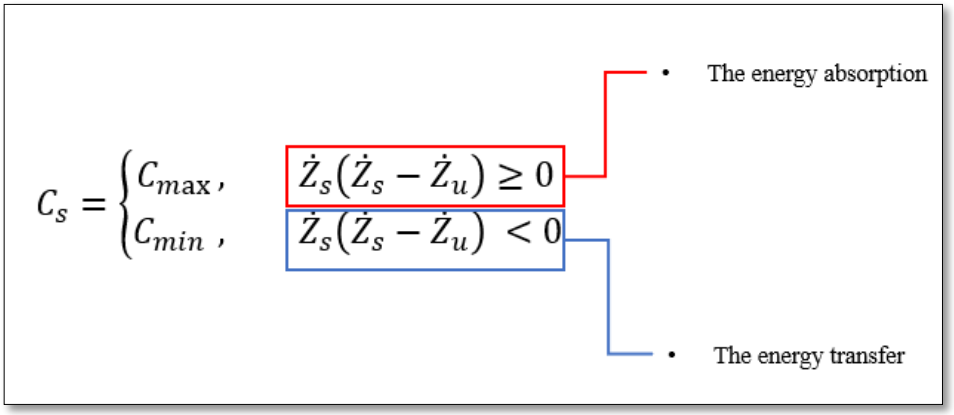

Figure 2.4: Breakdown of SH control from energy perspective.

- *The physical background of ADD*

The ADD was developed based on the port Hamiltonian technic by targeting to reduce the sprung mass acceleration instead of the velocity variable of SH. The body acceleration term, $\ddot{z}_s$, in the policy of the ADD, $\ddot{z}_s(\dot{z}_s - \dot{z}_u) \geq 0$, is replaced in Equation 2.4 (The sprung mass motion equation), then, Equation 2.20 is obtained. Thus, it can be inferred that ADD tries to balance the power by considering minimization of the acceleration with respect to the power of spring as in expression given in Equation 2.22. The alternative (explicit) form of ADD is given in Equation 2.21.

$$\ddot{Z}_s(\dot{Z}_s - \dot{Z}_u) = [-k_s(Z_s - Z_u) - C_s(\dot{Z}_s - \dot{Z}_u)](\dot{Z}_s - \dot{Z}_u) \tag{2.20}$$

$$C_s = \begin{cases} C_{min}, & \&[k_s(Z_s - Z_u) + C_s(\dot{Z}_s - \dot{Z}_u)](\dot{Z}_s - \dot{Z}_u) \leq 0 \quad (2.21) \\ C_{max}, & \&[k_s(Z_s - Z_u) + C_s(\dot{Z}_s - \dot{Z}_u)](\dot{Z}_s - \dot{Z}_u) > 0 \quad (2.22) \end{cases}$$

$$\text{ADD} \Leftrightarrow \min_{C_s} J(C_s \triangleq |P_{net}|) \in \{C_{min}, C_{max}\}$$

- *The physical background of PDD*

PDD behaves like ADD and energy sharing between sprung and unsprung mass is a capability of the suspension system. If the P_{net} is close to zero, suspension can have better isolation, which was also addressed by (Liu and Zuo, 2016). Elements of P_{net} and sign analysis are shown in Table 2.2, always taking into account the positive sign spring stiffness and damping coefficient.

Table 2.2: The PDD/ADD conditions truth table (For Equation 2.20).

Condition	k_s	Z_s-Z_u	$\dot{Z}_s$-$\dot{Z}_u$	C_s	$\dot{Z}_s$-$\dot{Z}_u$	$\dot{Z}_s$-$\dot{Z}_u$	$\lvert P_{net}\rvert$
1	+	-	-	+	-	-	**>0**
2	+	+	-	+	-	-	
3	+	-	+	+	+	+	
4	+	-	-	+	-	-	**>0**

When $P_{net}>0$, C_s must be set to minimum C_{min} for conditions 1 and 4. Spring power is always negative while damper power is always positive for conditions 2 and 3. To minimize P_{net}, C_s must be set to maximum, C_{max} .

If the damper and spring forces are equal, Equation 2.23 can be derived from P_{net}.

$$\frac{-k_s(Z_s-Z_u)}{\dot{Z}_s-\dot{Z}_u} \tag{2.23}$$

PDD is significantly the same as ADD (alternative form of ADD is given in Equation 2.21), except for one condition, if $(\dot{Z}_s-\dot{Z}_u)=0$ & $(Z_s-Z_u)=0$, then the damping is set to average as $C_s=(C_{max}+C_{min})/2$, just to smooth out the damping. The expression 2.24 gives the function of the PDD.

$$\text{PDD} \Leftrightarrow \min_{C_s} J(C_s \triangleq |P_{net}|) \tag{2.24}$$

- *The physical background of SH-ADD / PDD*

SH or ADD is switched by the design parameter α and SH or PDD is switched based on the rule $\dot{Z}_s^2-\dot{Z}_u^2 \geq 0$. The physical background is the same as the structure of ADD/PDD, and a detailed explanation is given in sections 2.3 and 2.4.

2.7 Model Predictive Control

Model Predictive Control was developed for chemical process control and mainly for slowly changing systems. On the other hand, increasing CPU performance and memory capacity made MPC attractive for chassis control applications due to its preview capability and flexible structure that enables it to consider actuator constraints (Hrovat et al., 2012). One of the first MPCs for active suspension control was studied by (Mehra et al., 1997). They used the road disturbance as a preview information with multiple point and a preview horizon of 0.32 with 0.02 s sampling time. This study took into account the bump stop rate and results were compared with LQR control method. Another research using preview information to account for bump stop in the

quarter car system model showed that MPC outperformed SH on rounded pulse and pseudo random road profiles (Cho, 1999). Another research focused on a full car model using MPC without considering tyre dynamics due to low bandwidth-energy saving actuators. The control variable was actuator displacement instead of force in this research, and interestingly, proactive actuator engagement was only obtained, when the constraints of the actuator displacement rate were included in the optimization problem (Gohrle et al., 2012). In another study, but this time MPC design for semi-active suspension control, road profile estimator was used instead of preview, and the estimator was 10 times faster than the closed loop, and the step time of the closed loop was 5ms (Nguyen et al., 2016). Implementation seemed infeasible as the proposed controller had a very challenging step time of 5ms and 0.5ms for the controller and observer, respectively, in terms of standard vehicle communication system speed with on-board sensors.

Another research focused on developing different MPCs for active and semi-active suspension systems with available road profile data. Due to the nonlinear semi-active damper characteristics considered in Quadratic programming, the first controller was nonlinear MPC and was referenced in this paper. The second MPC was proposed by linearizing the semi-active damper characteristics using the approximate stroke speed calculated with the passive vehicle model on the preview horizon. The third MPC used the clipping approach, thus unconstrained optimization was performed. It is possible to calculate and distribute the optimal force to the actuators for the case controlling both active and semi-active suspensions. However, the authors found it difficult to combine the active suspension and semi-active damper constraints, simultaneously. Therefore, they separately optimized both the damper force and the active suspension displacement. The optimization of both actuators was compared with active suspension with passive hard and soft damper configurations and the optimized configuration outperformed the others as expected (Göhrle et al., 2013). The same authors proposed a model predictive trajectory optimization controller which uses an inverse vehicle model that optimizes bounce, roll and pitch instead of four actuators. This was a novel formulation of a nonlinear control method relying on MPC rather than predictive control. Thus, it reduced the computational complexity (Göhrle, 2014). Another experimental research focused on implementation of nonlinear MPC for semi-active suspension control without preview. The authors used chirp road profile

representing a 5-20Hz and 2.5mm amplitude and a square wave type signal which represents the speed bump with 7mm amplitude. They achieved only a 3.5% reduction compared to the SH control; this was interpreted as MPC not having significant performance without preview information (Madhavan Rathai et al., 2019). Another study reformulated the semi-active suspension controller problem in the Volvo S90 by considering the control variable as damping instead of force for real-time implementation with the front camera. According to this study, real-time test performance was lower than simulation results compared to optimally tuned passive dampers. (Kjellberg and Sundell, 2018). In the studies carried out so far, either no information was given about the accuracy of the road profile perception, or a perfect road profile measurement was assumed. (Göhrle et al., 2015) shared a comprehensive study on road profile estimation with the preview sensor. In the study, they found that the feedforward with Skyhook and the MPC with preview of active suspension had the same performance. Another study focused on the effect of actuator limitations on comfort using linear MPC. Different type of speed bumps, country roads, city roads were used in the simulations. They found that the suspension rate had more of an effect than the lower and upper force generating capability to reject the disturbances on the quarter car model with a 2s horizon and a 10ms sampling rate (Enders et al., 2020). After promising results with various MPC studies in the literature, the focus of the research has been moved towards implementing MPC to the vehicle. Thus, explicit MPC has gained much more importance as they have less computational effort than implicit ones.

The force-velocity characteristics of the semi-active suspension are highly nonlinear. Therefore, these curves can be separated to the straight lines and these lines are linear. Thus, these linear characteristic curves were used as a linear constraint by switching them according to the stroke speed on the prediction horizon. This approach gave the opportunity to identify the highly nonlinear characteristic in the quadratic optimization problem to create the piecewise affine function to build the explicit MPC (Houzhong et al., 2020)

The MPC controller requires the system model, which can be provided by the discretized state-space matrix form. A zero-order hold discretization can be used for this. The plant model can be written in matrix form as in Equations 2.25 and 2.26. It can then be discretized as in Equations 2.27-2.30. (Camacho and Bordons, 2007;

Kjellberg and Sundell, 2018) In this study, the sources in which the formulas are given explicitly were used in writing the MPC formulas.

$$\dot{x}=Ax+B\begin{bmatrix}u\\w\end{bmatrix} \quad (2.25)$$

$$y=Cx+Du \quad (2.26)$$

$$A_d=e^{AT} \quad (2.27)$$

$$B_d=A^{-1}(e^{AT}-I)B \quad (2.28)$$

$$C_d=C \quad (2.29)$$

$$D_d=D \quad (2.30)$$

The discretized plant model can be given in Equations 2.31 and 2.32.

$$x[k+1]=A_dx[k]+B_du[k] \quad (2.31)$$

$$y[k]=C_dx[k]+D_du[k] \quad (2.32)$$

The discretized plant without d subscription can be written in the form in Equations 2.33 and 2.34 for simplicity,

$$x[k+1]=Ax[k]+Bu[k] \quad (2.33)$$

$$y[k]=Cx[k]+Du[k] \quad (2.34)$$

x is the state vector, A is the state matrix, B is the input matrix, C is the output matrix, D is the feedthrough matrix, y is the output vector, u is the control signal vector. The input matrix B can be divided into two parts, B_u and B_w as the control signal matrix and the disturbance input matrix, respectively. Therefore, equation 2.35 and 2.36 are obtained.

$$x[k+1]=Ax[k]+B_uu[k]+B_ww[k] \quad (2.35)$$

$$y[k]=Cx[k]+Du[k] \quad (2.36)$$

- *State estimations*

The system model in Equation 2.35 can be written over a finite horizon as in Equations from 2.37 to 2.41. Equation 2.41 inherently includes the previous states, as they are added into the $\hat{x}[k|k]$ term. Then the final state vector can be obtained as in Equation 2.41.

$$\hat{x}[k+1|k]=A\hat{x}[k|k]+B_uu[k|k]+B_ww[k|k] \quad (2.37)$$

$$\hat{x}[k+2|k]=A\hat{x}[k|k]+B_uu[k|k]+B_ww[k+1|k] \quad (2.38)$$

$$\hat{x}[k+2|k]=A(A\hat{x}[k|k]+B_u u[k|k]+B_w w[k|k])+B_u u[k|k+1]+B_w w[k|k+1] \quad (2.39)$$

$$\hat{x}[k+2|k]=A^2\hat{x}[k|k]+AB_u u[k|k]+AB_w w[k|k])+B_u u[k|k+1]+B_w w[k|k+1] \quad (2.40)$$

$$\hat{x}[k+N|k]=A^N\hat{x}[k|k]+A^{N-1}B_u u[k|k]+A^{N-1}B_w w[k|k]) \\ +A^{N-2}B_u u[k|k+1]+A^{N-2}B_w w[k|k+1]+...+B_u u[k+N-1|k]+ B_w w[k+N-1|k]) \quad (2.41)$$

- *Output estimations*

The output estimation vector includes the concatenated system matrices including the previous state matrices as in the state estimation equations. Therefore, the output Equations, from *k* to *k+N,* 2.42 to 2.47 are added together in the equation 2.48 which expresses all outputs in the horizon.

$$\hat{y}[k+1|k]=C\hat{x}[k+1|k]+Du[k+1|k] \quad (2.42)$$

$$\hat{y}[k+1|k]=C(A\hat{x}[k|k]+B_u u[k|k]+B_w w[k|k])+Du[k+1|k] \quad (2.43)$$

$$\hat{y}[k+1|k]=CA\hat{x}[k|k]+CB_u u[k|k]+CB_w w[k|k]+Du[k+1|k] \quad (2.44)$$

$$\hat{y}[k+2|k]=C(A^2\hat{x}[k|k]+AB_u u[k|k]+AB_w w[k|k])+ \\ B_u u[k|k+1]+B_w w[k|k+1])+Du[k+2|k] \quad (2.45)$$

$$\hat{y}[k+2|k]=CA^2\hat{x}[k|k]+CAB_u u[k|k]+CAB_w w[k|k]) \\ +CB_u u[k|k+1]+CB_w w[k|k+1]+Du[k+2|k] \quad (2.46)$$

$$\hat{y}[k+N|k]=CA^N\hat{x}[k|k]+CA^{N-1}B_u u[k|k]+CA^{N-1}B_w w[k|k])+ \\ CA^{N-2}B_u u[k|k+1]+CA^{N-2}B_w w[k+1|k]+\ldots+CB_u u[k+N-1|k] \\ +CB_w w[k+N-1|k]+Du[k+N|k] \quad (2.47)$$

The output estimations can be written in the matrix form as given in Equation 2.48.

$$\underbrace{\begin{bmatrix}\hat{y}[k+1|k]\\ \hat{y}[k+2|k]\\ \vdots\\ \hat{y}[k+N|k]\end{bmatrix}}_{\hat{y}} = \underbrace{\begin{bmatrix}CA\\ CA^2\\ \vdots\\ CA^N\end{bmatrix}}_{\hat{\Theta}} \hat{x}[k|k] + \underbrace{\begin{bmatrix}CB_u & D & 0 & \dots & 0\\ CAB_u & CB_u & D & 0 & \vdots\\ \vdots & \ddots & \ddots & \ddots & 0\\ CA^{N-1}B_u & CA^{N-2}B_u & \dots & \ddots & CB_w\end{bmatrix}}_{r_u} \underbrace{\begin{bmatrix}u[k|k]\\ u[k+1|k]\\ \vdots\\ u[k+N|k]\end{bmatrix}}_{\hat{u}} + \underbrace{\begin{bmatrix}CB_w & 0 & \dots & 0\\ CAB_w & CB_w & \ddots & \vdots\\ \vdots & \ddots & \ddots & 0\\ CA^{N-1}B_w & CA^{N-2}B_w & \ddots & CB_w\end{bmatrix}}_{r_w} \underbrace{\begin{bmatrix}w[k|k]\\ w[k+1|k]\\ \vdots\\ w[k+N-1|k]\end{bmatrix}}_{\hat{w}} \quad (2.48)$$

The Equation 2.48 is written in a simple form as given in Equation 2.49.

$$\hat{y} = \Theta x[k] + r_u \hat{u} + r_w \hat{w} \quad (2.49)$$

Equation 2.49 can be formulated as a quadratic optimization problem to minimize the output of the system, as given in Equation 2.50.

$$\min_{\hat{u}} \hat{y}^T Q \hat{y} + \hat{u}^T R \hat{u} \quad (2.50)$$

Q is the output penalty matrix and R is the control signal penalty matrix. Equation 2.49 is substituted into the Equation 2.50 to get the Equation 2.51.

$$\hat{y}^T Q \hat{y} + \hat{u}^T R \hat{u} = (\Theta x[k] + r_u \hat{u} + r_w \hat{w})^T Q (\Theta x[k] + r_u \hat{u} + r_w \hat{w}) + \hat{u}^T R \hat{u} \quad (2.51)$$

The Equation 2.52 is obtained after the modifications in the Equation 2.51.

$$\hat{y}^T Q \hat{y} + \hat{u}^T R \hat{u} = (x[k]^T \Theta^T + \hat{u}^T r_u^T + \hat{w}^T r_w^T) Q (\Theta x[k] + r_u \hat{u} + r_w \hat{w}) + \hat{u}^T R \hat{u} \quad (2.52)$$

The Equation 2.53 can be obtained after the distribution of the variables in the parenthesis in Equation 2.52.

$$\begin{aligned}\hat{y}^T Q \hat{y} + \hat{u}^T R \hat{u} = {} & x[k]^T \Theta^T Q \\ & \Theta x[k] + x[k]^T \Theta^T Q r_u \hat{u} + x[k]^T \Theta^T Q r_w \hat{w} + \dots + \hat{u}^T r_u^T Q\, \Theta x[k] \\ & + \hat{u}^T r_u^T Q r_u \hat{u} + \hat{u}^T r_u^T Q r_w \hat{w} + \hat{w}^T r_w^T Q \Theta x[k] \\ & + \hat{w}^T r_w^T Q r_u \hat{u} + \hat{w}^T r_w^T Q r_w \hat{w} + \hat{u}^T R \hat{u}\end{aligned} \quad (2.53)$$

Equation 2.52 is obtained by subtracting terms that do not depend on the optimization variable $\hat{u}$ in equation 2.53.

$$x[k]^T\Theta^T Q r_u \hat{u} + \hat{u}^T r_u{}^T Q\,\Theta x[k] + \hat{u}^T r_u{}^T Q r_u \hat{u} + \cdots \tag{2.54}$$
$$+\hat{u}^T r_u{}^T Q r_w \hat{w} + \hat{w}^T r_w{}^T Q r_u \hat{u} + \hat{u}^T R \hat{u} = \hat{u}^T \underbrace{(r_u{}^T Q r_u + R)}_{H} \hat{u} +$$
$$2\underbrace{(x[k]^T\Theta^T Q r_u + \hat{w}^T r_w{}^T Q r_u)}_{f} \hat{u}$$

The problem given in Equation 2.50 can be written as equation 2.55.

$$\min_{\hat{u}} \frac{1}{2}\hat{u}^T H \hat{u} + f\hat{u} \tag{2.55}$$

The problem was rearranged to be solved in a quadratic programming (QP) solver. The Hessian matrix, H, must be positive definite to have a convex optimization problem. The MPC problem and constraints are generally expressed in the form of Equation 2.56. The constraints lb and ub are lower bound and upper bound, respectively and are linear.

$$\min_{\hat{u}} \frac{1}{2}\hat{u}^T H \hat{u} + f\hat{u} \tag{2.56}$$
$$\text{Subject to } A\hat{u} \leq b$$
$$lb \leq \hat{u} \leq ub$$

2.8 Vehicle Model Validation

The full car model validated using Renault's high fidelity vehicle model in IPG-Carmaker®. The CRG digitalized Renault test track was used in simulation for model validation, and Figures 2.5 to 2.7 show the comparison between the high-fidelity vehicle model and the estimated vehicle model. The digitalized test track has a wide frequency spectrum up to 200Hz. Therefore, estimation of the model was not an easy task. The initial peaks in roll rate and vertical speed were the results of choosing a constant damping coefficient rather than nonlinear damping. The nonlinear damper characteristic depends on stroke speed and for a small stroke speed up to ~0.2 m/s; the slope of the damping coefficient curve is high, and then the slope of the curve is small to resist more movements resulted by handling and less for bumps. Therefore, having an average damping value for all regions of damper causes undesirably high forces for small road inputs. Another reason for the first peak is that the rear wheels start without

input when the front wheels are started with a non-zero input value, causing an unbalanced initialization in simulation for the linear vehicle model.

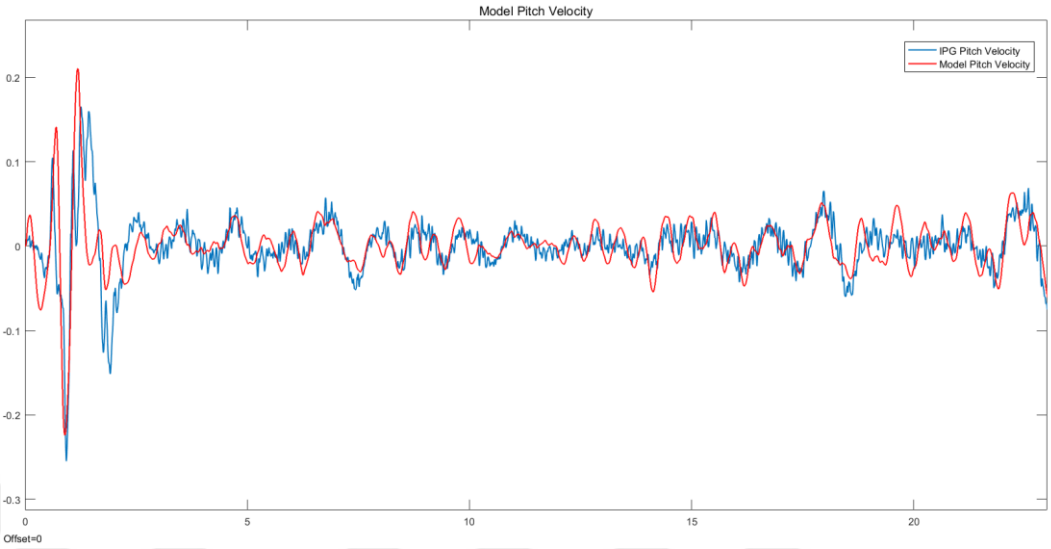

Figure 2.5: Validation of vehicle model: Pitch velocity.

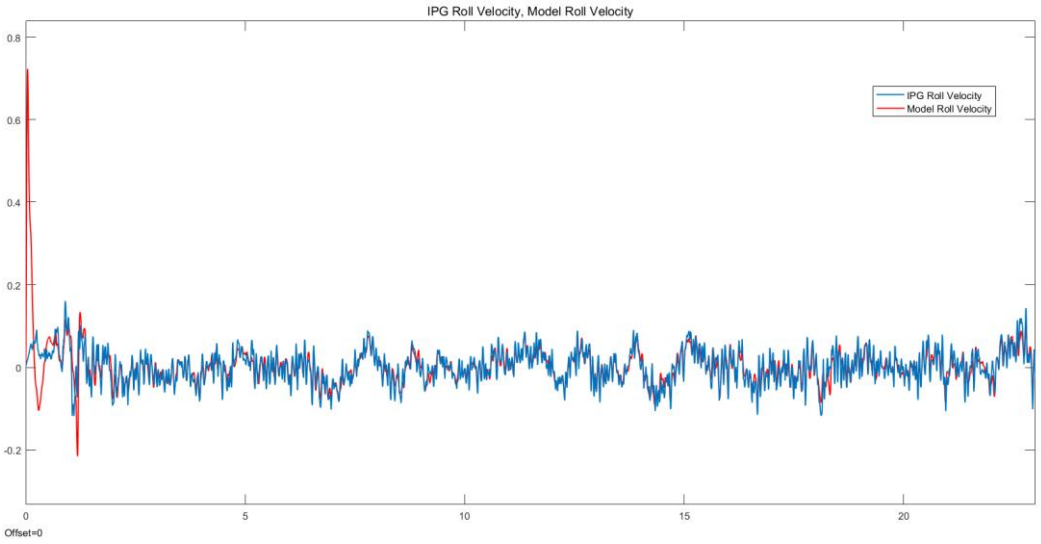

Figure 2.6: Validation of vehicle model: roll velocity.

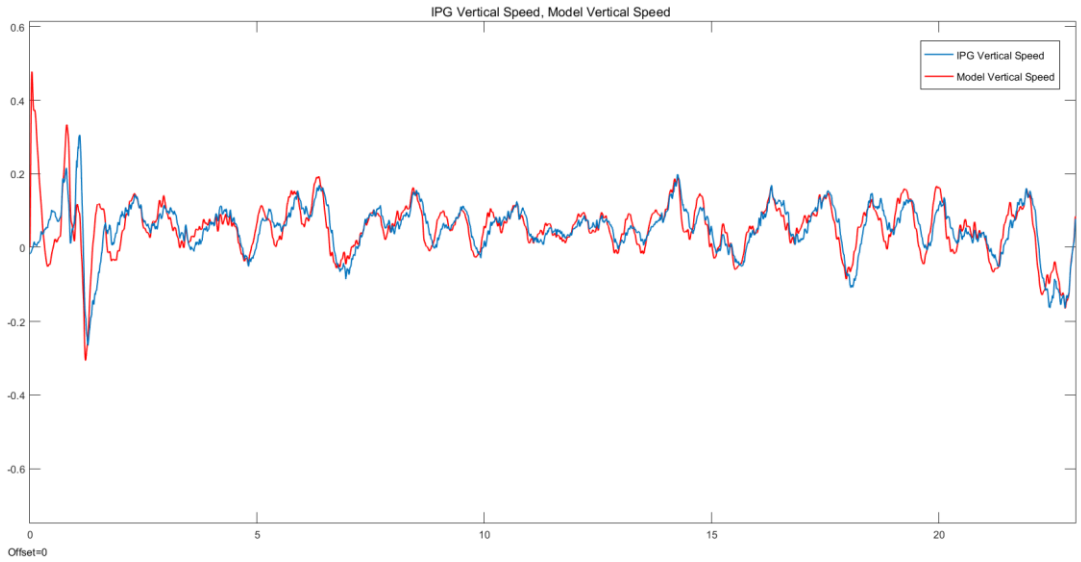

Figure 2.7: Validation of vehicle model: vertical speed.

2.9 Implementation Of Suspension Control Methods In The Full Car

The suspension system has a complex kinematic structure, and its complexity varies according to the axle type. On the other hand, the quarter car model approach used in modelling reduces the three-dimensional interconnected wheel and body motion to two DoFs, generally. Therefore, the relationship between body, wheel and stroke motions can be easily investigated. This is the reason that the quarter car has widely been used to investigate the response of the vehicle system. Moreover, most of the semi-active suspension control policy has been developed or represented by the quarter car model, but some control policies developed based on optimality are not suitable for use with global control logics. Because they operate with maximum, minimum and some intermediate damping coefficients. On the other hand, the output of the global control logic is force, not damping, hence it cannot be used in control policies. But it is also possible to think of a vehicle as four quarter car, i.e., the full car model is divided into four and each part can be controlled independently (Ahmadian and Blanchard, 2008). Therefore, a "four quarter car" approach was used for vehicle implementation especially for "optimal" control policies (Buyukkopru et al., 2022a).

If a control policy allows the use of force instead of damping, it is possible to apply the global control force requests to each actuator. For instance, continuously variable damping allows an infinite number of damping, can be used in the global frameworks, and the global control output can be distributed to the actuators.

- *Centralized and decentralized Control Approach*

Recently, vehicles have sophisticated chassis control systems to improve vehicle stability, handling and comfort. Some examples of well-known chassis control systems are vehicle stability control (VSC), Active suspension system (ASS), Semi-active suspension system (SAS), electrical power assisted steering system (EPAS), four-wheel steering control (4WS), and four wheel-hub motor control. These control systems have been developed by different suppliers to control different components for different objectives or functionalities. Moreover, these systems operate independently of each other and cause parallel vehicle control architecture. Therefore, since vehicle motions in vertical, lateral and longitudinal directions are inherently interconnected, it is inevitable for such systems to experience interaction and performance conflicts (W. Chen et al., 2016).

2.9.1 Four quarter car approach

Simplicity is the main reason for using the well-known quarter car model, so it is easy to define a relationship between sprung and unsprung masses. Therefore, most of the rule-based control approaches, particularly optimal ones, have been developed based on the quarter car model. However, the quarter-car model-based control application does not allow the vehicle to be controlled around the CoG, moreover, each corner of the vehicle must be controlled locally, which means the decentralization of the control action. Also, (Hac and Brook, 1994) introduced decentralised controller to decouple vehicle body dynamics (slow dynamics) and unsprung mass dynamics (fast dynamics) even in 2 DoF quarter car model to reduce computational effort. A Recent study, called region-free (regionless) explicit MPC, also used decentralized architecture to reduce computational cost, controller generation time, memory requirements and implementation complexity (Theunissen et al., 2020). On the other hand, even though the decentralized approach allows the control logic development and computational requirements can be satisfied efficiently, it can be quite difficult to prioritise one motion over another. For instance, assuming that a vehicle is decelerated by the adaptive cruise control system while cornering and is simultaneously subjected to body roll and pitch motions; in this case, it is an open question which motion must be predominantly suppressed for the non-prioritized option. A typical decentralized suspension control block diagram can be seen in Figure 2.8. Individual controllers in

blue, executes the control action based on the measured outputs of each corner, as shown in Figure 2.9, then the control force requests, $Fd_{i,j}$, are transmitted to the actuators to produce the output forces $Fd'_{i,j}$.

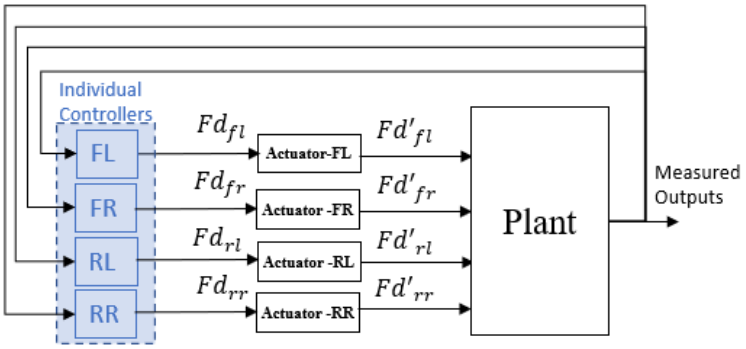

Figure 2.8: Decentralized Approach: Four quarter car control.

Controlling the ride dynamics affects the handling dynamics. Controlling the vehicle roll in corners will affect lateral dynamics because normal forces on the tyres are changed by lateral load transfer and actuator interventions, active or semi-active suspension, on each tyre. Therefore, the longitudinal and lateral force generation capacity of each tyre will be affected. Vehicle handling characteristics will change, indirectly, i.e., from oversteer to understeer or vice versa. The same situation may occur as the decentralized control approach aims to reduce undesired motion of the body in its control zone, which is a quarter of the vehicle.

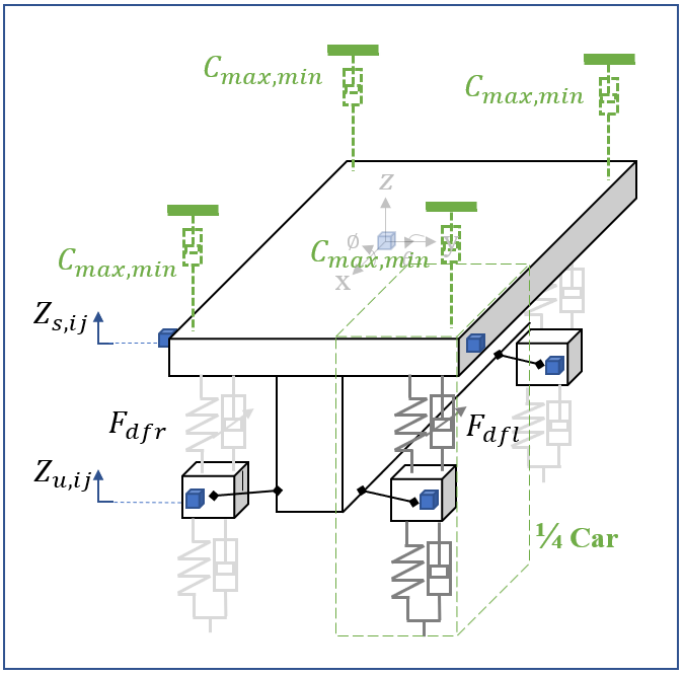

Figure 2.9: Four quarter car control-decentralized control.

2.9.2 Global control approach of suspensions

Today, vehicles have made impressive progress towards autonomous vehicle technology, with the inclusion of environmental sensing systems. As a result, while comfort requirements change (Iskander et al., 2019), comfort expectations also change, autonomous vehicle users want to have leisure time in the car while travelling (Correia et al., 2019). Therefore, it will be a significant advantage for a vehicle to have proactive vertical control concepts by knowing the upcoming road inputs in order to adapt itself appropriately to the vehicle trajectory. Proactive adaptation of the vehicle also includes the possible consequences of future manoeuvres, such as future roll motion as an output of vehicle cornering. Therefore, execution of proactive high-level controller requires global control approach to control vertical motions. There are some studies conducted the motion sickness reduction of the vehicle by considering the future trajectory (Jurisch, 2021). In the centralized control approach, the high-level controller-1 calculates the restoring forces, F_z, and moments, M_θ and $M_\emptyset$, around the CoG. The calculated forces and moments are distributed to the actuators by the Input Decoupling Transformation (IDT) as shown in Figure 2.10. If the controller has multi-input-multi-output (MIMO) capability, the force distribution can be done on its own. MPC can handle difficulties in control design of MIMO systems.

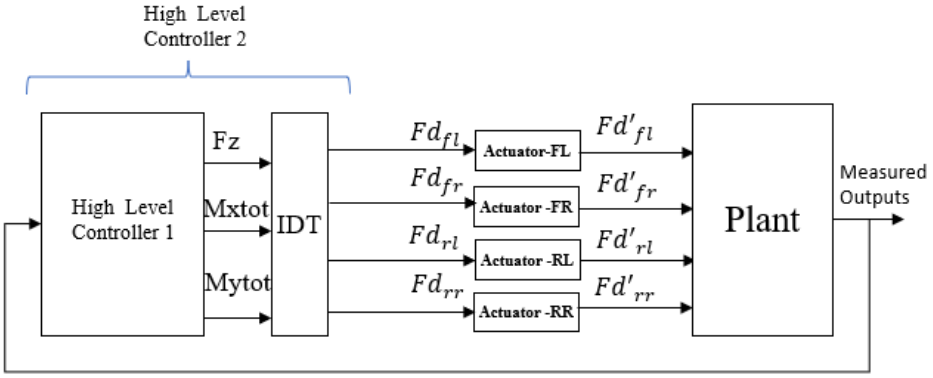

Figure 2.10: Centralized suspension control.

The full vehicle model in Figure 2.11 has four control inputs as Fd_{fl}, Fd_{fr}, Fd_{rl}, Fd_{rr}. Considering the control of the four unsprung masses in addition to the body motions points to the problem of under-actuation problem due to the number of actuators and the control variable. This problem was solved by excluding the control of the unsprung mass. The unsprung mass control problem can be solved externally, for example, by groundhook control. Hence, a four-input three-output control problem was obtained.

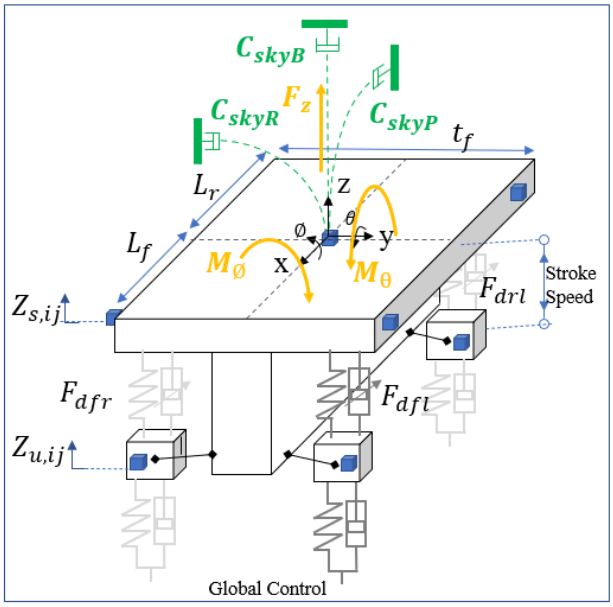

Figure 2.11: Global Control Strategy for SH continuous.

Measured outputs were bounce, pitch and roll velocities multiplied by continuous SH gains in Equations from 2.57 to 2.59.

$$F_z = C_{skyB}\,\dot{Z}_s \tag{2.57}$$

$$M_\theta = C_{skyP}\,\dot{\theta} \tag{2.58}$$

$$M_\emptyset = C_{skyR}\,\dot{\emptyset} \tag{2.59}$$

Equivalent forces and moments for bounce, pitch and roll motions are defined in Equations 2.60, 2.61 and 2.62 based on their geometrical relationships. L_f, L_r and t_f are the distance of front and rear axles to the CoG and the front axle width, respectively. For simplicity, it is assumed that the rear and front axle widths are equal.

$$F_z = -Fd_{fl} - Fd_{fr} - Fd_{rl} - Fd_{rr} \tag{2.60}$$

$$M_\theta = L_f.Fd_{fl} + L_f.Fd_{fr} - L_r.Fd_{rl} - L_r.Fd_{rr} \tag{2.61}$$

$$M_\emptyset = 0.5\,t_f\,(-Fd_{fl} + Fd_{fr} - Fd_{rl} + Fd_{rr}) \tag{2.62}$$

The equations 2.60, 2.61 and 2.62 were written in matrix form in equation 2.63.

$$\begin{bmatrix} F_z \\ M_\theta \\ M_\emptyset \end{bmatrix} = \begin{bmatrix} -1 & -1 & -1 & -1 \\ L_f & L_f & -L_r & -L_r \\ -0.5\,t_f & 0.5\,t_f & -0.5\,t_f & 0.5\,t_f \end{bmatrix} \begin{bmatrix} Fd_{fl} \\ Fd_{fr} \\ Fd_{rl} \\ Fd_{rr} \end{bmatrix} \tag{2.63}$$

The linear equations $\mathbf{y}=\mathbf{W}\mathbf{x}$ and $\mathbf{W}\in R^{\mathbf{mxn}}$ have full row rank, in which the right inverse (pseudo-inverse) can be calculated a$\mathbf{W}^{\dagger}$=s $\mathbf{W}^{\mathbf{T}}(\mathbf{W}\mathbf{W}^{\mathbf{T}})^{-\mathbf{1}}$. Thus, the Equation 2.63 can be transformed to Equation 2.64.

$$\begin{bmatrix} Fd_{fl} \\ Fd_{fr} \\ Fd_{rl} \\ Fd_{rr} \end{bmatrix} = \begin{bmatrix} \frac{-L_r}{2(L_f+L_r)} & \frac{1}{2(L_f+L_r)} & -\frac{1}{2t_f} \\ \frac{-L_r}{2(L_f+L_r)} & \frac{1}{2(L_f+L_r)} & \frac{1}{2t_f} \\ \frac{-L_f}{2(L_f+L_r)} & -\frac{1}{2(L_f+L_r)} & -\frac{1}{2t_f} \\ \frac{-L_r}{2(L_f+L_r)} & -\frac{1}{2(L_f+L_r)} & \frac{1}{2t_f} \end{bmatrix} \begin{bmatrix} F_z \\ M_\theta \\ M_\emptyset \end{bmatrix} \tag{2.64}$$

(Campos et al., 1999; Ikenaga et al., 2000) first proposed IDT for active suspension control. Then it was extended to the global continuous SH control (Buyukkopru et al., 2021). IDT is pseudo inverse and can also be defined as unconstrained control allocation. There are also some studies using control allocation with optimisation and

quadratic programming to distribute forces to actuators while considering actuator constraints (Binder and Khajepour, 2014; Schofield and Hägglund, 2008).

2.10 Road profile generation2

The road surface directly influences the ride characteristics. Knowing the upcoming road surfaces can significantly improve ride comfort, many studies have been done to estimate the road surface; some make use of accelerometers where sensor measurements are evaluated and then an idea of the road characteristic can emerge (González et al., 2008; Wen, 2008; Yang et al., 2022). These studies can be considered as vibration-based approaches. Most approaches use vibration signals to define frequency content as they can be constrained to certain frequency bandwidths and then RMS values or amplitudes can be compared with each other. Vibration based approaches inherently provide an understanding of the road surface after passing over a pothole or uneven surface. In this way, a road characteristic can be defined after some accumulation period and this period is an unused gap without automatic control action. However, individual road roughnesses such as pothole or bump may need to be subtracted from the accumulated data prior to evaluation to statistically exclude their effect on the data (Ward and Iagnemma, 2009). Moreover, individual shocks can affect ride comfort directly and without taking an action. On the other hand, if the road surface can be measured in the preview, the time gap can be used to improve the comfort level. At this point, preview control logics can be introduced with the recently developed sensing devices such as lidar and camera. These devices make it possible to measure the road surface before the vehicle passes through its trajectory(Gong et al., 2019; Oniga et al., 2007).

Streiter was one of the first researchers to propose road profile generation study for preview control of the vehicle body (Streiter, 2008). Then, Schindler introduced the lidar sensor to have preview information. In his study, a regression analysis method was developed to construct the road profile from the point cloud of lidar and the least squares approach was used to match the consecutive sensor measurements (Schindler, 2009a). In another study, a compact ADAS Lidar was placed in front of the radiator

[2] Some of work presented in the road profile generation chapter were published with the article (Buyukkopru et al., 2022b)

grill, and the scanned raw data was converted into a road profile with statistical and deterministic sensor models (Bouzouraa et al., 2014). Gong et. al used gyro near the lidar to compensate for the variation between consecutive measurements. Noise was removed and the dense point cloud was interpolated to generate a road profile for recognition of the off-road profile(Gong et al., 2019). Ego motion is an important parameter for aligning consecutive measurements, because change of sensor orientation with respect to the road surface is inevitable. Optimal fitting of consecutive images of a camera allows for estimation of ego motion, as does the least squares approximation of consecutive measurements and the use of gyro (Stein et al., 2000; Wu et al., 1995).

Göhrle et al. used a stereo camera to specifically recognize the low frequency and long wavelength road profile. In this study, as with Schindler's approach, two consecutive measurements were used to align the actual and previous approach. This author also used statistical approaches such as maximum-likelihood and probability density functions to estimate the probable mean of several measurements of a point in a measurement window (Göhrle et al., 2015)

Mercedes-Benz has introduced the Magic Body Control based on Active Body Control with a changing laser sensor with stereo Camera in serial production for the S-Class. In the study, road surface scanning was performed with a stereo multi-purpose camera placed on the windshield. The scan of this camera was accumulated during every 60.3ms and the camera was able to scan the front of the vehicle up to 15m and the accumulated measurements were statistically evaluated to improve the accuracy of the scan. However, the details of the method have not been disclosed, publicly (Weist et al., 2013). Deigmoeller et al. of Honda, conducted a study to check the feasibility of detecting bumpy roads with high accuracy in extreme conditions. They also preferred to use a stereo camera, as the monocular approach has limited precision and has higher latency for high speeds than a stereo camera. The stereo camera was able to detect the events in the range of 5mm and 3 cm with a low false positive rate of 2.5% for the speed range of 100-150kph (Deigmoeller et al., 2018).

The scanning quality of a camera's road surface depends on the texture, lighting reflectance of the road, weather conditions and ego motion. Studies also showed that accuracy of the road profile generation decreases proportionally with measuring distance (Shen et al., 2014). Therefore, confidence values were assigned to each pixel

or a group of pixels to compare the measurement with the ground truth (Hu and Mordohai, 2010). (Pfeiffer et al., 2013) The literature includes many ways to calculate the confidence of camera measurements, such as the left-right difference and Naïve peak ratio (Hu and Mordohai, 2012). Thus, statistical methods can be used to reduce the impact of less confident measurement, if any, in order to have a more reliable road profile.

- *Expected Sensor Output: The road profile*

If the road profile recognition procedure by the cameras is handled in two steps, the first step is image processing and elevation profile creation, and the second step is the conversion of the obtained elevation data to the road profile. The literature has mostly been conducted on the image processing step to obtain a height profile. Information on how to effectively combine height profile data to create a road profile is extremely limited (Buyukkopru et al., 2022b). Recent research has also highlighted the lack of research on the effect of road information on the performance of a preview controller (Theunissen et al., 2021). Suspension control studies in the literature mostly assume excellent sensor measurements for road information. In fact, the camera measurement can have significant errors like any other imperfect measurement.

The control target, i.e., the actuator bandwidth, usually gives an idea of the preview information requirement level. For example, the control bandwidth of industrial slow-active suspension systems is around 4 Hz, which covers dominant vehicle body motions. For this purpose, research has been carried out to provide necessary and sufficient preview information. On the other hand, if the actuator control bandwidth is greater than 4 Hz, as in full active suspension or semi-active damper applications, having more accurate preview information provides significant advantages in control. In this chapter, our motivation is to focus on short-range and high-frequency road profiles as well as low-frequency content. Due to the dissipative constraint, the semi-active damper does not allow control under all conditions. In these cases, since the damper is not energized, changing the damping coefficient can reduce oscillation or prevent underdamped results.

Accurate detection of a singular object is also quite important for accurate control. Speed bumps are an example of a singular object, and there are various types of speed bumps. Since their dimensions and geometries are different, their effects on the vehicle

are also different. For this reason, the control applied must be specific to each case. Incorrect estimation can damage the suspension system in case of low damping or untimely parameter change.

A sensor (camera or lidar) located at the front of the vehicle for preview control affected by body movement as the vehicle body rotates around CoG or roll and pitch centres. The sensors are not referenced with respect to the earth reference frame. Indeed, they are fixed to their own frame of reference and hence to the vehicle reference frame. As the vehicle moves on the road, the road profile is positioned below or above the reference plane as shown in Figure 2.12. The reference plane of the sensor is the imaginary line passing through the road contact points of the rear and front wheels.

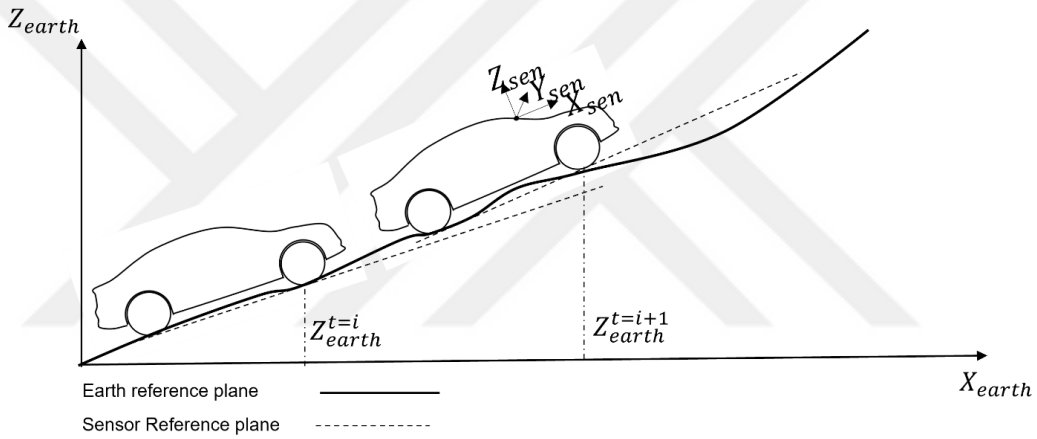

Figure 2.12: Vehicle and sensor reference systems.

As mentioned above, the vehicle body is suspended by springs and dampers, therefore, the sensor is translated (in the Z axis) and rotates relative to the centres of rotation. The sensor measures a certain distance (with multiple measurement points) from the road surface instead of a single point. This means that the same location on the road surfaces is measured redundantly as the vehicle moves forward. Therefore, previous and current measurements can be interrelated, at each time step. This interrelationship can be very helpful in reducing sensor noise, which will be discussed later. It also helps correct sensor position changes caused by vehicle body translations and rotations. The linear regression method can be used to match two successive measurements (Göhrle et al., 2015; Schindler, 2009a).

As seen in Figure 2.13, the same or very close points on the road are measured more than once. Therefore, the new measurement overlaps with previous measurements. As an advantage, multiple measurement of the same point can be used to reduce sensor noises.

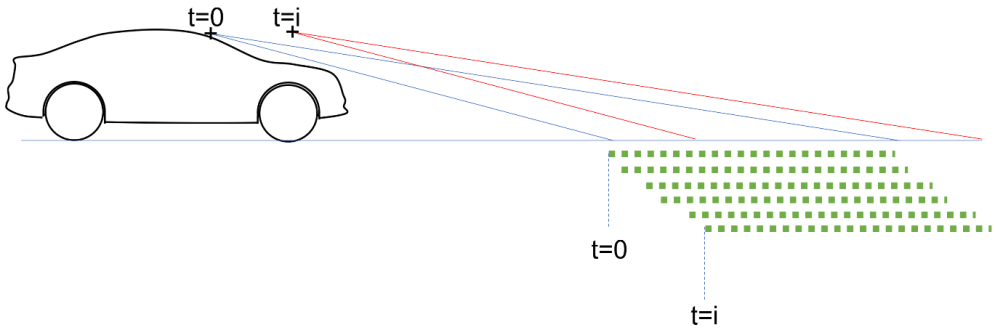

Figure 2.13: Sensor location and sensor measurement on the road profile between time t=0 and t=i.

- *Measurement Point Alignment*

The sensor at the windshield scans a certain area and produces a predefined number of measurement points. Even if the vehicle speed changes, the predefined number of measurement points is fixed. It should therefore be understood that the relationship of the measuring points to each other depends on the vehicle speed. The distance between two successive points can be expressed by Equation 2.65.

At the time t_j, the distance between the points X_i andX_{i+1} is

$$|X_i - X_{i+1}| = V_j \cdot \Delta t \qquad (2.65)$$

As a constant, Δt is the processing time, and Z_i is the road height at point X_i. The vehicle speed varies in each measurement instance, which means that the distribution of measurement points in an instance is not uniform. Also, the sensor position shifts forward as the vehicle moves. This moves the initial point of the following measurement forward. In such cases, the points in the same measurement set need to be aligned and measurement sets need to be positioned with each other. The measurement points in the point cloud can be seen in Figure 2.14.

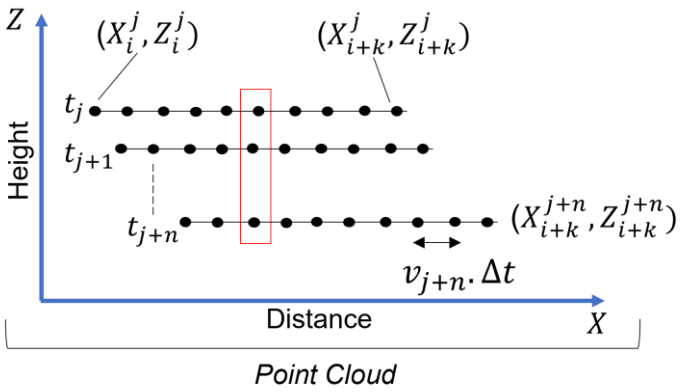

Figure 2.14 : Measurement points in the point cloud.

The above-mentioned measurement set positioning is only possible when the measurement sets are corrected relative to each other. Measurement set matching can be done by image processing with linear regression or ego motion estimation before generating a road height profile (Göhrle et al., 2015; Stein et al., 2000).

- *Sensor Noise Reduction*

The same or very close points on the path are measured multiple times. The position of the points with respect to the sensor and the distance between the points are known. But those points may be partially nonuniformly scattered throughout the scanned area. The term, "Partially", refers to the fact that vehicle speed changes the density of the points in a region. For this reason, some places are dense, while others are finely measured.

It is known that the camera produces a confidence value for each measurement point. If the same points or two very close points are measured fairly frequently, confidence values can be used to weight more accurate measurements. On the other hand, how to distinguish the same or closer points in a different set of measurements is an open question.

Assuming for now that the points are vertically concentric, basically the weighted arithmetic mean can be used to calculate the probable location of the height values. It is obvious that the spacing of the successive points increases for higher speed. Under the assumption that known standard deviations increase with distance, a more complex statistical approach, such as maximum likelihood estimation, can be used (Göhrle et al., 2015).

$$\bar{Z}=\frac{\sum_{i=1}^{n}\omega_i.Z_i}{\sum_{i=1}^{n}\omega_i} \quad (2.66)$$

Simple weighted arithmetic mean was applied to obtain most probable road height, $\bar{Z}$, given in the Equation 2.66. Weighting factors were selected according to the confidence values of the points. Weighting factors are $\omega_i=\{\omega_1,\omega_2,.....,\omega_n\}$ and for $\omega_i>0, Z_i=\{Z_1,Z_2,.....,Z_n\}$ are the measured heights of each of the points.

- *Density Based Spatial Clustering of Applications with Noise (DBSCAN)*

The measured points in the point cloud are sorted from the first point to the last point according to the measurement start position. Sorting is required to find the most probable height. Therefore, the points are segmented to determine the points to be averaged. Also, the literature in this field is quite limited, and Göhrle's study appears to be the only study in which the windowing approach was used prior to this PhD study (Göhrle et al., 2015; Schindler et al., 2019). For example, a for loop can be used to group these points into cells for a fixed window length. The window length determines the resolution of the output profile, as shown in Figure 2.15. If the length is too short, the number of iterations increases the processing time. Otherwise, a window length that is too long can reduce resolution while reducing processing time. The windowing approach does not take into account the proximity of points, and some windows may have more points than others, and these deviations may cause additional complexity in the signal, which is a redundant junction (Buyukkopru et al., 2022b). If the distance between points close to each other in the horizontal direction is less than the theoretical minimum distance of the two points that the camera can produce, the road signal may contain additional noise. These redundant junctions cause relatively high frequency artificial noise due to process. For this reason, the necessity of grouping the points appropriately has emerged. At this point, DBSCAN is a powerful algorithm that allows clustering of points due to their position in a plane. DBSCAN has the ability to identify points as core, neighbour, and noise (Ester et al., 1996). The points to be statistically averaged or merged, can be grouped with this algorithm.

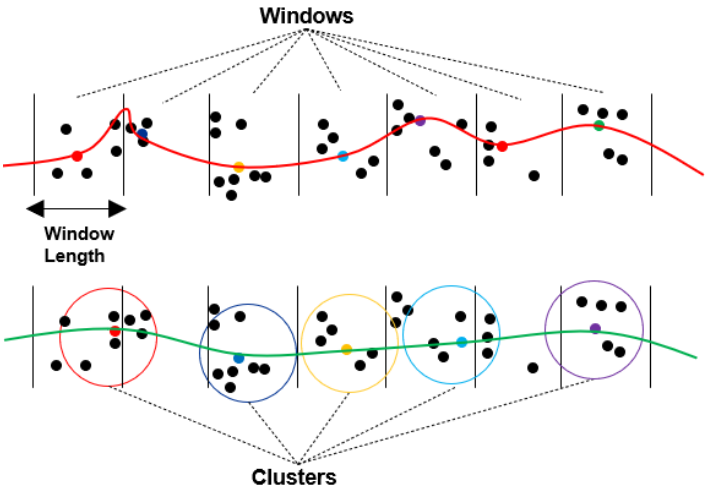

Figure 2.15: Windowing approach and DBSCAN comparison.

This technique first checks the proximity of all points and then determines the core points. Then, neighbouring points are defined around the core points within the radius (ε) for the neighbourhood range and the minimum point threshold. If the neighbours are defined around the core point, the points outside the circle are defined as noise. It should be noted that the point outside the circle is also outside the circles of the other clusters. Finally, clusters are labelled and at the same time noise and neighbouring points are assigned by the DBSCAN algorithm as in Figure 2.16.

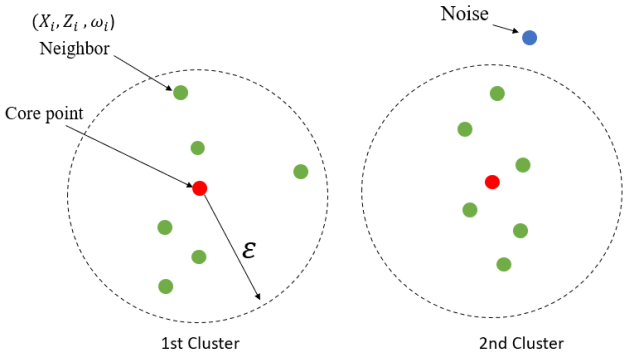

Figure 2.16: Different length measurements in X and Z directions with DBSC clustering.

The pseudo code of original DBSCAN is given in the Table 2.3 (Schubert et al., 2017)

Table 2.3 : Pseudocode of original sequential DBSCAN algorithm.

Line	Pseudocode
	Input: DB: Database
	Input: ε: Radius Input: minPts: Density threshold
	Input: dist: Distance function
	Data: label: Point labels, initially undefined
1	**foreach** point p **in** database DB do // Iterate over every point
2	**if** label(p) undefined **then continue** // Skip processed points
3	Neighbours N ← RangeQuery(DB, dist,p,ε) // Find initial neighbours
4	**if** |N | < minPts **then** // Non-core points are noise
5	label(p) ← Noise
6	**continue**
7	c ← next cluster label // Start a new cluster
8	label(p) ← c
9	Seed set S ← N \ {p} // Expand neighbourhood
10	**foreach** q in S **do**
11	**if** label(q) = Noise then label(q) ← c
12	**if** label(q) undefined then continue
13	Neighbours N ← RangeQuery(DB, dist,q,ε)
14	label(q) ← c
15	**if** |N | < minPts then continue // Core-point check
16	S ← S ∪ N

2.11 Data acquisition and sensors to measure body movements and stroke speed

As briefly introduced in the sensor section, vehicle motions can only be measured with accelerometers and stroke sensors. Accelerometers are noisy. Thus, proper filtering should remove bias and drift in the sensor, as acceleration must eventually be converted to velocity. An additional filter can be designed as the sensor exceeds the relatively broad spectrum of frequencies more than the controller can. A high pass filter can reduce the slope effect of the road, drifting and sensor's bias. A low pass filter can then be used, acting as an integral to convert acceleration into velocity. An advantage of the low pass filter is that the phase of the signal is less than integral and can be tuned to the desired frequency. A typical first order HPF and LPF can be seen in Figure 2.17.

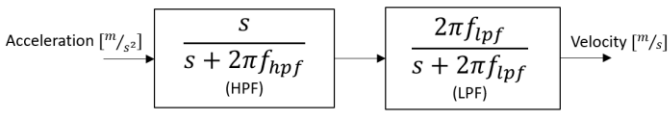

Figure 2.17: Basic filter design for transformation of acceleration into the velocity.

Two accelerometers placed on the sprung and unsprung mass can, as a product of subtracting the two sensor, give the acceleration, velocity of the sprung mass and the acceleration, velocity and stroke speed of the unsprung mass. The subtraction and stroke speed calculation must consider the motion ratio of suspension geometry for the front and rear.

3. SIMULATIONS AND TESTS

3.1 Road Profile Generation With Monocular Camera

A monocular prototype camera, as shown in Figure 3.1, was used to collect road profile data from the proving ground at the Renault test centre. The camera had a 100° field of view and 1820 x950 pixels. Vehicle speed during these tests ranged from 15kph to 44kph.

Figure 3.1: Test vehicle equipped with monocular camera.

The first track includes concrete slabs placed side-by-side. The mean confidence value was greater than 3 in the range of 0 to 5. The camera scanning was stored in a data logger, and then the data was processed offline. It should be noted that the scanned surface distance is limited to a few meters. Scanned surfaces are collected cumulatively as the camera scans continuously after the threshold vehicle speed is exceeded. Therefore, the graphs show some parts of the total measurements, without providing information for a single measurement length. It is worth reminding that the generated road profile does not have road elevation since it is built based on the vehicle reference system. The raw measurement was processed to compare the DBSCAN and windowing approaches. Eps, ε, value and window length were set to 0.015m and 0.005m, respectively. The minpths value for DBSCAN was set to 2. The results of the first track can be seen in Figure 3.2 and DBSCAN produced smooth profile compared

to the windowing approach. It can be clearly seen that windowing approach can cause artificial noises as in the detailed view of Figure 3.2.

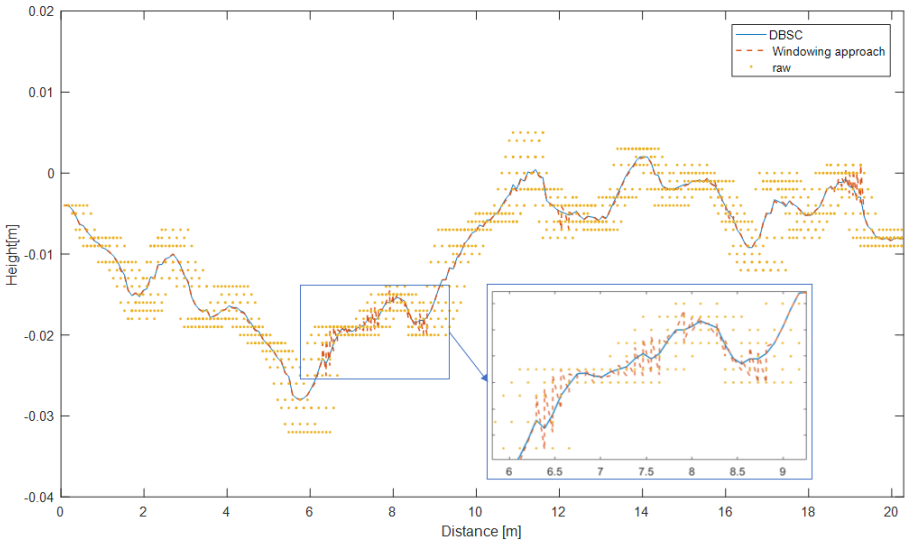

Figure 3.2: Test track concrete blocks, DBSC and windowing approach comparison, ε =0.015 minpts=2, window length=0.005m on the LH wheel trajectory.

In Figure 3.3, some process noise is clearly visible as a result of the windowing approach. It can be seen that the distance between the points increases depending on the sudden changes on the measured surface shape. The fixed length windowing approach causes a sudden change in profile at 14m. Low amplitude process noise can also be seen in the entire profile in the detailed view in Figure 3.3.

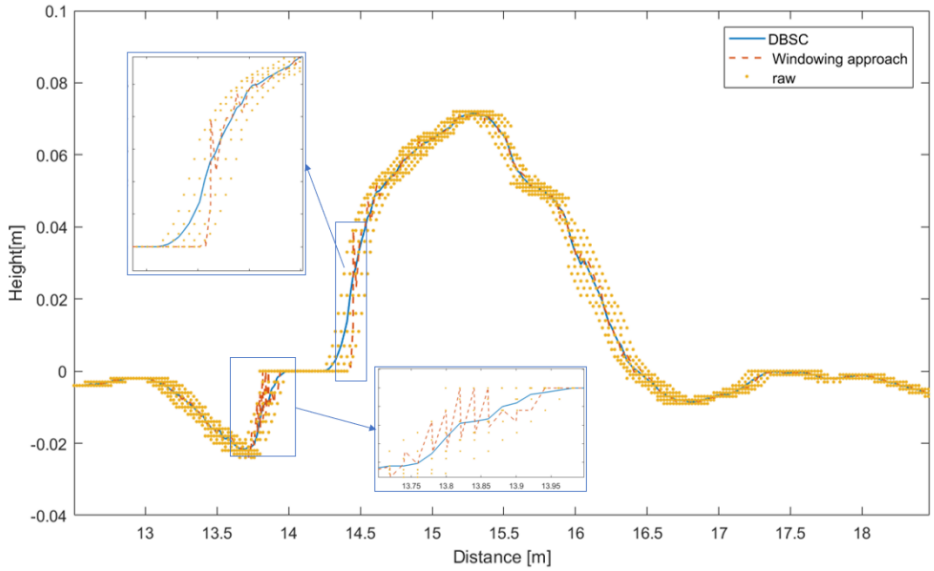

Figure 3.3: Test route speed bump, DBSC and windowing approach comparison, ε =0.015 minpts=2, window length=0.005m for a speed bump on the LH wheel trajectory.

The main problem was aligning and arranging the points based on their confidence values to find the most probable height. Camera accuracy causes deviations in height measurements. The use of DBSCAN reduced processing noise and detection of high frequency road profile contents without any additional filtering and signal loss.

A window length of 0.005m was chosen by trial-and-error method to obtain accurate results. A larger value will significantly reduce the detection accuracy. However, this value can be determined by averaging the distances between the points in the point set. On the other hand, minpts must be chosen at least two. Another point of DBSCAN was the determination of the radius, ε. If the radius is not small enough, the accuracy of the profile will decrease. However, if it is too small, the number of clusters will be increased, which may increase the computational cost. The radius can be determined by averaging the distances in the x and y directions in the point cloud. Since the points are generated as a result of the vehicle instantaneous speed, the radius ε can be formulated as a function of the vehicle speed. DSBCAN has a significant advantage over the windowing method as it produces the signal smoothly and uses the elements of the signal by connecting them in a more natural way. On the other hand, the significant drawback of DBSCAN is the computational cost, as the preview control requires fast computation. The resolution of a camera available and the resolution and computational time requirement in a specific road surface scanning application give an insight of which method is to be preferred.

3.2 Actuator Properties And Control

The output of the controller is the force or damping coefficient in high-level control. However, actuators can be controlled by current and voltage in general. Therefore, the force or damping request must be converted to current or voltage. In this study, the semi-active damper was electro-hydraulic type, and the valve could be controlled by current. The damper force depends on both the stroke speed and the damping coefficient provided by the valve. The semi-active force - stroke speed curve is highly nonlinear and continuously variable with an infinite number of damping. On the other hand, linearization causes significant amount of error. It was decided to use maximum (F_{max}) and minimum (F_{min}) curves to calculate the equivalent current based on the force requested ($F_{request}$) at a given time by using equations 3.1 to 3.3. Thus, the force was calculated by determining the position of the requested force on the force-stroke speed map, as shown in Figure 3.4.

$$I=f^{-1}(F_{d,}\dot{Z}_s-\dot{Z}_u) \tag{3.1}$$

$$I_{control}=\frac{F_{request}-F_{min}}{F_{max}-F_{min}}(I_{max}-I_{min})+I_{min} \tag{3.2}$$

$$I_{max}\geq I_{control}\geq I_{min} \tag{3.3}$$

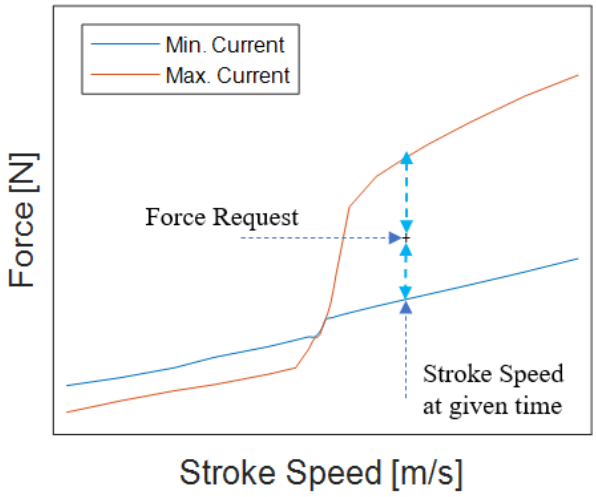

Figure 3.4: Semi-active damper stroke speed and force curve – front.

Stroke speed, extension-compression condition, and amount of instantaneous force request are the parameters that affect the actuator delay. When the settling time is

examined; Although the time to reach 90% of the damper force occurs at different lag values in the compression and expansion regions with different speeds of the damper, it has been determined that the damper generally exhibits 1st order system behaviour. T=10 ms delay is defined as a first-order system to reflect the above average system dynamics.

$$G(s)=\frac{1}{Ts+1} \tag{3.4}$$

3.3 Simulations with Quarter Car and Full Car Model for semi-active suspension[3]

In this section, it is aimed to present the feedback and preview controller performances with and without preview information, particularly in semi-active suspension systems. For this reason, 600m of the CRG road profile was selected and the speed was set to 50 kph. It is worth noting that the selected road profile offers a broad spectrum of road inputs that excite the body, wheels, engine and other body parts. This road profile is a digital version of a test track at the Renault test centre in France. Sinusoidal and ISO profiles are generally used in controller evaluation because the input-output relationship is simple to understand. ISO profiles are stationary even if they include more complex frequency content than sinusoidal inputs (Loprencipe and Zoccali, 2017). Thus, CRG gives a more realistic evaluation compared to simple sinusoidal road inputs or ISO profiles, as both profiles are artificial, stationary and do not contain road slope and non-symmetrical characteristics. Inclusion of a slope and bank angle in the road inputs requires some filters to be designed to remove the effect of slope and bank angle on the sensors, even though the sensors are virtual. In this regard, the slightly delayed filtering result of imperfect sensor data also contributes to a more realistic assessment in addition to the high-fidelity vehicle model. Co-simulation was performed with Matlab-Simulink® and IPG-Carmaker®, and the quarter car and full car parameters are presented in Table 3.1. Note that the CRG road profiles are not symmetrical in the lateral axis. The simulation outputs were sampled at 1 kHz and filtered to ‘window size=15Hz’ with a moving average filter for better readability.

[3] Some of work presented in this chapter were published with the article (Buyukkopru et al., 2022a)

How the front camera can detect the road surface in front of the vehicle is explained in Section 3.1. A similar strategy must be used to represent the strategy of front camera in the simulation environment. IPG Carmaker's library includes a virtual road property sensor that perfectly represents the road surface at the defined position. However, this sensor provides road profile data in the earth fixed reference system which includes the elevation of the road profile. On the other hand, the front camera detects the road surface with respect to the vehicle coordinate system, by aligning the front and rear wheels with the reference line, as described in Section 2.9.

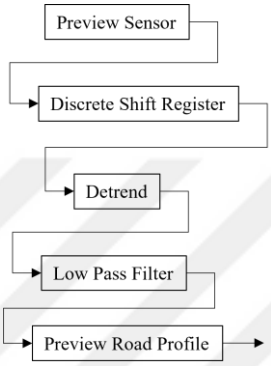

Figure 3.5: Virtual Preview sensor signal conditioning.

The output of the preview sensor was discretised first with the shift register, as shown in Figure 3.5. Then the signals were transferred to the detrend block which removes the linear trend from the certain length of the input vector. The linear trend, straight line was calculated by using least square approximation. Since the raw road profile contains high frequency inputs outside of the control logic, it has been removed using a low pass filter with a cut off frequency of 20Hz. It was aimed that the preview sensor strategy used in the simulation is as close as possible to the front camera road profile estimation strategy. Hence, the converted road profile contained some errors compared to the original data, especially on sloppy sections of the road profile.

Table 3.1: Vehicle Parameters.

Parameters	
Sprung mass	M_s=1500kg (Quarter car M_s=450 kg)
Unsprung mass	M_{uf} = M_{ur}=45kg
Spring constant	k_{sf}=29kN/m , k_{sr}=32kN/m
Anti-roll bar stiffness	k_{rf}=21kN/m k_{rr}=11kN/m
Max and Min. damping coefficient front, rear	$C_{maxf,r}$ =4000Ns/m $C_{minf,r}$ =300Ns/m
Front, rear lower and upper damping force limits at extension - compression	$F_{df,r}$=[-550N,-750N;650N,2500N] F_{dr}=[-1000N,-1500N; 1500N,5000N
Tyre spring constant, damping coefficient	$k_{tf,r}$ =350 kN/m, $C_{tf,r}$ = 1000Ns/m.
Distance between axles and -CoG, and Axle width	L_f=1.1m L_r=1.8m t_f=1.6m

- *MPC and Clipped Approach*

MPC uses a defined vehicle model inside to estimate the future trajectory of model outputs, taking into account multi-input multi-output relationships using Kalman estimators to perform optimal control action. Although a linear vehicle model is used with some acceptable errors, due to the high nonlinearity and passivity constraints of the dampers, nonlinear dampers cannot be considered in vehicle models or as a constraint in quadratic optimization. Therefore, the clipping approach can help design a controller. In this method, the controller is built without considering passivity constraints. The required control force is then transferred to the actuators that can produce the requested force. For this reason, this approach has drawbacks as it is not guaranteed to produce the requested force, and passivity is not considered in the optimization step (S. Savaresi et al., 2010). Consequently, using linear MPC with constant upper and lower constraints, instead of nonlinear passivity constraint as shown in Figure 3.6, can provide a computationally efficient solution.

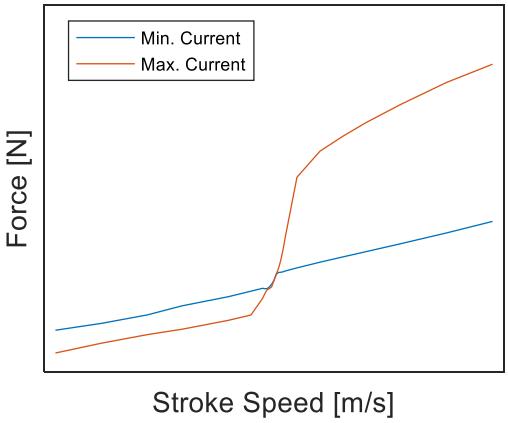

Figure 3.6:Constraints on the damping force of a variable damper.

Another way to incorporate constant linear constraints in the optimization is to use the force-velocity map of the damper to calculate the lower and upper bound, $lb \leq \hat{u} \leq ub$, in each time step. This methodology is known in the literature as the clipped-optimal approach for semi-active suspensions (Göhrle et al., 2013). On the other hand, these methods sometimes give infeasible results since the actuator-dependent lower and upper bounds changes quickly. This is the period of no control for a certain period of time and should be considered in applying appropriate damping to prevent undamped condition as a fail-safe mode. As shown in Figure 3.7, co-simulation was performed in Matlab-Simulink and IPG Carmaker environments. The full vehicle model has 14 states. Matlab active-set solver uses the KWIK algorithm (Schmid and Biegler, 1994).

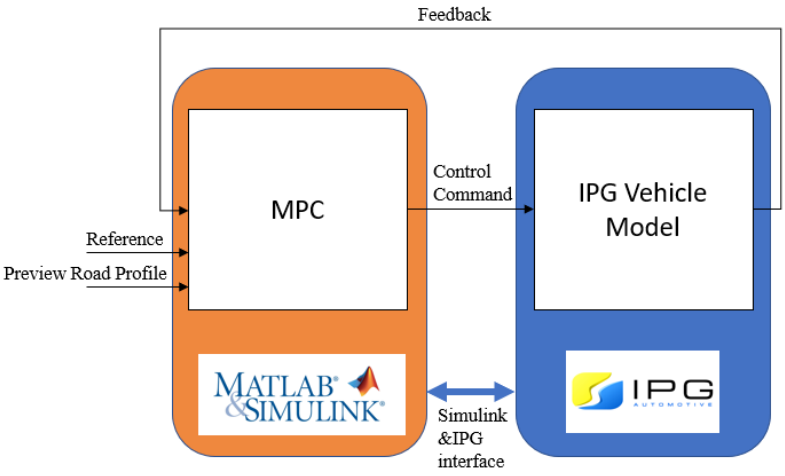

Figure 3.7: Matlab Simulink & IPG Carmaker interface for MPC control example.

- *Rule based control logics and their tuning*

The rest of the semi active suspension controllers desribed in Chapter 2 was also simulated in the Matlab-IPG Carmaker co-simulation. As explained in Section 2.9, some optimally designed methods are not suitable for the global control approach. Therefore, these methods were simulated with the four quarter car approach. All semi-active control methods were compared in terms of performance and also motion priorization capability. It should be noted that SH based approaches are also model-free and there is no need to use a vehicle model.

SH-Continuous gains were tuned to 32 kNs/m (rotational movements kNms/rad) and C_{skyB}=C_{skyP}=C_{skyR} were tuned equally. C_{max} was tuned to 4kNs/m. In fact, there is no developed method to determine the gain of the SH control, but the control force need to be tuned within the capabilities. Otherwise, if excessive gain is set, the system will be overdamped, giving a feeling of discomfort. In a study by Ghasemalizadeh, the optimal SH gain that minimize RMS body acceleration and suspension stroke was determined iteratively by testing gains between 0 and 20kNs/m (Ghasemalizadeh, 2016). The four quarter car approach gains were increased until the best value was obtained thus the best gain was found to be 5 kNs/m.

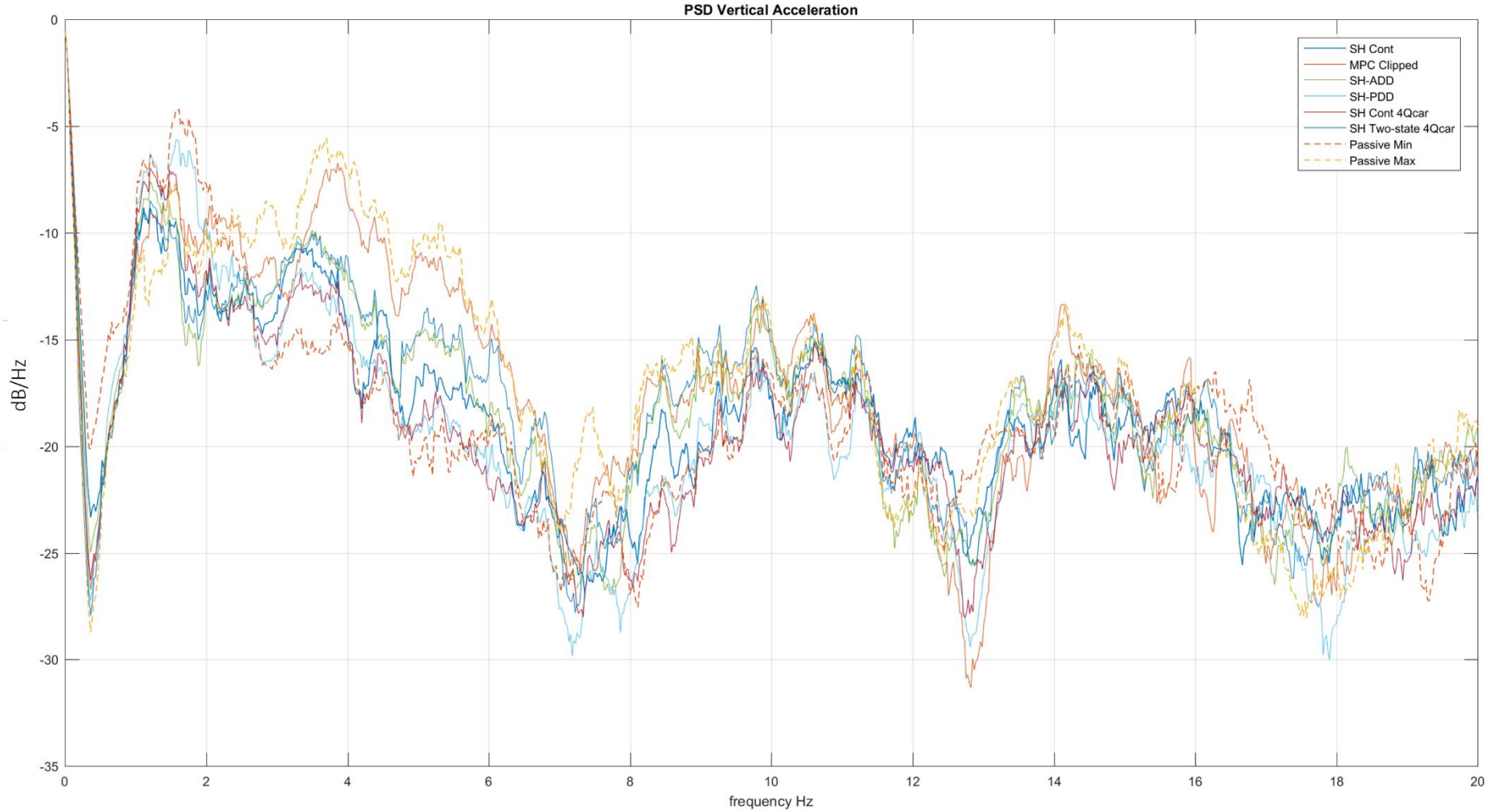

Figure 3.8:PSD of vertical acceleration.

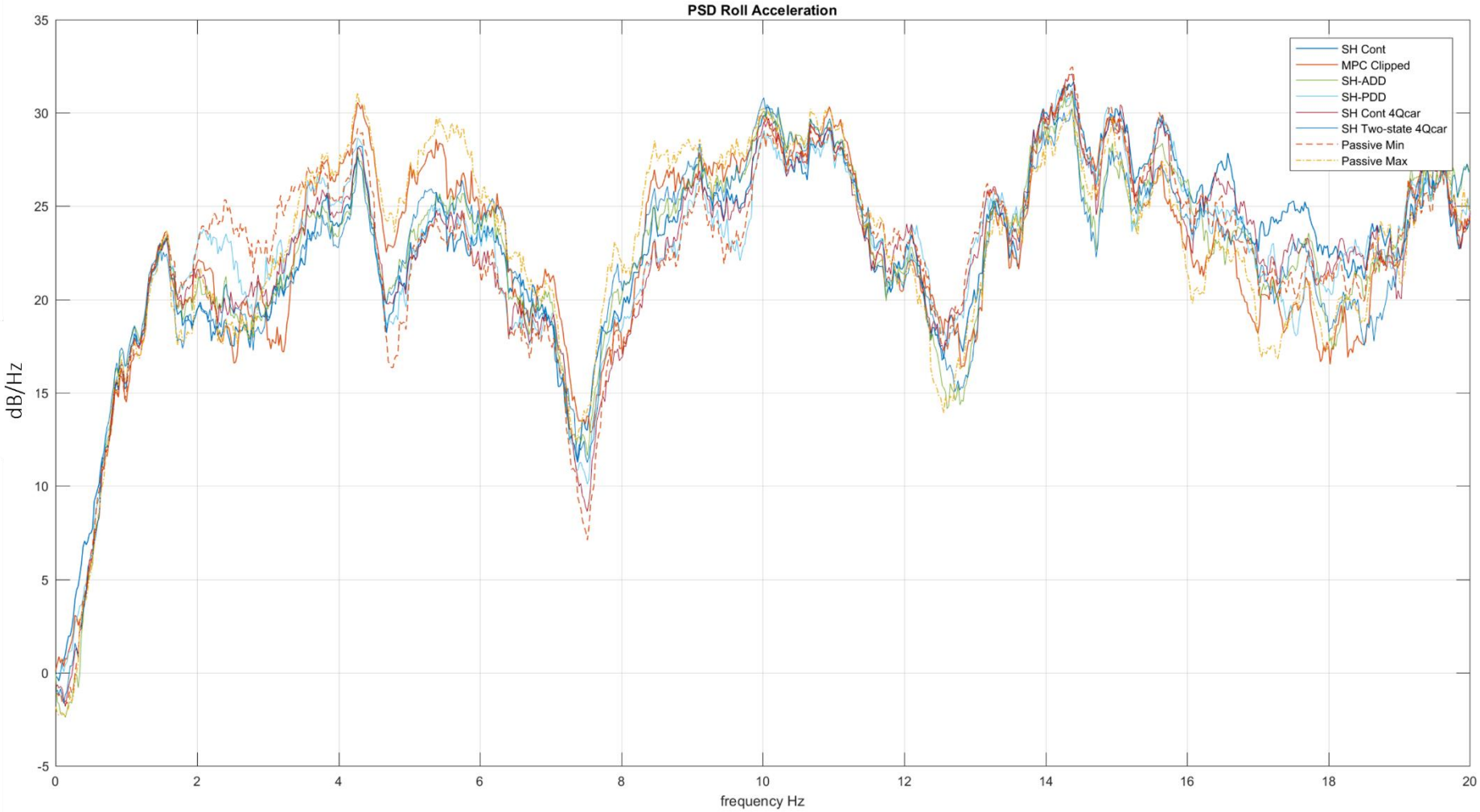

Figure 3.9: PSD of roll acceleration.

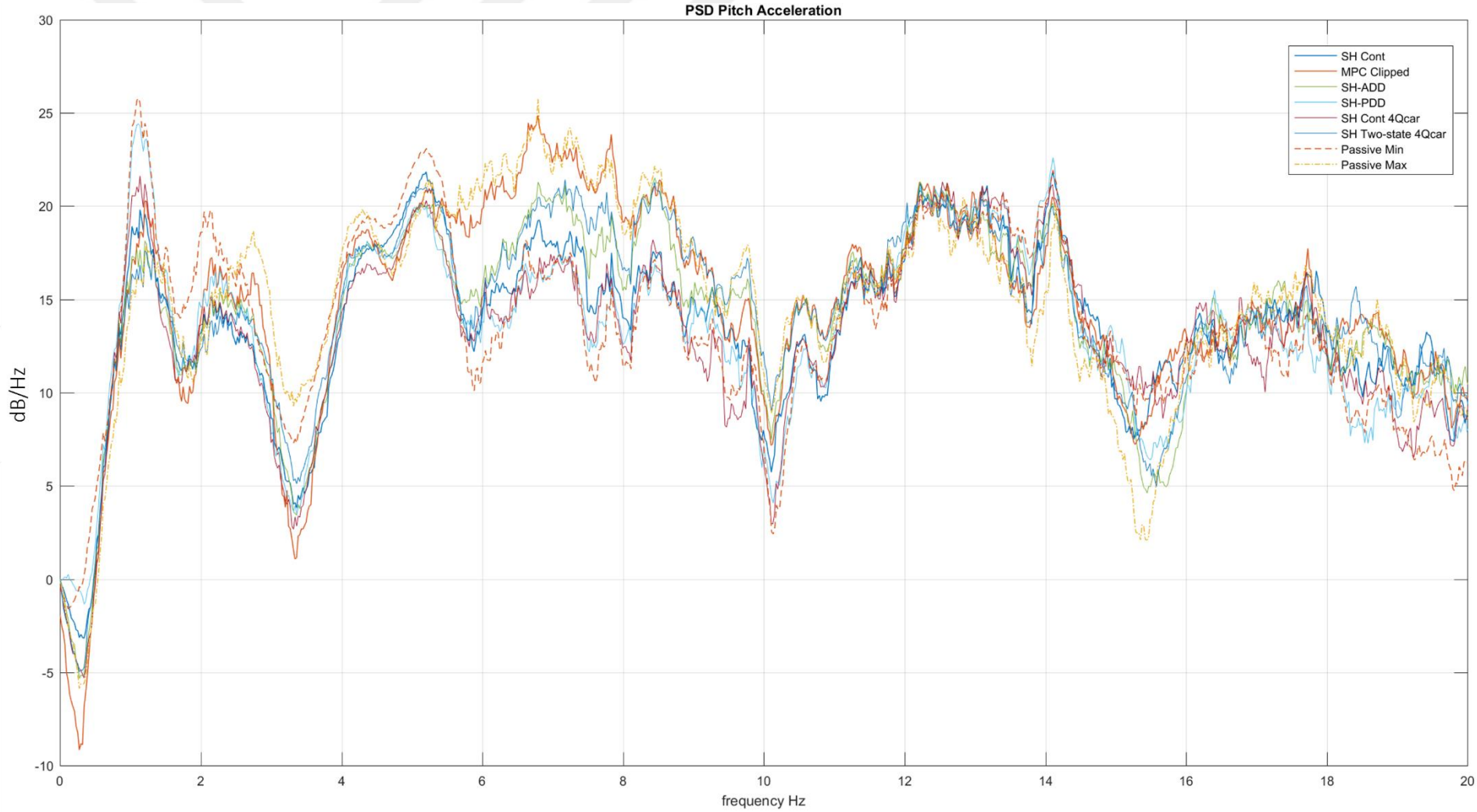

Figure 3.10: PSD of pitch acceleration.

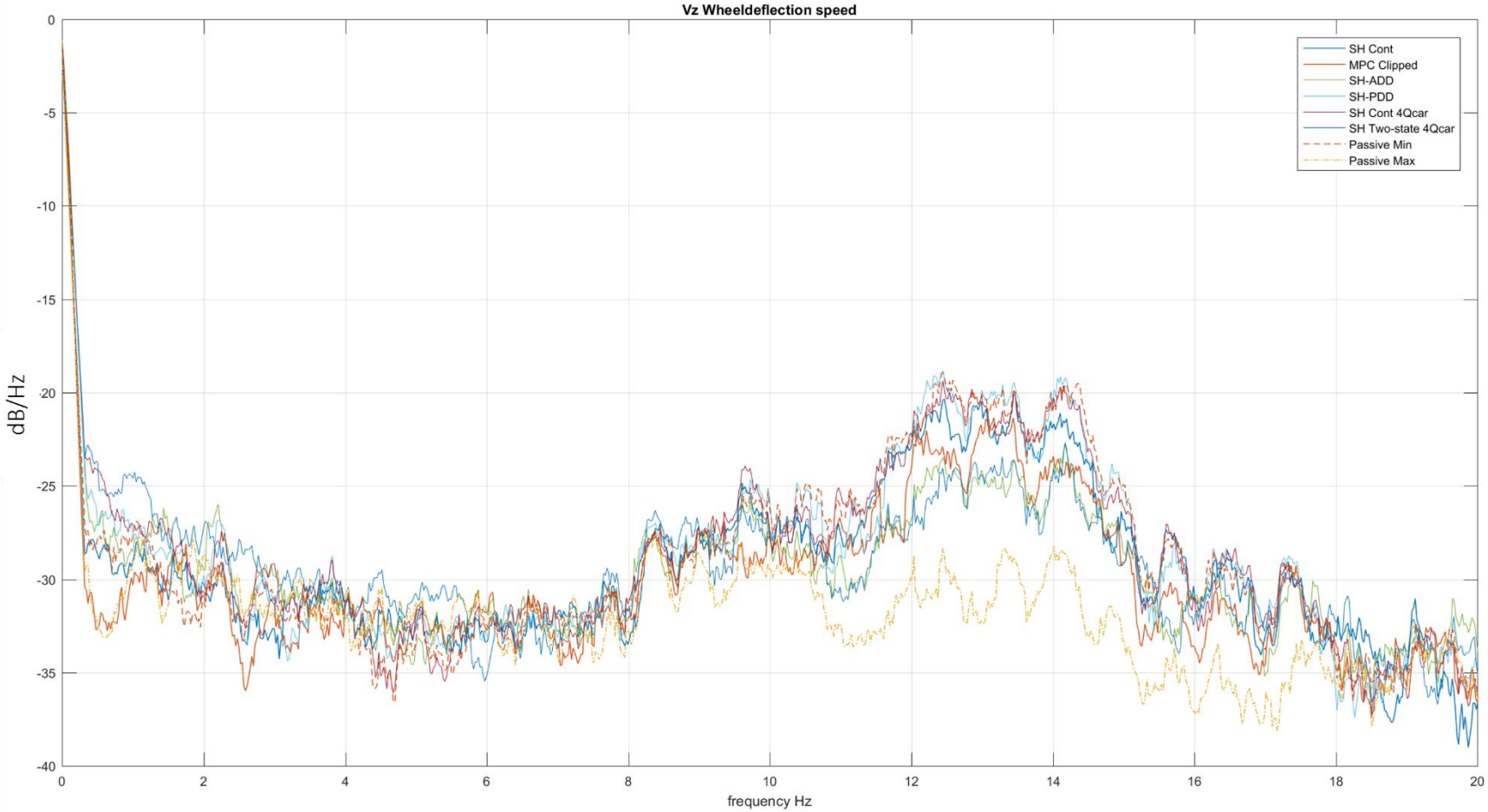

Figure 3.11: PSD of wheel deflection speed FL wheel.

Table 3.2: RMS values of the vehicle states according to control logic.

		RMS Body Acc. [m/s^2]	RMS body Jerk [m/s^3]	RMS FL Wheel Z speed [m/s]	RMS RL Wheel Z speed [m/s]	RMS Suspension Travel FL Wheel [m]	RMS Suspension Travel RL Wheel [m]	RMS Pitch Acc. [deg/s^2]	RMS Roll Acc. [deg/s^2]	RMS Pitch rate [deg/s]	RMS Roll rate [deg/s]	RMS Pitch angle [deg]	RMS Roll angle [deg]
Global	SH Cont. 32/32/32 kNs/m	0.911	76.950	0.505	0.485	0.015	0.008	39.170	114.000	1.900	2.666	2.056	4.247
	SH Cont. 2-100/100/100 kNs/m	1.012	101.100	0.495	0.479	0.013	0.007	46.170	131.500	1.679	2.710	2.062	4.341
	SH Cont. 4 - 100/100/120 kNs/m	1.005	101.900	0.013	0.007	0.013	0.007	46.930	133.800	1.662	2.688	2.059	4.317
Four Quarter Car	MPC Clipped	1.259	141.500	0.494	0.468	0.012	0.006	59.340	149.800	1.939	3.017	2.073	4.368
	ADD 5kNs/m	1.098	115.600	0.493	0.479	0.017	0.009	43.630	120.200	2.884	2.370	2.054	4.309
	SH ADD 5kNs/m	0.998	86.390	0.491	0.474	0.014	0.007	44.110	123.200	1.845	2.768	2.056	4.282
	PDD 5kNs/m	1.019	56.720	0.520	0.491	0.021	0.012	40.400	106.800	3.426	3.004	2.065	4.273
	SH PDD 5kNs/m	0.942	57.650	0.518	0.489	0.020	0.010	38.940	108.700	2.947	2.868	2.049	4.270
	SH Cont. 5kNs/m	0.886	61.980	0.512	0.490	0.018	0.009	36.940	107.800	2.246	2.715	2.048	4.240
	SH Two state 5kNs/m	1.028	95.390	0.491	0.472	0.013	0.007	47.490	126.900	1.747	2.735	2.054	4.304
	Passive min (0.32A)	1.077	58.720	0.520	0.491	0.021	0.011	39.840	106.500	3.444	2.995	2.064	4.300
	Passive Hard (1.6A)	1.520	200.800	0.477	0.469	0.010	0.008	74.530	202.900	1.774	3.217	2.057	4.403

According to the simulation result in Figure 3.8, Passive maximum had the best performance in damping vertical acceleration between 0.01 and 1.8 Hz, as expected. Then MPC achieved the second-best performance up to 1.5Hz. SH-continuous-global had the third best performance around the body resonant frequency. On the other hand, Passive-maximum and MPC performed worst between 2-10Hz. Passive-minimum had the worst performance around body resonant frequency but performed best between 2-10Hz as it had the least transmissibility. ADD and PDD were less effective around the body resonant frequency, therefore their performance was not adequate as expected. However, SH-ADD and SH-PDD were significantly better for roll and pitch acceleration as shown in Figure 3.9 and 3.10, but success was not the same for roll and pitch rate as these logics were developed with damping of acceleration in mind. PDD and SH-PDD had superior performance in terms of jerk. SH-continuous-Four-quarter-car had superior performance in terms of RMS of acceleration according to Table 3.2 but SH continuous-global had better performance around the body resonant frequency. It can be clearly seen that the SH –continuous-four-quarter-car has less transmissibility between 2 and 10Hz compared to the SH-global. It seems there were still some margin to increase SH-continuous-four-quarter-car gain. For comparison, it was decided to keep the gain of all controllers the same. In terms of handling performance, roll and wheel deflection can simply be considered as handling performance measures. Based on the wheel deflection speed results in Figure 3.11, the passive maximum performed best around the unsprung mass resonant frequency, the same as the passive maximum performance around the body roll resonant frequency in Figure 3.9. The remaining controllers did not performed well around the body resonant frequency compared to the passive maximum, as their concern is to reduce body motions rather than unsprung mass.

- *SH control gain scheduling for motion prioritization: "Virtual Vehicle"*

Varying road surface characteristics cause different body motions during vehicle movement. Having preview road surfaces can be used to anticipate upcoming vehicle motions. If the road profile is known, a vehicle model representing the real vehicle can be fed with the road profile data in advance. Thus, potential vehicle motions can be estimated. Then, SH gains can be scheduled, or any other controller targets or gains can be tuned to upcoming conditions. Continuous SH is effective around body resonant frequencies. Therefore the estimated representative vehicle model outputs need to be

filtered at a certain bandwidth, for example 0.1 to 3 Hz. This is to prevent increased gain in the ineffective zones of the SH controller. The filtered signals were then used to calculate the inclusion ratios of each relative to the other. Weighting constants can then be used to prioritize one motion over another. The block diagram of the strategy is given in Figure 3.12. 7 DOF vehicle model was discussed in section 1.2.5.4, and this model was used to estimate bounce, roll and pitch motions. Vehicle speed was constant 50kph and CRG road profile and second-order band pass filters (BPF) were used in the simulation. SH continuous was tuned to 64kNs/m. Then, 32kNs/m was tuned as a basis for adaptive controllers. Another gain of 64KNs/m was shared between bounce, roll and pitch motions based on their inclusion and weight.

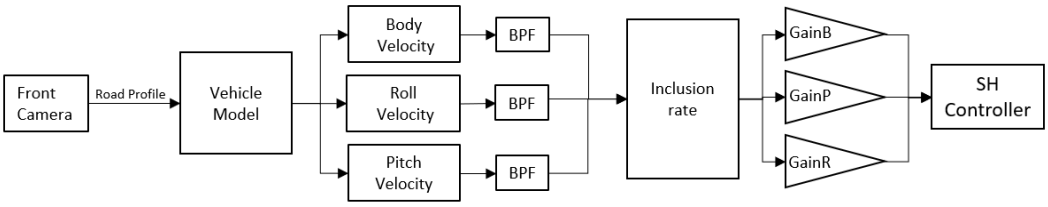

Figure 3.12: Vehicle motion estimation block diagram.

According to Figure 3.13, the results showed that giving the controller high gains as baseline resulted in significant damping around 1.4 Hz. In addition, roll and pitch prioritized controllers had more bounce around 1.4Hz. On the other hand, adaptive controllers had less transmissibility around 2 and 3.5 Hz, as their damping coefficients (constant: 32kNs/m, adaptive :64kNs/m) were mostly adaptive. The main idea was to give weight to the rotational movements since they are more annoying for the passenger and driver. Therefore, pitch and roll were more weighted than bounce.

According to Figure 3.14, pitch motion was not well damped compared to the roll motion in Figure 3.15. The reason may be an insufficient roll damping coefficient due to the road profile prone to generate significant roll in mixed bounce and pitch. The virtual sensor placed in the IPG vehicle may have also been affected by the roll motions when the vehicle motions were coupled, however, we used an equation for each motion excluding the couplings. Roll prioritized controller remarkably reduces the roll acceleration around 2 Hz compared to other controllers. There was no obvious difference of the controller in terms of wheel deflection speed as shown in Figure 62. It is also worth noting that all controllers were designed for body control purposes.

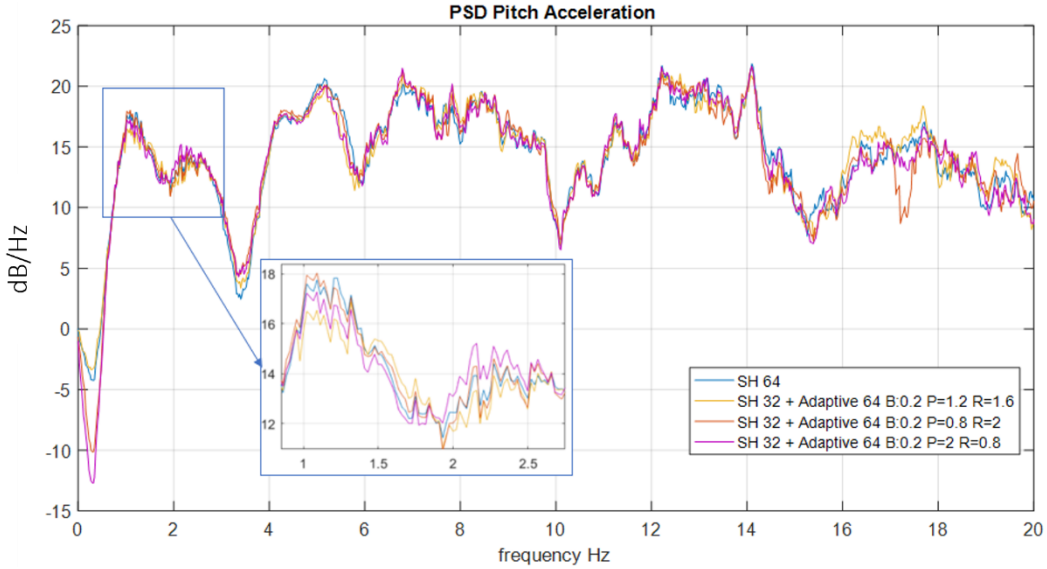

Figure 3.13: PSD of pitch acceleration.

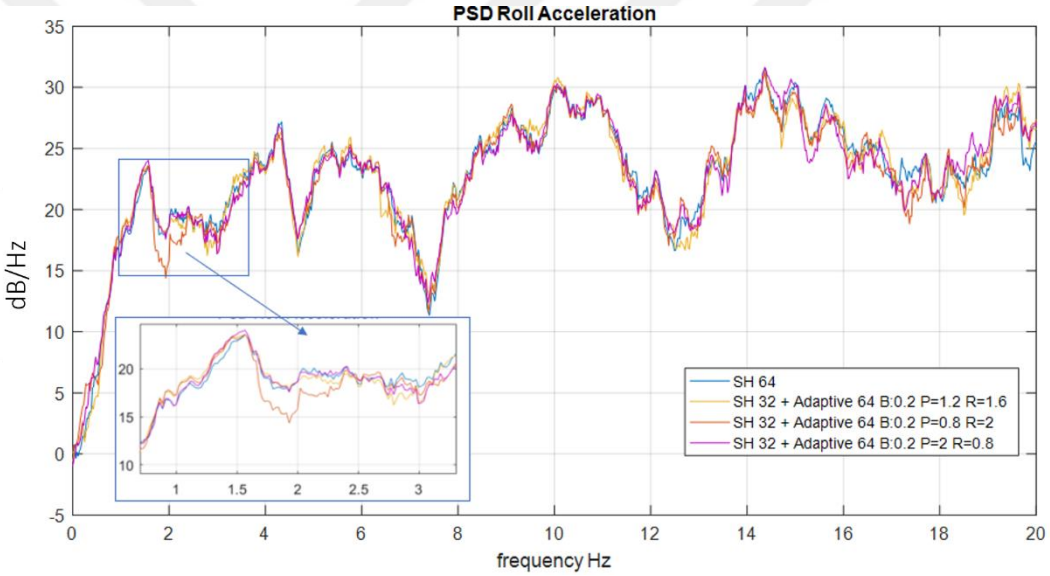

Figure 3.14: PSD of roll acceleration.

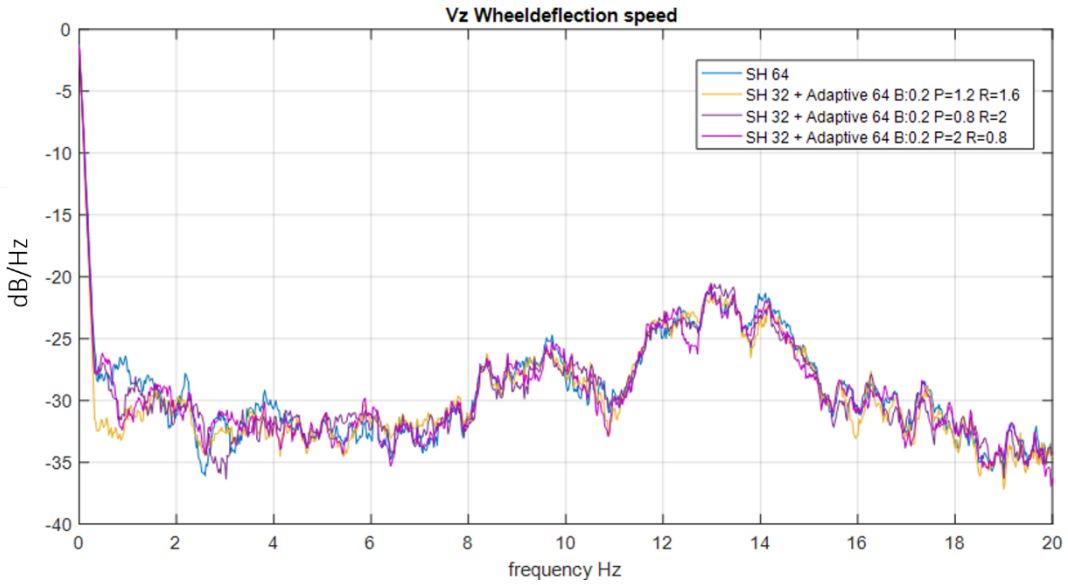

Figure 3.15: PSD of wheel deflection speed.

- *SH control forces optimization with MPC*

The central continuous-SH-control calculates virtual forces and moments around the CoG as a result of the virtual damper's movements with respect to the X, Y and Z imaginary reference frame in principle. Then, the virtual dampers generate restoring forces and moments. It is also possible to consider these restoring forces and moments in an optimization problem. They can be calculated considering that they are manipulated variables instead of four actuators in a MPC controller, as shown in Figure 3.16. This approach can be a computational cost advantage as one of the manipulated variables is eliminated. Moreover, MPC provides flexibility to prioritize one motion over another and allows defining lower and upper constraints for states. Once optimally manipulated variables are found on a finite horizon, these values can be distributed to the actuators by the IDT. This approach can be thought of as finding the optimal virtual damping values of SH.

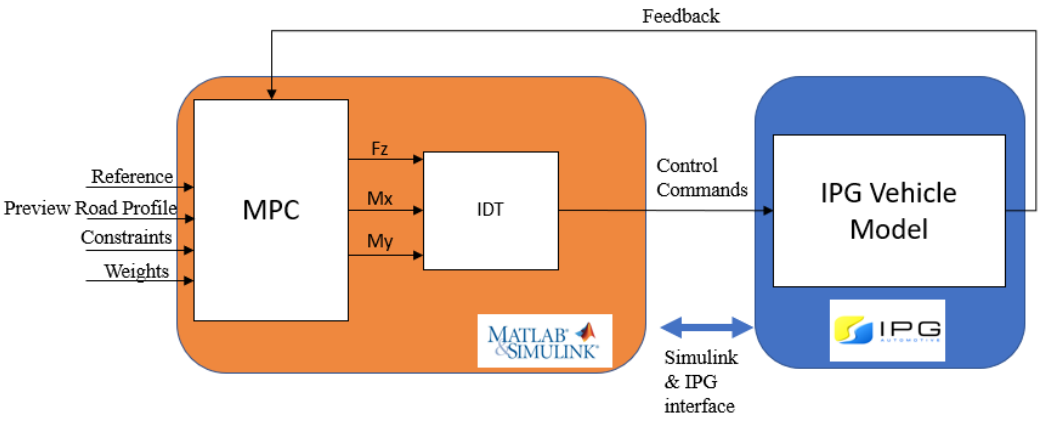

Figure 3.16: Scheme of SH control force optimization with MPC.

The 7 DOF vehicle has a total of seven inputs; four for standard actuators and three for vertical forces and moments about the x and y axis. Global forces and moments are given priority, as the flexibility of the MPC makes it possible to penalize one actuator over another. Thus, the system behaves as if it has three inputs.

CRG road profile was utilized as the road input and the vehicle speed was kept constant at 50kph as before in the simulation. The lower and upper bound of the control forces and moments were defined using the logic given in Equation 3.5. The body vertical velocity variable, $\dot{Z}_s$, in the logic can be replaced by the pitch rate, $\dot{\theta}$, and roll rate $\dot{\emptyset}$ to have the lower and upper bounds of global moments. This is the way to represent the virtual skyhook dampers in MPC.

$$\begin{cases} \text{if } \dot{Z}_s > 0 & F_{z,min} = -C_{sky}\dot{Z}_s \\ \dot{Z}_s \leq 0 & F_{z,max} = -C_{sky}\dot{Z}_s \end{cases} \tag{3.5}$$

SH-continuous was tuned to 64 kNs/m, (rotational motions: 64 kNms/rad) and selected as the benchmark controller. The lower and upper bound of the MPC controller was tuned to 64kNs/m to be coherent with SH-continuous. The prediction horizon and control horizon were set to 10 and 2, respectively. According to Figure 3.17, SH had better results for vertical acceleration, around 1 and 3Hz. The MPC SH 64 and MPC SH 128 had similar performance around body resonant frequencies. The performance difference of the controller in the 4-20 Hz range was not significant compared to the body resonant frequencies.

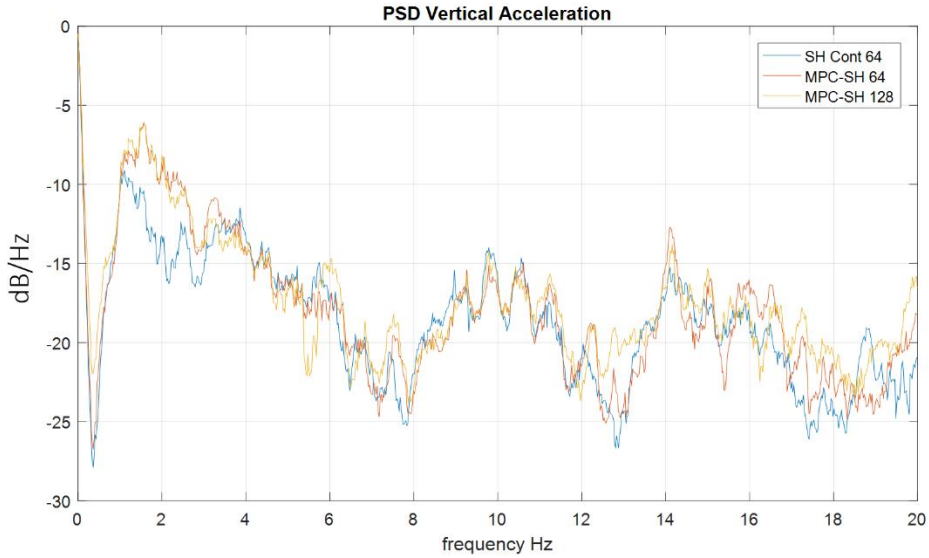

Figure 3.17: PSD of vertical acceleration MPC SH.

SH had better performance in terms of pitch acceleration compared to MPCs around 1-6 Hz, as shown in Figure 3.18.

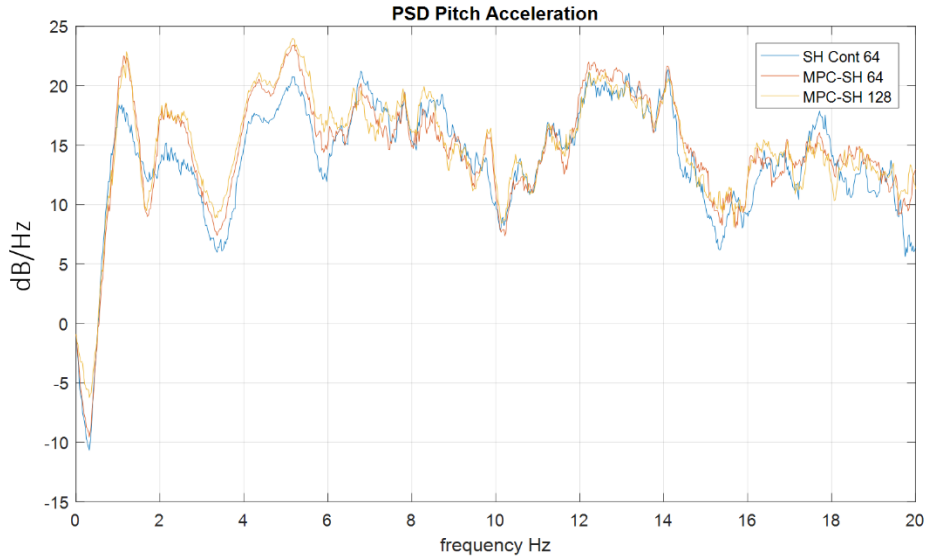

Figure 3.18: PSD of pitch acceleration.

SH had better roll acceleration performance around 2-4.3 Hz compared to MPCs, as shown in Figure 3.19.

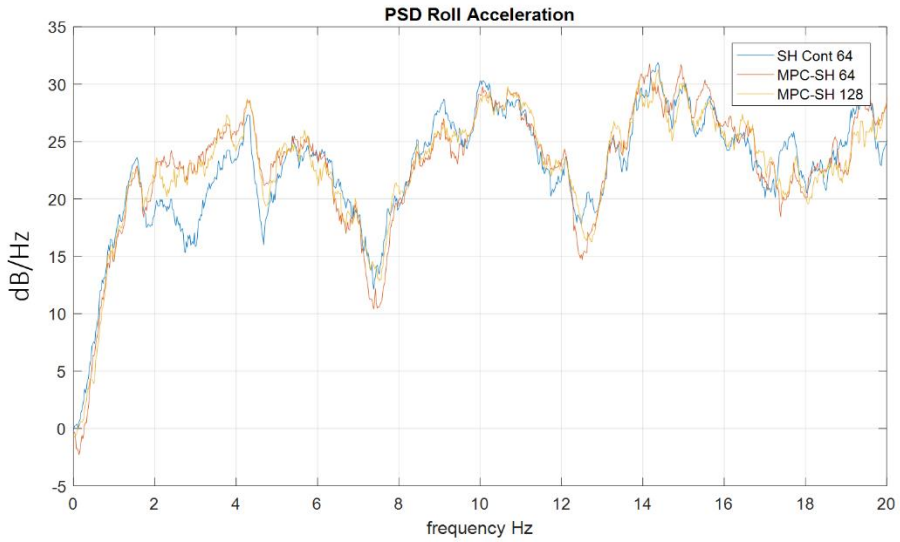

Figure 3.19: PSD of roll acceleration.

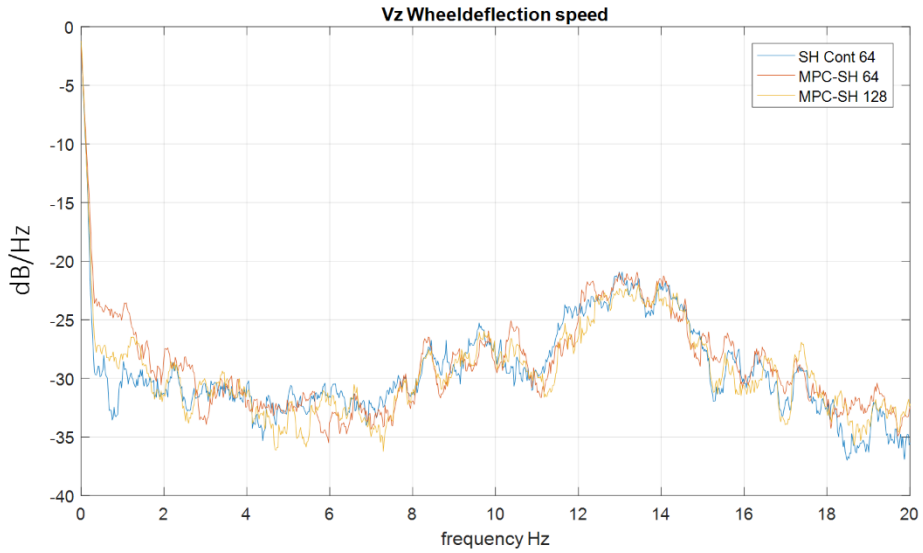

Figure 3.20: PSD of wheel displacement.

All configurations were designed to control body motions. Therefore, there was no significant difference in wheel deflection speed, as shown in Figure 3.20. The reason for the gap around 1Hz is the relatively low damping application of MPC.

- *Potential reasons for the lack of performance*:

The SH-continuous formulation calculates virtual damper forces at global level without considering the passivity constraint of virtual actuators. Then the calculated forces and moments were distributed for the actuators and SH rule was applied in this stage. Therefore, there were no discontinuities in global forces and moments. On the

other hand, force discontinuity was initiated in the high-level controller when the virtual force and moment applied as MPC SH control as lower and upper bound. Therefore, the force distributed to the actuators had lack of damping compared to SH-continuous. This was one of the reasons for the underperformance.

Second, SH control is effective in the body resonant frequency region. Therefore, virtual damper forces and moments directly consider the body resonant frequency region. However, MPC does not focus on a specific frequency range. Another reason could be an imperfection in the prediction model and inaccurate preview information.

3.4 Simulations with Full Car Model for active suspension

The same section of the road profile was selected, but this time for active suspension control simulations. Vehicle speed was set to 50kph as in previous simulations. The prediction horizon and the control horizon were selected 10 and 4, respectively. The sampling time was 10ms. The lower and upper bounds and constraints of the actuator were defined as ±5000N. The output lower and upper bound, scale factors, and weights have been tuned until the best results are obtained. For a constant 50kph speed, a 1m long preview road profile was fed into the MPC controller. As passive dampers, semi-active suspension was used by keeping the current constant. The damper was tuned to the comfort characteristic. This damper setting was used during simulation for MPC and SH. Since the SH control was not capable of considering the actuator constraints like MPC, a saturation was added to limit the output of each actuator to ±5000N. The road profile was filtered by the LPF with a cut off frequency of 5Hz.

SH active virtual damper gains were tuned to 4kNs/m, 4kNs/m and 4kNs/m for bounce, roll and pitch motions, respectively. Three scenarios, which are SH -active, MPC-active with preview and MPC-active with non-preview information, were simulated. According to the body vertical acceleration PSD in Figure 3.21, the SH controller gave the best results around the body resonant frequency compared to the two types of MPC; both MPCs had similar performance across the entire range except 7Hz. The performance of the SH control is significant around 0.5 to 3Hz. According to the roll acceleration PSD in Figure 3.22, SH control performed best between 1.8Hz and 4.2 Hz, while the MPCs outperformed SH between 0.8Hz to 1.8Hz. MPC-active preview and without preview had similar performance around 1.8Hz to 4.2Hz. All controllers gave similar performance between 4.2Hz and 20Hz.

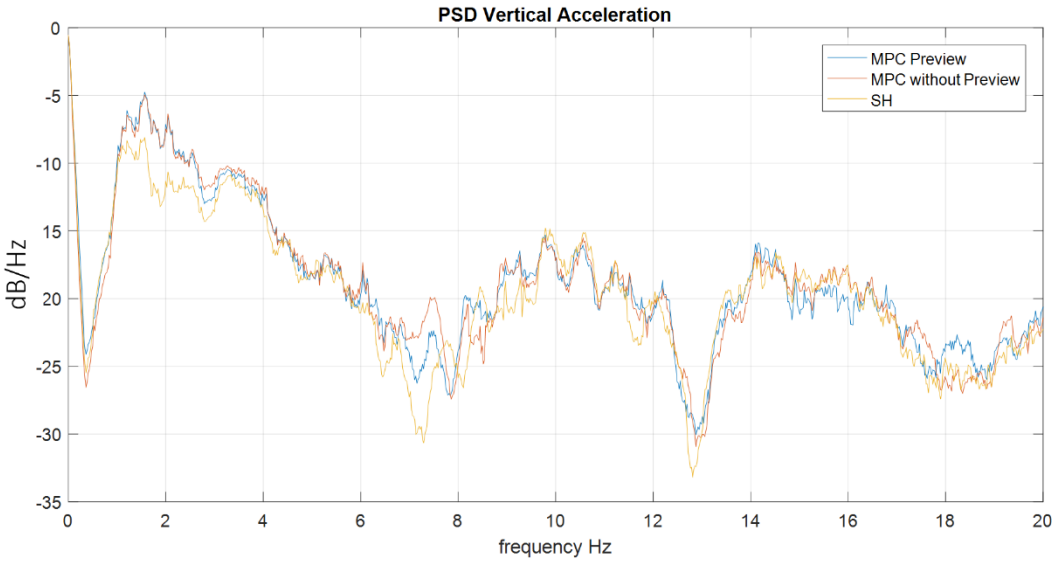

Figure 3.21: PSD of vertical acceleration.

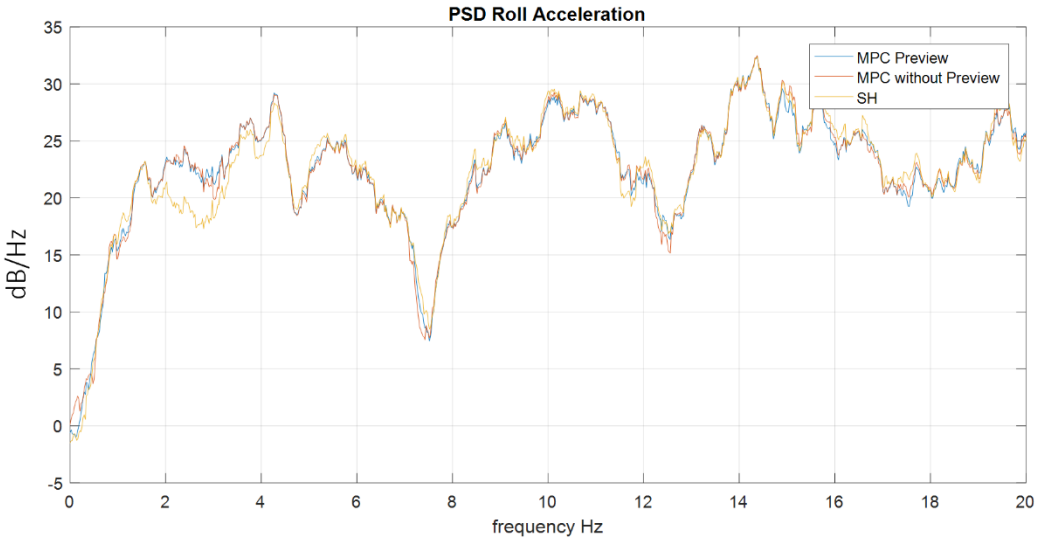

Figure 3.22: PSD of roll acceleration.

According to the pitch acceleration PSD in Figure 3.23, MPC active with preview and without preview had the same and worst result between 1 and 2Hz. The SH controller performed best at 0.1 to 3Hz. All controllers had similar performance from 5Hz to 20Hz.

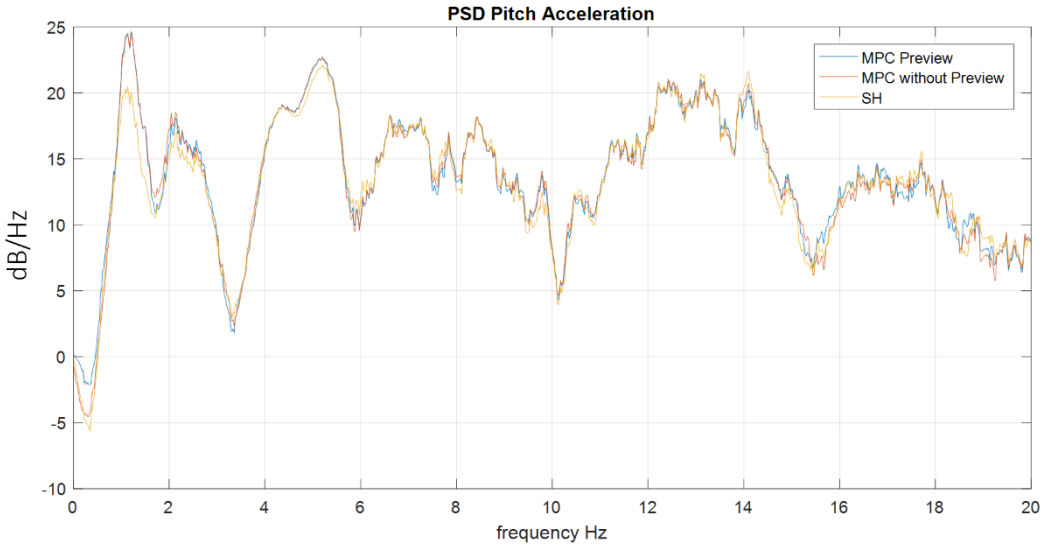

Figure 3.23: PSD of Pitch Acceleration.

According to the wheel deflection speed PSD, Figure 3.24, which can be a measure of road holding, there was no significant difference between the controllers over the entire frequency range, although the MPC controller wheel deflection speed outputs were constrained, and the SH did not have this capability.

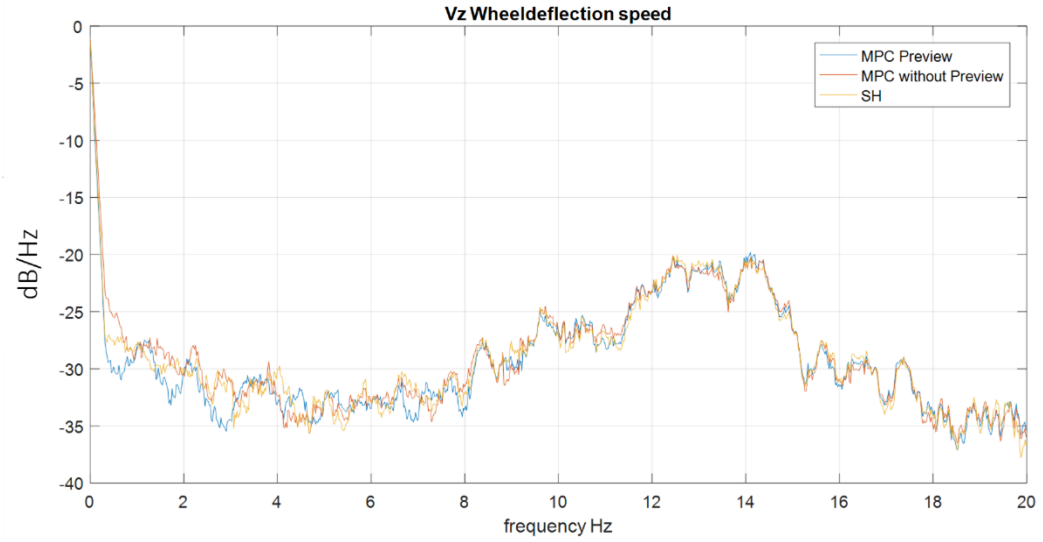

Figure 3.24: PSD of Wheel deflection speed.

It is worth noting that MPC controller performance depends on the optimization results. Therefore, in some iterations, the results shown in PSD diagrams had significant deviations indicating that the estimated performance of MPCs may not be constant. On the other hand, according to the overall results, it can be interpreted that

the use of imperfect preview road profile as disturbance, may degrade MPC performance.

3.5 Overall ride comfort evaluation of semi-active suspension control logics

The evaluation of comfort in the car is a multidimensional problem consisting of translational and rotational accelerations, jerk, seat vibrations, steering wheel, floor, and tyre noises that can be heard by the driver and passenger. The standards in the literature are not sufficient to evaluate all these variables in the problem for comfort assessment since comfort is studied with limited use cases based on acceleration which is evaluated depending on frequencies and weights. On the other hand, there are many real-life use cases for vehicle suspension systems. The suspension system works on paved, highway, city, gravel, asphalt, and concrete road. There are also individual use cases on the road such as speed bumps, potholes, and low and high-frequency irregularities. Often some of the above use cases are combined. Some people are sensitive to small vibrations causing the audible sounds, while others are sensitive to peak acceleration. On the other hand, if the vehicle has a controlled suspension system, the comfort characteristics expected from the vehicle will vary depending on the vehicle segment and driving mode. The RMS of accelerations in vertical and rotational directions are reasonable indicators for observing vibration energy on the vehicle body, but can sometimes be misleading as it does not give the other expected components of comfort expectations. Nearly undamped soft damping settings usually put less energy into the vehicle body, and it has the lowest RMS. However, this almost undamped vehicle body can be quickly noticed by an ordinary driver. Additionally, the nearly undamped settings allow the unsprung mass to move easily over uneven surfaces. Thus, even significant noises can be heard in the cabin. Speed bumps, potholes and any impact input will cause the suspension to reach the bump stop, which for example, causes sudden shocks. Therefore, the system must be evaluated considering all these use cases, ideally. However, making such an assessment in this detail would go beyond the scope of this study. Additionally, there is no ready to use standard since the criteria, such as weighted RMS in ISO 2631 are based on acceleration measured on seat surfaces.

Then, other criteria, such as wheel deflection speeds as a measure of road holding, have not been previously associated with the measurement of comfort in the vehicle body. It would not be meaningful to obtain a comfort result by weighting the results that have not been associated with each other in the literature or that have not been

taken into account by detailed tests and analysis or within the scope of a study. Therefore, it is more reasonable to expect a minimum value for any parameter for a fair evaluation than to give unequal weighting factors. For this reason, the average of the equally weighted RMSs of the relevant parameters was evaluated by ordering them from the smallest to the largest. The equally weighted RMS parameters are added and divided by the number of parameters to obtain the average, overall ride value.

The RMS of body acceleration is filtered by Low-pass filters and Band-pass filters to separate the 0.1-2 Hz and 2-10 Hz region. Only the RMS vertical acceleration is weighted according to ISO 2631 standard with factors of 0.5 and 0.8 as in Figure 3.25. Factors were reproduced as $\frac{0.5}{(0.5+0.8)} = 0.38$ and $\frac{0.8}{(0.5+0.8)} = 0.62$ according to their ratios, providing equal weighting with other RMS criteria.

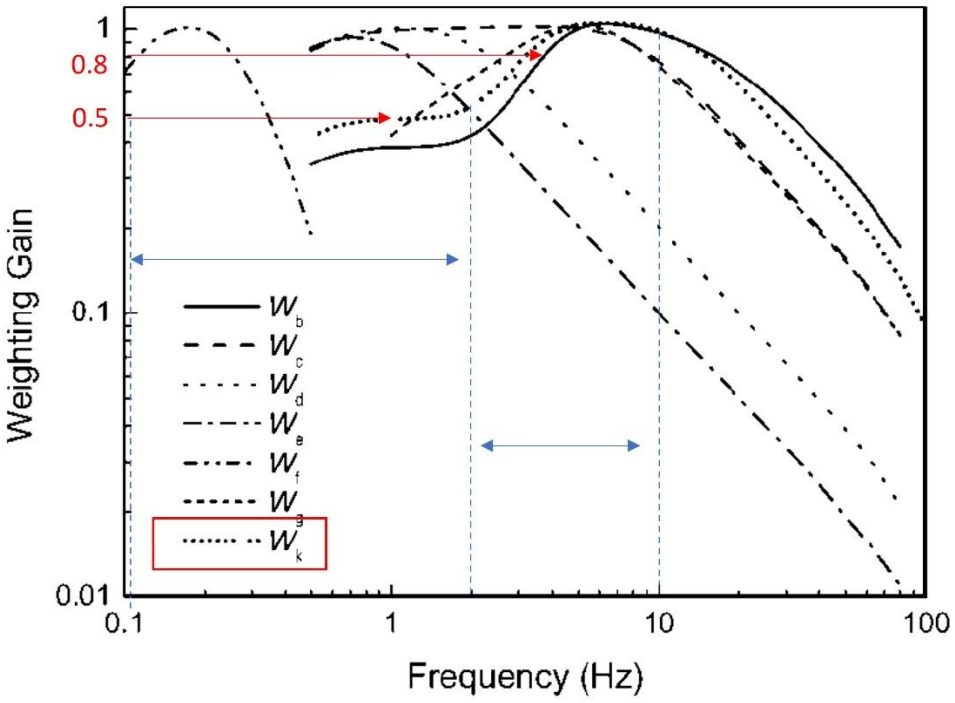

Figure 3.25 Acceleration frequency weightings for whole-body vibration and motion sickness as defined in the BS 6481:1987 and ISO :1997 (Griffin, 2007)

RMS vertical acceleration was also kept in the evaluation to have the effects of vibration beyond 10Hz. Table 3.3 is an extension of Table 3.2 and has a low and medium frequency range for vertical acceleration. The minimum and maximum RMS values are dark green and red, respectively. Therefore, the colour scale from dark green to red also gives the degree of preference of the element under consideration. Table

3.4 gives the normalized and weighted RMS values. Each RMS value for a characteristic is multiplied by the weights, then the overall ride values are obtained for each row at the far-right of the table. Overall ride value metric takes into account the level of comfort parameters such as body vertical accelerations, jerk, pitch and roll acceleration and their rates and angles. On the other hand, it also measures handling parameters, such as suspension stroke speed, vertical wheel speeds as a measure of road holding, and roll rate and roll angle. According to the overall ride value, the SH Global has the best performance with 32kNs/m and SH Cont. for quarter car has the second-best performance with 5kNs/m. There was no significant difference between the two controllers. All values in Table 3.3 and Table 3.4 are in agreement with the PSD graphs in Section 3. The passive maximum setting had the worst overall ride performance except for road holding and the wheel's vertical speed. Similarly, but this time opposite side Passive minimum setting had one of the worst overall ride performances. The overall ride performance of any controller can also be seen by its adaptation capability of changing conditions and minimizing the capability of all metrics. The Continuous SH-based controllers provided good comfort in the low and medium frequency ranges by reducing vehicle body motions and not significantly reducing the road holding metrics.

Table 3.3: RMS values of the vehicle states according to control logic and their comparison

		RMS Body Acc. [m/s^2]	RMS Body Acc [0-2 Hz] [m/s^2]	RMS Body Acc. [2-10Hz] [m/s^2]	RMS body Jerk [m/s^3]	RMS FL Wheel Z speed [m/s]	RMS RL Wheel Z speed [m/s]	RMS Suspension Travel FL Wheel [m]	RMS Suspension Travel RL Wheel [m]	RMS Pitch Acc. [deg/s^2]	RMS Roll Acc. [deg/s^2]	RMS Pitch rate [deg/s]	RMS Roll rate [deg/s]	RMS Pitch angle [deg]	RMS Roll angle [deg]
Global	SH Cont. 32/32/32 kNs/m	0.911	0.400	0.447	76.950	0.505	0.485	0.015	0.008	39.170	114.000	1.900	2.666	2.056	4.247
	SH Cont. 2-100/100/100 kNs/m	1.012	0.390	0.539	101.100	0.495	0.479	0.013	0.007	46.170	131.500	1.679	2.710	2.062	4.341
	SH Cont. 4 - 100/100/120 kNs/m	1.042	0.389	0.566	107.700	0.497	0.479	0.013	0.007	48.030	137.600	1.662	2.718	2.064	4.294
Four Quarter Car	MPC Clipped	1.259	0.506	0.634	141.500	0.494	0.468	0.012	0.006	59.340	149.800	1.939	3.017	2.073	4.368
	ADD 5kNs/m	1.098	0.494	0.539	115.600	0.493	0.479	0.017	0.009	43.630	120.200	2.884	2.370	2.054	4.309
	SH ADD 5kNs/m	0.998	0.424	0.493	86.390	0.491	0.474	0.014	0.007	44.110	123.200	1.845	2.768	2.056	4.282
	PDD 5kNs/m	1.019	0.563	0.388	56.720	0.520	0.491	0.021	0.012	40.400	106.800	3.426	3.004	2.065	4.273
	SH PDD 5kNs/m	0.942	0.507	0.373	57.650	0.518	0.489	0.020	0.010	38.940	108.700	2.947	2.868	2.049	4.270
	SH Cont. 5kNs/m	0.886	0.437	0.393	61.980	0.512	0.490	0.018	0.009	36.940	107.800	2.246	2.715	2.048	4.240
	SH Two state 5kNs/m	1.028	0.415	0.531	95.390	0.491	0.472	0.013	0.007	47.490	126.900	1.747	2.735	2.054	4.304
	Passive min (0.32A)	1.077	0.563	0.388	58.720	0.520	0.491	0.021	0.011	39.840	106.500	3.444	2.995	2.064	4.300
	Passive Hard (1.6A)	1.520	0.544	0.806	200.800	0.477	0.469	0.010	0.008	74.530	202.900	1.774	3.217	2.057	4.403

Table 3.4: Overall ride value, weighted and normalized RMS values of vehicle states according to control logic and their comparisons

		RMS Body Acc. [m/s^2]	RMS Body Acc [0-2 Hz] [m/s^2]	RMS Body Acc. [2-10Hz] [m/s^2]	RMS body Jerk [m/s^3]	RMS FL Wheel Z speed [m/s]	RMS RL Wheel Z speed [m/s]	RMS Suspension Travel FL Wheel [m]	RMS Suspension Travel RL Wheel [m]	RMS Pitch Acc. [deg/s^2]	RMS Roll Acc. [deg/s^2]	RMS Pitch rate [deg/s]	RMS Roll rate [deg/s]	RMS Pitch angle [deg]	RMS Roll angle [deg]	Overall ride value
	Weights	1	0.38	0.62	1	1	1	1	1	1	1	1	1	1	1	-
Global	SH Cont. 32/32/32 kNs/m	0.071	0.071	0.073	0.066	0.084	0.084	0.080	0.076	0.070	0.074	0.069	0.079	0.083	0.082	0.082
	SH Cont. 2-100/100/100 kNs/m	0.079	0.069	0.088	0.087	0.082	0.083	0.070	0.071	0.083	0.086	0.061	0.080	0.083	0.084	0.085
	SH Cont. 4 - 100/100/120 kNs/m	0.081	0.069	0.093	0.093	0.083	0.083	0.071	0.073	0.086	0.090	0.060	0.080	0.084	0.083	0.087
Four Quarter Car	MPC Clipped	0.098	0.090	0.104	0.122	0.082	0.081	0.065	0.058	0.106	0.098	0.071	0.089	0.084	0.085	0.095
	ADD 5kNs/m	0.086	0.088	0.088	0.100	0.082	0.083	0.088	0.086	0.078	0.078	0.105	0.070	0.083	0.083	0.092
	SH ADD 5kNs/m	0.078	0.075	0.081	0.074	0.082	0.082	0.077	0.067	0.079	0.080	0.067	0.082	0.083	0.083	0.084
	PDD 5kNs/m	0.080	0.100	0.064	0.049	0.086	0.085	0.114	0.119	0.072	0.070	0.125	0.089	0.084	0.083	0.094
	SH PDD 5kNs/m	0.074	0.090	0.061	0.050	0.086	0.085	0.104	0.101	0.070	0.071	0.107	0.085	0.083	0.083	0.088
	SH Cont. 5kNs/m	0.069	0.078	0.065	0.053	0.085	0.085	0.095	0.090	0.066	0.070	0.082	0.080	0.083	0.082	0.083
	SH Two state 5kNs/m	0.080	0.074	0.087	0.082	0.082	0.082	0.071	0.072	0.085	0.083	0.064	0.081	0.083	0.083	0.085
	Passive min (0.32A)	0.084	0.100	0.064	0.051	0.087	0.085	0.114	0.113	0.071	0.069	0.125	0.089	0.084	0.083	0.094
	Passive Hard (1.6A)	0.119	0.097	0.132	0.173	0.079	0.081	0.051	0.076	0.133	0.132	0.065	0.095	0.083	0.085	0.108

4. CONCLUSION AND RECOMMENDATIONS

4.1 Conclusion

In this study, four concepts for preview suspension vertical chassis control were proposed. First, well-known closed loop control logics were evaluated in terms of different requirements and implementation methods, especially centralized and decentralized approaches. Then, the process noise preventive road profile estimation method was introduced. Secondly, the SH virtual vehicle concept was introduced for scheduling the SH controller's gain based on the preview road information. Afterwards, MPC Clipped approach was introduced and compared with closed-loop control approaches in a high-fidelity simulation environment. Finally, an SH-like derivative MPC controller was introduced to control the vehicle body by controlling global forces and moments instead of forces on the actuators.

Of particular interest for this study is to evaluate the controller's performance as close to real conditions as possible. For this reason, the CRG road profile was used in the co-simulations. Furthermore, accelerometers were chosen from virtual sensors of the co-simulation environment (IPG Carmaker's virtual sensors) to get closer to reality, although in fact velocity sensors were already available to provide accurate output. In this way, the output of the virtual accelerometer was processed, for example, with high-pass and low-pass filters to remove the effect of road slope.

The passivity constraint of a semi-active damper makes direct preview control applications extremely difficult. Because the system is usually modelled as an actuator that can generate force but absolutely cannot. Moreover, the vehicle model in receding horizon can only be modelled linearly if linear MPC is required. Then, during optimization, the lower or upper bound is sometimes zero, as it cannot generate damping forces and it is not possible to find feasible results. If the passivity constraint is not considered in the problem, the optimizer can find feasible results, while the damper cannot. This is called clipped approach and can cause instabilityfor semi-active dampers. The MPC clipped approach was compared with well-known semi-active

suspension control methods. Therefore, SH control and its variants were also simulated in a realistic environment. Then, it was found that Global SH control had better performance compared to other semi-active suspension control logics in terms of motion prioritisation and overall performance.

To elaborate the study, specifically to indirectly benefit from the preview road profile, a virtual vehicle model with 7 DOF was moved at the same speed as the vehicle. The proposal was to pre-determine the skyhook gains according to the RMS of bounce, roll, pitch rates, which can be considered indirect control. The results were promising, and it could be seen that it was possible to dampen one motion more than others around body resonant frequencies.

To further refine the study, specifically combining MPC with SH control and road profile directly, MPC was utilised to optimize the damping coefficient of virtual skyhook dampers. Therefore, the external forces and moments were added over the CoG in the vehicle model, these forces and moments were optimized according to the vehicle motions taking into account the road profile and constraints of the virtual damper. This approach somehow mimics the skyhook control. Its performance appears to lag behind SH control around body resonant frequencies, but it is similar to SH beyond body resonant frequencies. On the preview horizon, it has still the potential to optimize virtual damping forces by reformulating the problem considering skyhook damper in the vehicle model. Preview information was used directly and indirectly in MPC and SH control, respectively, and it can be seen that preview information can improve comfort. The accuracy of the vehicle model has a significant impact on the MPC and indirect control. SH had superior performance around body resonant frequencies and the resonant frequency region is the highest amplitude that makes the controller performance is decisive.

After performing various simulations, the Global SH control was found to outperform other controllers in terms of various requirements; especially its overall ride performance, adaptability, flexibility, and modularity, which does not require complex tuning and optimization. Consequently, the above advantages make SH preferable for active and semi-active suspension systems.

4.2 Recommendations

The SH control and their variants consider semi-active dampers as force generators. Semi-active dampers can produce force, reaction force when they have disturbance. Moreover, if there is vibration in the vehicle body, the SH control requests force. Frequently, the controller does not request force or the force generators cannot produce force. This causes a lack of damping for a while. Therefore, a lack of damping can result in undamped body and wheel motion. Eventually, it should be noted that a certain amount of minimum damping is required to guarantee adequate damping for the vehicle body, wheels and suspension stroke. In the context of SH control, where ideally zero damping is required, having minimal damping may at first glance seem like a loss of performance on the indicators. On the other hand, for instance, body acceleration is not a single indicator that defines comfort, it must be evaluated within the total vibration and noise environment which includes road induced noise in the cabin, steering wheel vibrations, the vibrations on the vehicle floor, etc. In summary, the performance indicators change to "negative" in graphs when the minimum damping demand is considered.

Complexity of vehicle model in MPC has a significant effect on the state estimation. The linear damping coefficient creates equal damping force for compression and extension. At the same time, suspension kinematics and complex tyre behaviour are not considered. Moreover, the preview information of the camera is not perfect. Having more accurate vehicle and tyre model and preview information can help improve performance. More realistic targets, non-zero references, can improve the performance of the MPC if the controller’s references can be generated taking into account the upcoming road surfaces.

For future studies, a linear but more detailed and accurate vehicle model will be designed, including suspension kinematics and tyre contact model. Reformulating the problem to optimize fictitious damping forces in a preview horizon can improve performance and provide flexibility as the number of parameters decreases. Another future study can be the reformulation of same problem but this time is optimization of fictitious skyhook damper in a vehicle model.

REFERENCES

Ahmadian, M., and **Blanchard, E.** (2008). Ride performance analysis of semiactive suspension systems based on a full-car model. *2007 Proceedings of the ASME International Design Engineering Technical Conferences and Computers and Information in Engineering Conference, DETC2007*, *3 PART B*, 1261–1270. https://doi.org/10.1115/DETC2007-35658

Ahmadian, M., **Song, X.**, and **Southward, S. C.** (2004). No-jerk skyhook control methods for semiactive suspensions. *Journal of Vibration and Acoustics, Transactions of the ASME*, *126*(4), 580–584. https://doi.org/10.1115/1.1805001

Akçay, H., and **Türkay, S.** (2008). RMS performance limitations and constraints for quarter-car active suspensions. *2008 Mediterranean Conference on Control and Automation - Conference Proceedings, MED'08*, 425–430. https://doi.org/10.1109/MED.2008.4601978

Albak, E. İ., **Solmaz, E.**, and **Öztürk, F.** (2021). Simplified optimization model and analysis of twist beam rear suspension system. *Proceedings of the Institution of Mechanical Engineers, Part D: Journal of Automobile Engineering*, *235*(5), 1434–1445. https://doi.org/10.1177/0954407020963988

ASAM OpenCRG®. (n.d.). 2022. Retrieved 22 February 2022, from https://www.asam.net/standards/detail/opencrg/

Badalamenti, J. M., and **Doyle, G. R.** (1988). Radial-interradial spring tire models. *Journal of Vibration and Acoustics, Transactions of the ASME*, *110*(1), 70–75. https://doi.org/10.1115/1.3269483

Bakker, E., **Nyborg, L.**, and **Pajecka, H. B.** (1987). Tyre Modelling for Use in Vehicle Dynamics Studies. *Intenational Congress and Exposition*. https://doi.org/https://doi.org/10.4271/870421

Bayar, K. (2006). *MODELING OF THE DYNAMICS OF MULTI-AXLE STEERED VEHICLES*. Midde East Technical University.

Bender, E. K. (1968). Optimum Linear Preview Control With Application to Vehicle Suspension. *Journal of Basic Engineering*, *90*(2), 213–221. https://doi.org/10.1115/1.3605082

Besinger, F. H., **Cebon, D.**, and **Cole, D. J.** (1995). Force Control of a Semi-Active Damper. *Vehicle System Dynamics*, *24*(9), 695–723. https://doi.org/10.1080/00423119508969115

Binder, M. K., and **Khajepour, A.** (2014). Optimal control allocation for coordinated suspension control. *Proceedings of the American Control Conference*, 2126–2131. https://doi.org/10.1109/ACC.2014.6859119

Blundell, M. ., and **D., H.** (2017). *The Multibody System Approach to Vehicle Dynamics* (Vol. 91).

Bouzouraa, M. E., **Kellner, M.**, **Hofmann, U.**, and **Lutz, R.** (2014). Laser scanner based road surface estimation for automotive applications. *Proceedings of IEEE Sensors*, *2014-Decem*(December), 2034–2037. https://doi.org/10.1109/ICSENS.2014.6985434

Brezas, P., **Smith, M. C.**, and **Hoult, W.** (2015). A clipped-optimal control algorithm for semi-active vehicle suspensions: Theory and experimental evaluation. *Automatica*, *53*, 188–194. https://doi.org/10.1016/j.automatica.2014.12.026

Buyukkopru, M., **Uzunsoy, E.**, and **Mouton, X.** (2021, September 7). Global Skyhook And Groundhook Control Of Vehicle With Semi-Active Dampers. *10th International Automotive Conference*.

Buyukkopru, M., **Uzunsoy, E.**, and **Mouton, X.** (2022a). Implementation of semi-active suspension control methods in a full car model and a comparative study in terms of ride comfort and road holding. *Journal of Automobile Engineering*, *177*. https://doi.org/10.1177/09544070221133153

Buyukkopru, M., **Uzunsoy, E.**, and **Mouton, X.** (2022b). Vision Based Road Profile Estimation for Preview Controlled Vehicle Suspension Systems. *Vision Based Road Profile Estimation for Preview Controlled Vehicle Suspension Systems*, *October*, 6–7.

Camacho, E. F., and **Bordons, C.** (2007). *Model Predictive Control - Second edition*. Springer.

Campos, J., **Davis, L.**, **Lewis, F. L.**, **Ikenaga, S.**, **Scully, S.**, and **Evans., M.** (1999). *Active Suspension Control of Ground Vehicle Heave and Pitch Motions*. 68–70.

Carratù, M., **Pietrosanto, A.**, **Sommella, P.**, and **Paciello, V.** (2017, July 5). Velocity prediction from acceleration measurements in motorcycle suspensions. *I2MTC 2017 - 2017 IEEE International Instrumentation and Measurement Technology Conference, Proceedings*. https://doi.org/10.1109/I2MTC.2017.7969943

Chen, D., **Danielson, C.**, and **Di Cairano, S.** (2021). A Predictive Controller for Drivability and Comfort in Multi-Motor Electric Vehicles. *IFAC-PapersOnLine*, *54*(20), 650–656. https://doi.org/10.1016/j.ifacol.2021.11.245

Chen, W., **Zhao, L.**, **Wang, Q.**, **Zhu, M.**, and **Xiao, H.** (2016). *Integrated Vehicle Dynamics and Control*. John Wiley & Sons Singapore Pte. Ltd. https://www.ptonline.com/articles/how-to-get-better-mfi-results

Cho, B. K. (1999). Active suspension controller design using MPC with preview information. *KSME International Journal*, *13*(2), 168–174. https://doi.org/10.1007/BF02943668

Choi, S. B., **Choi, Y. T.**, **Chang, E. G.**, **Han, S. J.**, and **Kim, C. S.** (1998). Control characteristics of a continuously variable ER damper. *Mechatronics*, *8*(2), 143–161. https://doi.org/10.1016/s0957-4158(97)00019-6

Collette, C., and **Preumont, A.** (2010). High frequency energy transfer in semi-

active suspension. *Elsevier*. https://doi.org/10.1016/j.jsv.2010.05.026

Correia, G. H. de A., **Looff, E.**, **van Cranenburgh, S.**, **Snelder, M.**, and **van Arem, B.** (2019). On the impact of vehicle automation on the value of travel time while performing work and leisure activities in a car: Theoretical insights and results from a stated preference survey. *Transportation Research Part A: Policy and Practice*, *119*(September 2017), 359–382. https://doi.org/10.1016/j.tra.2018.11.016

Cosine scientific software AG. (n.d.). *FTire Product Brochure*. https://www.cosin.eu/wp-content/uploads/2018-FTire-flyer-brochure.pdf

Coxworth, B. (2022). *Continental forward braking system to get stereo vision*. https://newatlas.com/continental-forward-braking-system-stereo-vision/18594/

Deigmoeller, J., **Einecke, N.**, **Fuchs, O.**, and **Janssen, H.** (2018). Road surface scanning using stereo cameras for motorcycles. *VISIGRAPP 2018 - Proceedings of the 13th International Joint Conference on Computer Vision, Imaging and Computer Graphics Theory and Applications*, *5*(Visigrapp), 549–554. https://doi.org/10.5220/0006614805490554

Demić, M., **Lukić, J.**, and **Milić, Ž.** (2002). Some aspects of the investigation of random vibration influence on ride comfort. *Journal of Sound and Vibration*, *253*(1), 109–128. https://doi.org/10.1006/jsvi.2001.4252

Dixon, J. C. (2007). The Shock Absorber Handbook: Second Edition. In *The Shock Absorber Handbook: Second Edition*. https://doi.org/10.1002/9780470516430

Do, A. L., **Sename, O.**, and **Dugard, L.** (2010). An LPV control approach for semi-active suspension control with actuator constraints. *Proceedings of the 2010 American Control Conference, ACC 2010*, 4653–4658. https://doi.org/10.1109/acc.2010.5531069

Dogru, E. (2017). *Burulma Kirişli Bir Arka Aks Tasarımı Ve Taşıt Dinamik Davranışı Üzerine Etkileri* [Bursa Teknik Universitesi]. http://acikerisim.btu.edu.tr/xmlui/bitstream/handle/20.500.12885/188/456989.pdf?sequence=1&isAllowed=y

Duven, E. (2007). Tasitlar icin aktif suspansiyon denetiminin gelistirilmesi [Uludag Universitesi Fen Bilimleri Enstitusu]. In *Uludag Universitesi Fen Bilimleri Enstitusu*. https://www.infodesign.org.br/infodesign/article/view/355%0Ahttp://www.abergo.org.br/revista/index.php/ae/article/view/731%0Ahttp://www.abergo.org.br/revista/index.php/ae/article/view/269%0Ahttp://www.abergo.org.br/revista/index.php/ae/article/view/106

Eager, D., **Pendrill, A. M.**, and **Reistad, N.** (2016). Beyond velocity and acceleration: Jerk, snap and higher derivatives. *European Journal of Physics*, *37*(6), 1–11. https://doi.org/10.1088/0143-0807/37/6/065008

Eichler, M. (1997). Ride comfort tyre model for vibration analysis in full vehicle simulations. *Vehicle System Dynamics*, *27*(Suppl), 37–41. https://doi.org/10.1080/00423119708969648

Els, P. S. (2005). The applicability of ride comfort standards to off-road vehicles.

Journal of Terramechanics, *42*(1), 47–64. https://doi.org/10.1016/j.jterra.2004.08.001

Els, P. S., **Theron, N. J.**, **Uys, P. E.**, and **Thoresson, M. J.** (2007). The ride comfort vs. handling compromise for off-road vehicles. *Journal of Terramechanics*, *44*(4), 303–317. https://doi.org/10.1016/j.jterra.2007.05.001

Emura, J., **Kakizaki, S.**, **Yamaoka, F.**, and **Nakamura, M.** (1994). Development of the semi-active suspension system based on the sky-hook damper theory. *SAE Technical Papers*, *41 2*. https://doi.org/10.4271/940863

Enders, E., **Burkhard, G.**, and **Munzinger, N.** (2020). Analysis of the influence of suspension actuator limitations on ride comfort in passenger cars using model predictive control. In *Actuators* (Vol. 9, Issue 3). https://doi.org/10.3390/ACT9030077

Ester, M., **Kriegel, H.-P.**, **Sander, J.**, and **Xu, X.** (1996). *A Density-Based Algorithm for Discovering Clusters in Large Spatial Databases with Noise*. www.aaai.org

Fischer, D., and **Isermann, R.** (2004). Mechatronic semi-active and active vehicle suspensions. *Control Engineering Practice*, *12*(11), 1353–1367. https://doi.org/10.1016/j.conengprac.2003.08.003

Fleming, W. J. (2001). Overview of Automotive Sensors. *IEEE Sensors Journal*, *1*(4), 296–308. https://doi.org/10.1109/7361.983469

Fukushima, N., **Hidaka, K.**, and **Iwata, K.** (1983). Optimum Characteristics of Automotive Shock Absorbers Under Various Driving Conditions and Road Surfaces. *International Journal of Vehicle Design*, *4*(5), 463–472.

G, L. C. S., and **Serpa, A. L.** (2010). Semi-Active Suspension Control With One Measurement Sensor Using H ∞ Technique. *Control*, 878–884. http://www.sbmac.org.br/dincon/trabalhos/PDF/optimization/67793.pdf

Ghasemalizadeh, O. (2016). *Analysis and Development of Control Methodologies for Semi-active Suspensions Analysis and Development of Control Methodologies for Semi-active Suspensions*. Virginia Polytechnic Institute and State University.

Gillespie, T. D. (1992). *Fundamentals of Vehicle Dynamics - Thomas D.Gillespie*. SAE International.

Göhrle, C. (2014). *Methods and implementation of a predictive chassis control for active and semi-active suspension systems*. University of Stuttgart.

Göhrle, C., **Schindler, A.**, **Wagner, A.**, and **Sawodny, O.** (2013). Model Predictive Control of semi-active and active suspension systems with available road preview. *2013 European Control Conference, ECC 2013*, 1499–1504. https://doi.org/10.23919/ecc.2013.6669185

Göhrle, C., **Schindler, A.**, **Wagner, A.**, and **Sawodny, O.** (2015). Road Profile Estimation and Preview Control for Low-Bandwidth Active Suspension Systems. *IEEE/ASME Transactions on Mechatronics*, *20*(5), 2299–2310. https://doi.org/10.1109/TMECH.2014.2375336

Gohrle, C., **Wagner, A.**, **Schindler, A.**, and **Sawodny, O.** (2012). Active suspension controller using MPC based on a full-car model with preview information. *Proceedings of the American Control Conference*, 497–502. https://doi.org/10.1109/acc.2012.6314680

Gong, M., **Wang, H.**, and **Wang, X.** (2019). Active Suspension Control Based on Estimated Road Class for Off-Road Vehicle. *Mathematical Problems in Engineering*, *2019*. https://doi.org/10.1155/2019/3483710

González, A., **O'Brien, E. J.**, **Li, Y. Y.**, and **Cashell, K.** (2008). The use of vehicle acceleration measurements to estimate road roughness. *Vehicle System Dynamics*, *46*(6), 483–499. https://doi.org/10.1080/00423110701485050

Griffin, M. (2007). Discomfort from feeling vehicle vibration. *Vehicle System Dynamics : International Journal of Vehicle Mechanics and Mobility*, *53*(March 2014), 37–41.

Hac, A. (2007). Optimal Linear Preview Control of Active Vehicle Suspension. *Http://Dx.Doi.Org/10.1080/00423119208969008*, *21*(1), 167–195. https://doi.org/10.1080/00423119208969008

Hac, A., and **Brook, S.** (1994). Decentralized control of active vehicle suspensions with preview. *Proceedings of the American Control Conference*. https://doi.org/10.1109/ACC.1994.752416

Hamzah, R. A., **Rahim, R. A.**, and **Noh, Z. M.** (2010). Sum of absolute differences algorithm in stereo correspondence problem for stereo matching in computer vision application. *Proceedings - 2010 3rd IEEE International Conference on Computer Science and Information Technology, ICCSIT 2010*, *1*, 652–657. https://doi.org/10.1109/ICCSIT.2010.5565062

Hirao, R., **Kasuya, K.**, and **Ichimaru, N.** (2018). *A Semi-Active Suspension System Using Ride Control Based on Bi-linear Optimal Control Theory and Handling Control Considering Roll Feeling*. https://doi.org/10.4271/2015-01-1501.Copyright

Hironobu, K., and **Kazuaki, I.** (2022). RIDE PERFORMANCE ON WHEEL ROTATION SPEED DRIVEN. *International Journal of Automotive Technology*, *23*(5), 1451–1470.

Hong, K. S., **Sohn, H. C.**, and **Hedrick, J. K.** (2002). Modified skyhook control of semi-active suspensions: A new model, gain scheduling, and hardware-in-the-loop tuning. *Journal of Dynamic Systems, Measurement and Control, Transactions of the ASME*, *124*(1), 158–167. https://doi.org/10.1115/1.1434265

Houzhong, Z., **Jiasheng, L.**, **Chaochun, Y.**, **Xiaoqiang, S.**, and **Yingfeng, C.** (2020). Application of explicit model predictive control to a vehicle semi-active suspension system. *Journal of Low Frequency Noise Vibration and Active Control*, *39*(3), 772–786. https://doi.org/10.1177/1461348418822170

Hrovat, D., **Cairano, S. Di**, **Tseng, H. E.**, and **Kolmanovsky, I. V**. (2012). *The Development of Model Predictive Control in Automotive Industry : A Survey*.

Hu, X., and **Mordohai, P.** (2010). Evaluation of stereo confidence indoors and outdoors. *Proceedings of the IEEE Computer Society Conference on Computer*

Vision and Pattern Recognition, 1466–1473. https://doi.org/10.1109/CVPR.2010.5539798

Hu, X., and **Mordohai, P.** (2012). A quantitative evaluation of confidence measures for stereo vision. *IEEE Transactions on Pattern Analysis and Machine Intelligence*, *34*(11), 2121–2133. https://doi.org/10.1109/TPAMI.2012.46

Ikenaga, S., **Lewis, F. L.**, **Campos, J.**, and **Davis, L.** (2000). Active suspension control of ground vehicle based on a full-vehicle model. *Proceedings of the American Control Conference*, *6*(June), 4019–4024. https://doi.org/10.1109/ACC.2000.876977

Iskander, J., **Attia, M.**, **Saleh, K.**, **Nahavandi, D.**, **Abobakr, A.**, **Mohamed, S.**, **Asadi, H.**, **Khosravi, A.**, **Lim, C. P.**, and **Hossny, M.** (2019). From car sickness to autonomous car sickness: A review. *Transportation Research Part F: Traffic Psychology and Behaviour*, *62*, 716–726. https://doi.org/10.1016/J.TRF.2019.02.020

ISO 2631. (1997). *ISO - ISO 2631-1:1997*. https://www.iso.org/standard/7612.html

ISO 8608:2016(E). (2016). *INTERNATIONAL STANDARD ISO Mechanical vibration — Road surface profiles — Reporting of measured data IS=8608:2016(E)* (Vol. 2016).

Janeway, R. N. (1975). Human vibration tolerance criteria and applications to ride evaluation. *SAE Technical Papers*. https://doi.org/10.4271/750166

Jazar, R. N. (2017). Vehicle Dynamics: Theory and Application: Third Edition. In *Vehicle Dynamics: Theory and Application: Third Edition*. https://doi.org/10.1007/978-3-319-53441-1

Jurisch, M. (2021). Vertical trajectory planning: an optimal control approach for active suspension systems in autonomous vehicles. *Vehicle System Dynamics*. https://doi.org/10.1080/00423114.2021.1979238

Kaneko, A. M., and **Yamamoto, K.** (2017). Monocular depth estimation by two-frame triangulation using flat surface constraints. *IEEE International Conference on Intelligent Robots and Systems*, *2017-Septe*, 574–581. https://doi.org/10.1109/IROS.2017.8202210

Karnopp, D., **Crosby, M. J.**, and **Harwood, R. A.** (1973). VIBRATION CONTROL USING SEMI-ACTIVE FORCE GENERATORS. *ASME Pap*, *73-DET-122*.

Kishi, T., and **Yamamoto, Y.** (1985). *United States Patent (19) Kishi et al. (54) ULTRA-SONIC SENSORSYSTEM FOR MONITORING ROLLING AND/OR PITCHING MOTION OF VEHICLE* (Patent No. 4,722,547).

Kissai, M., **Monsuez, B.**, **Mouton, X.**, **Martinez, D.**, and **Tapus, A.** (2019). Adaptive robust vehicle motion control for future over-actuated vehicles. *Machines*, *7*(2), 1–31. https://doi.org/10.3390/machines7020026

Kjellberg, F., and **Sundell, S.** (2018). *Real-Time Nonlinear Model Predictive Control for Semi-Active Suspension with Road Preview*.

Koch, G., **Fritsch, O.**, and **Lohmann, B.** (2010). Potential of low bandwidth active

suspension control with continuously variable damper. *Control Engineering Practice*, *18*(11), 1251–1262. https://doi.org/10.1016/j.conengprac.2010.03.007

Krtolica, R., and **Hrovat, D.** (1990). Optimal active suspension control based on a half-car model. *Proceedings of the IEEE Conference on Decision and Control*, *4*, 2238–2243. https://doi.org/10.1109/cdc.1990.204023

Labayrade, R., **Aubert, D.**, and **Tarel, J.** (1998). Real Time Obstacle Detection in Stereovision on Non Flat Road Geometry Through "V-disparity" Representation. *Archivio Italiano Di Urologia, Andrologia : Organo Ufficiale [Di] Società Italiana Di Ecografia Urologica e Nefrologica / Associazione Ricerche in Urologia*, *70*(5), 211–266.

Lee, J. K., and **Yoon, K. J.** (2018). Temporally Consistent Road Surface Profile Estimation Using Stereo Vision. *IEEE Transactions on Intelligent Transportation Systems*, *19*(5), 1618–1628. https://doi.org/10.1109/TITS.2018.2794342

Li, Z., **Sun, W.**, and **Gao, H.** (2020). Energy-driven-damper (EDD): Comfort-oriented semiactive suspensions optimized from an energy perspective. *IEEE Transactions on Control Systems Technology*, *28*(5), 2069–2076. https://doi.org/10.1109/TCST.2019.2954793

Liu, Y., **Hozumi, J.**, **Morita, M.**, and **Higuchi, A.** (2015). Body attitude state estimation using wheel rolling speed variations. *International Journal of Automotive Engineering*, *6*(4), 135–142. https://doi.org/10.20485/jsaeijae.6.4_135

Liu, Y., **Waters, T. P.**, and **Brennan, M. J.** (2005). A comparison of semi-active damping control strategies for vibration isolation of harmonic disturbances. *Journal of Sound and Vibration*, *280*(1–2), 21–39. https://doi.org/10.1016/j.jsv.2003.11.048

Liu, Y., and **Zuo, L.** (2016). Mixed Skyhook and Power-Driven-Damper: A New Low-Jerk Semi-Active Suspension Control Based on Power Flow Analysis. *Journal of Dynamic Systems, Measurement and Control, Transactions of the ASME*, *138*(8), 1–10. https://doi.org/10.1115/1.4033073

Loprencipe, G., and **Zoccali, P.** (2017). Use of generated artificial road profiles in road roughness evaluation. *Journal of Modern Transportation*, *25*(1), 24–33. https://doi.org/10.1007/s40534-017-0122-1

Łuczko, J., and **Ferdek, U.** (2020). Nonlinear dynamics of a vehicle with a displacement-sensitive mono-tube shock absorber. *Nonlinear Dynamics*, *100*(1), 185–202. https://doi.org/10.1007/s11071-020-05532-7

Madhavan Rathai, K. M., **Alamir, M.**, and **Sename, O.** (2019). Experimental Implementation of Model Predictive Control Scheme for Control of Semi-active Suspension System. *IFAC-PapersOnLine*, *52*(5), 261–266. https://doi.org/10.1016/j.ifacol.2019.09.042

Maher, D., and **Young, P.** (2011). An insight into linear quarter car model accuracy. *Vehicle System Dynamics*, *49*(3), 463–480. https://doi.org/10.1080/00423111003631946

Margolis, D. L., and **Goshtasbpour, M.** (1984). The Chatter of Semi-Active On-Off Suspensions and its Cure. *Vehicle System Dynamics*, *13*(3), 129–144. https://doi.org/10.1080/00423118408968771

Mastinu, G., and **Manfred, P.** (2014). *Road and off-road vehicle system dynamics handbook*.

Mehra, R. K., **Amin, J. N.**, **Hedrick, K. J.**, **Osorio, C.**, and **Gopalasamy, S.** (1997). Active suspension using preview information and model predictive control. *IEEE Conference on Control Applications - Proceedings*, 860–865. https://doi.org/10.1109/CCA.1997.627769

Miller, L. R., and **Nobles, C. M.** (1990). Methods for eliminating jerk and noise in semi-active suspensions. *SAE Technical Papers*. https://doi.org/10.4271/902284

Milliken, William F. Milliken, D. L. (1995). *Race Car Vehicle Dynamics*. SAE International.

Missel, J. Mehren, D. Reichmann M., Lallinger, M. (2013). INTELLIGENT DRIVE ENTSPANNTER UND SICHERER FAHREN. *Fahrkomfort Der Extraklasse*, *18*(5), 124–128.

Morselli, R., and **Zanasi, R.** (2008). Control of port Hamiltonian systems by dissipative devices and its application to improve the semi-active suspension behaviour. *Mechatronics*, *18*(7), 364–369. https://doi.org/10.1016/j.mechatronics.2008.05.008

Nguyen, M. Q., **Canale, M.**, **Sename, O.**, and **Dugard, L.** (2016). A Model Predictive Control approach for semi-active suspension control problem of a full car. *2016 IEEE 55th Conference on Decision and Control, CDC 2016*, 721–726. https://doi.org/10.1109/CDC.2016.7798353

Oniga, F., **Nedevschi, S.**, **Meinecke, M. M.**, and **To, T. B.** (2007). Road surface and obstacle detection based on elevation maps from dense stereo. *IEEE Conference on Intelligent Transportation Systems, Proceedings, ITSC*, 859–865. https://doi.org/10.1109/ITSC.2007.4357734

Pellegrini, E. (2013). Model-Based Damper Control for Semi-Active Suspension Systems. *At-Automatisierungstechnik*, *61*(7), 515–516.

Pfeiffer, D., **Gehrig, S.**, and **Schneider, N.** (2013). *Exploiting the Power of Stereo Confidences*. https://doi.org/10.1109/CVPR.2013.45

Poussot-Vassal, C., **Sename, O.**, and **Dugard, L.** (2008). Attitude and handling improvements based on optimal skyhook and feedforward strategy with semi-active suspensions. *International Journal of Vehicle Autonomous Systems*, *6*(3–4), 308–329. https://doi.org/10.1504/ijvas.2008.023589

Prabakar, R. S., **Sujatha, C.**, and **Narayanan, S.** (2009). Optimal semi-active preview control response of a half car vehicle model with magnetorheological damper. *Journal of Sound and Vibration*, *326*(3–5), 400–420. https://doi.org/10.1016/j.jsv.2009.05.032

Qin, Y., **Dong, M.**, **Zhao, F.**, **Langari, R.**, and **Gu, L.** (2015). Road profile classification for vehicle semi-active suspension system based on Adaptive Neuro-Fuzzy Inference System. *Proceedings of the IEEE Conference on*

Decision and Control, *54rd IEEE*(May 2016), 1533–1538. https://doi.org/10.1109/CDC.2015.7402428

Rajamani, R. (2012). Vehicle Dynamics and Control. In *Vehicle Handling Dynamics* (Second Edi). https://doi.org/10.1016/b978-0-08-100390-9.00001-4

Šabanovič, E.; Kojis, P. ., Šukevičius, Š.; Shyrokau, B. . I., and **V.; Dhaens, M.; Skrickij, V.** (2021). Feasibility of a Neural Network-Based Virtual Sensor for Vehicle Unsprung Mass Relative Velocity Estimation. *Sensors*, *21*(21).

Savaresi, S. M., **Bittanti, S.**, and **Montiglio, M.** (2005). Identification of semi-physical and black-box non-linear models: The case of MR-dampers for vehicles control. *Automatica*, *41*(1), 113–127. https://doi.org/10.1016/j.automatica.2004.08.012

Savaresi, S. M., **Silani, E.**, and **Bittanti, S.** (2005). Acceleration-Driven-Damper (ADD): An optimal control algorithm for comfort-oriented semiactive suspensions. *Journal of Dynamic Systems, Measurement and Control, Transactions of the ASME*, *127*(2), 218–229. https://doi.org/10.1115/1.1898241

Savaresi, S. M., and **Spelta, C.** (2007). Mixed sky-hook and ADD: Approaching the filtering limits of a semi-active suspension. *Journal of Dynamic Systems, Measurement and Control, Transactions of the ASME*, *129*(4), 382–392. https://doi.org/10.1115/1.2745846

Savaresi, S., **Poussot-Vassal, C.**, **Spelta, C.**, **Sename, O.**, and **Dugard, L.** (2010). Semi-Active Suspension Control Design for Vehicles. *Semi-Active Suspension Control Design for Vehicles*, 71–90. https://doi.org/10.1016/C2009-0-63839-3

Saxena, A., **Jamie, S.**, and **Ng, A. Y.** (2007). Depth estimation using monocular and stereo cues. *IJCAI International Joint Conference on Artificial Intelligence*, 2197–2203.

Schindler, A. (2009a). *Neue Konzeption und erstmalige Realisierung eines aktiven Fahrwerks mit Preview-Strategie* (Vol. 31) [Universitätsverlag Karlsruhe]. https://doi.org/10.5445/KSP/1000013552

Schindler, A. (2009b). *New conception and first-time implementation of an active chassis with a preview strategy* [KIT Scientific Publishing]. https://doi.org/10.5445/KSP/1000013552

Schindler, A., **Göhrle, C.**, and **Sawodny, O.** (2019). *Method for precise scaling of an image of a camera sensor and system EP2916102B1*.

Schmeitz, A. J. C. (2004). *Semi-emperical three-dimensional model of the pneumatic tyre rolling over arbitrary uneven road surfaces, Ph.D. thesis*. Delft University of Technology.

Schmeitz, A. J. C., **Besselink, I. J. M.**, and **Jansen, S. T. H.** (2007). TNO MF-SWIFT. *Vehicle System Dynamics : International Journal of Vehicle Mechanics and Mobility*, *45*(March 2013), 37–41.

Schmid, C., and **Biegler, L. T.** (1994). Quadratic programming hessian. *Computers & Chemical Engineering*, *18*(9), 817–832.

Schofield, B., and **Hägglund, T.** (2008). Optimal control allocation in vehicle

dynamics control for rollover mitigation. *Proceedings of the American Control Conference*, *August*, 3231–3236. https://doi.org/10.1109/ACC.2008.4586990

Schramm, D., **Hiller, M.**, and **Bardini, R.** (2014). Vehicle dynamics: Modeling and simulation. In *Vehicle Dynamics: Modeling and Simulation* (Vol. 9783540360). https://doi.org/10.1007/978-3-540-36045-2

Schubert, E., **Sander, J.**, **Ester, M.**, **Kriegel, H.-P.**, **Xu, X.**, and **Kriegel, H.-P.** (2017). 9 DBSCAN Revisited, Revisited: Why and How You Should (Still) Use DBSCAN. *DBSCAN Revisited, Revisited: Why and How You Should (Still) Use DBSCAN. ACM Trans. Database Syst*, *42*(3). https://doi.org/10.1145/3068335

Shen, T., **Schamp, G.**, and **Haddad, M.** (2014). Stereo vision based road surface preview. *2014 17th IEEE International Conference on Intelligent Transportation Systems, ITSC 2014*, 1843–1849. https://doi.org/10.1109/ITSC.2014.6957961

Soliman, A. M. A., and **Kaldas, M. M. S.** (2021). *Semi-active suspension systems from research to mass-market – A review*. https://doi.org/10.1177/1461348419876392

Song, X., **Ahmadian, M.**, and **Southward, S. C.** (2005). Modeling magnetorheological dampers with application of nonparametric approach. *Journal of Intelligent Material Systems and Structures*, *16*(5), 421–432. https://doi.org/10.1177/1045389X05051071

Stamatov, S., **Krishnan, M.**, and **Yost, S.** (2008). Low jerk predictive force modulation for semi-active suspension control. *SAE Technical Papers*. https://doi.org/10.4271/2008-01-0904

Staniek, M. (2017). Stereo vision method application to road inspection. *Baltic Journal of Road and Bridge Engineering*, *12*(1), 38–47. https://doi.org/10.3846/bjrbe.2017.05

Stein, G. P., **Stein, G. P.**, **Mano, O.**, and **Shashua, A.** (2000). A Robust Method for Computing Vehicle Ego-motion. *IN IEEE INTELLIGENT VEHICLES SYMPOSIUM (IV2000*.

Stocia P., M. R. (2005). Spectral Analysis of Signals. In *Prentice Hall, Inc.* Prentice Hall, Inc. https://doi.org/10.1109/msp.2007.273066

Streiter, R. (2008). Active preview suspension system. *ATZ Worldwide 2008 110:5*, *110*(5), 4–11. https://doi.org/10.1007/BF03225003

Suhr, J. K., and **Jung, H. G.** (2015). Dense stereo-based robust vertical road profile estimation using hough transform and dynamic programming. *IEEE Transactions on Intelligent Transportation Systems*, *16*(3), 1528–1536. https://doi.org/10.1109/TITS.2014.2369002

Thenozhi, S., **Yu, W.**, and **Garrido, R.** (2012). A novel numerical integrator for structural health monitoring. *Proceedings - 2012 5th International Symposium on Resilient Control Systems, ISRCS 2012*, 92–97. https://doi.org/10.1109/ISRCS.2012.6309300

Theunissen, J., **Sorniotti, A.**, **Gruber, P.**, **Fallah, S.**, **Ricco, M.**, **Kvasnica, M.**, and **Dhaens, M.** (2020). Regionless Explicit Model Predictive Control of Active

Suspension Systems with Preview. *IEEE Transactions on Industrial Electronics*, *67*(6), 4877–4888. https://doi.org/10.1109/TIE.2019.2926056

Theunissen, J., **Tota, A.**, **Gruber, P.**, **Dhaens, M.**, and **Sorniotti, A.** (2021). Preview-based techniques for vehicle suspension control: a state-of-the-art review. *Annual Reviews in Control*, *51*(xxxx), 206–235. https://doi.org/10.1016/j.arcontrol.2021.03.010

Tseng, H. E., and **Hrovat, D.** (2015). State of the art survey: active and semi-active suspension control. *Http://Dx.Doi.Org/10.1080/00423114.2015.1037313*, *53*(7), 1034–1062. https://doi.org/10.1080/00423114.2015.1037313

Tudon-Martinez, J. C., **Fergani, S.**, **Varrier, S.**, **Sename, O.**, **Dugard, L.**, **Morales-Menendez, R.**, and **Ramirez-Mendoza, R.** (2013). Road adaptive semi-active suspension in an automotive vehicle using an LPV controller 1. *IFAC Proceedings Volumes (IFAC-PapersOnline)*, *7*(PART 1), 231–236. https://doi.org/10.3182/20130904-4-JP-2042.00090

Türkay, S., and **Akçay, H.** (2005). A study of random vibration characteristics of the quarter-car model. *Journal of Sound and Vibration*, *282*(1–2), 111–124. https://doi.org/10.1016/j.jsv.2004.02.049

Valášek, M., **Novák, M.**, **Šika, Z.**, and **Vaculín, O.** (1997). Extended ground-hook - New concept of semi-active control of truck's suspension. *Vehicle System Dynamics*, *27*(5–6), 289–303. https://doi.org/10.1080/00423119708969333

Wakeham, K. J., and **Rideout, D. G.** (2018). *MODEL COMPLEXITY REQUIREMENTS IN DESIGN OF HALF CAR ACTIVE SUSPENSION CONTROLLERS*.

Ward, C. C., and **Iagnemma, K.** (2009). *Speed-independent vibration-based terrain classification for passenger vehicles*. *47*(9), 1095–1113. https://doi.org/10.1080/00423110802450193

Weist, U., **Missel, J.**, **Cytrynski, S.**, **Mehren, D.**, **Schwarz, T.**, and **Kern, S.** (2013). Fahrkomfort der extraklasse. *ATZextra*, *18*(5), 124–128. https://doi.org/10.1365/s35778-013-0060-4

Wen, W. (2008). *Road roughness detection by analysing imu data* (Issue January). Royal Institute of Technology.

Wong, J. Y. (2008). *Theory of Ground Vehicles* (4th ed.). Wiley.

Wu, T. H., **Chellappa, R.**, and **Zheng, Q.** (1995). Experiments on estimating egomotion and structure parameters using long monocular image sequences. *International Journal of Computer Vision*, *15*(1–2), 77–103. https://doi.org/10.1007/BF01450850

Yang, H., **Kim, B. G.**, **Oh, J. S.**, and **Kim, G. W.** (2022). Simultaneous Estimation of Vehicle Mass and Unknown Road Roughness Based on Adaptive Extended Kalman Filtering of Suspension Systems. *Electronics (Switzerland)*, *11*(16), 1–20. https://doi.org/10.3390/electronics11162544

Zhao, S. E., **Li, Y.**, and **Qu, X.** (2014). Vehicle chassis integrated control based on multimodel and multilevel hierarchical control. *Mathematical Problems in Engineering*, *2014*. https://doi.org/10.1155/2014/248676

Ziebinski, A., **Cupek, R.**, **Erdogan, H.**, and **Waechter, S.** (2016). *A Survey of ADAS Technologies for the Future Perspective*. *2*, 135–146. https://doi.org/10.1007/978-3-319-45246-3

CURRICULUM VITAE

Name-Surname **: Mert BÜYÜKKÖPRÜ**

Place and Date of Birth **:**

E-mail **:**

EDUCATION:

- **B.Sc.** **:** 2013, Ege University, Engineering Faculty, Department of Mechanical Engineering
- **M.Sc.** **:** 2013, Ege University, Graduate School of Natural Applied Sciences, Department of Mechanical Engineering

PROFESSIONAL EXPERIENCE AND REWARDS:

- R&D Engineer at Ege Fren A.Ş.
- System Engineer Vehicle Chassis Control at Groupe Renault
- Specialist Semi-Active Suspension Control and Simulation Ride and Handling at Groupe Renault

PUBLICATIONS, PRESENTATIONS AND PATENTS ON THE THESIS:

- Patent Application: System And Method For Vision-Based Road Profile Estimation PCT/TR2021/050901, Mert Büyükköprü, Xavier Mouton, Erdem Uzunsoy.
- Patent Application: A method and system for energy-efficient control of semi-active damper and active suspension PCT/TR2021/051366, Mert Büyükköprü, Xavier Mouton, Erdem Uzunsoy
- Mert BÜYÜKKÖPRÜ, Erdem Uzunsoy, Xavier Mouton "Global Skyhook and Groundhook Control of Vehicle with Semi-Active Dampers" OTEKON 2021 International 10th Automotive Conference.
- Mert BÜYÜKKÖPRÜ, Erdem Uzunsoy, Xavier Mouton "Implementation of Semi-Active Suspension Control Methods In A Full Car Model And A Comparative Study In Terms Of Ride Comfort And Road Holding" Proc. IMechE, Part D: Journal of Automobile Engineering,2021
- Mert BÜYÜKKÖPRÜ, Erdem Uzunsoy, Xavier Mouton "Vision-Based Road Profile Estimation for Preview Controlled Vehicle Suspension Systems". Interdisciplinary Conference on Mechanics, Computers and Electronics 2022.

OTHER PUBLICATIONS, PRESENTATIONS AND PATENTS:

- Mert BÜYÜKKÖPRÜ, Erdem Uzunsoy "Reliability of Extended Kalman Filtering Technic on Vehicle Mass Estimation", Journal of Innovative Science and Engineering,2020.